

A dissertation submitted to the  
University of Manchester Institute of Science and Technology  
for the degree of MSc



**Lightning Protection of Buildings Using Active  
Finials**

**Daniel Charles Faircloth**

Department of Electrical Engineering and Electronics

1996

## **Abstract**

This dissertation investigates the efficacy of active lightning finials. The active lightning protection method studied involves the application of a voltage to the finial. An active finial working on this principle is simulated experimentally. The field experienced by a lightning finial during a lightning strike is analysed and simulated to allow investigation of the artificial active device in the laboratory.

**Declaration:** No portion of the work referred to in this dissertation has been submitted in support of another degree or qualification of this or any other institution of learning.

## **Acknowledgements**

Project Supervisor: Dr. K. J. Cornick  
Dr. N. Allen  
Derek Greaves  
Malcom Walker

# Contents

<b>1. INTRODUCTION</b>	<b>1</b>
<b>1.1 Background</b>	<b>1</b>
<b>1.2 Theory</b>	<b>2</b>
The Active Device	5
Method of operation	6
<b>1.3 Objectives</b>	<b>7</b>
<b>1.4 Summary of Work Conducted</b>	<b>7</b>
<b>2. APPARATUS</b>	<b>9</b>
<b>2.1 Introduction</b>	<b>9</b>
<b>2.2 Development of the Experimental Set up</b>	<b>9</b>
Electric field at ground level	9
Electric Field Simulation in the Laboratory	10
ESE Device Simulation	11
Experiments	12
<b>2.3 Laboratory set up</b>	<b>14</b>
<b>2.4 The Main Generator</b>	<b>16</b>
Circuit diagram	16
Wave shape	17
Voltage Calibration	18
<b>3. THE ARTIFICIAL ESE DEVICE</b>	<b>20</b>
<b>3.1 Introduction</b>	<b>20</b>
<b>3.2 System requirements</b>	<b>20</b>
<b>3.3 System design overview</b>	<b>21</b>
<b>3.4 Delay Unit</b>	<b>23</b>
Requirements:	23
Delay Circuit - design options	23
Monostable delay circuit design	24

Resistive Voltage Divider	25
Optical Transmitter Design	26
Delay Unit Construction	27
Delay Unit Modifications	30
<b>3.5 The Small Impulse Generator</b>	<b>36</b>
Introduction	36
Wave Shape	36
Available Impulse generator	39
Nominal Voltage Rating	40
Number of Stages	42
Nominal Capacitance	42
Nominal Energy	43
Sphere Gaps	43
Spark Gap Setting	45
Earthing and Safety	45
External Wave Front Components	46
Wave Shape Measurement	46
Voltage Calibration	47
Contingency Impulse Generator	48
<b>3.6 Firing The Small Impulse Generator</b>	<b>50</b>
Introduction	50
Triggering the generator	50
Pulse Feed Unit	51
Optical Receiver	52
Construction of the Firing Unit	53
Testing The Firing Unit	54
Firing the Contingency Impulse Generator	55
<b>3.7 Linking The Small Generator to the Finial</b>	<b>56</b>
Protecting the Small Impulse Generator	56
Gap Capacitance measurements	57
<b>3.8 Overall Artificial ESE Device Apparatus</b>	<b>59</b>
<b>4. EXPERIMENTS</b>	<b>60</b>
<b>4.1 Introduction</b>	<b>60</b>
<b>4.2 Preliminary Experiments- The Passive Finial</b>	<b>60</b>
V50% for Finial-Sphere Gap	60
Corona Inception Times	61
Time to Breakdown	66

<b>4.3 Pre-stressing the Finial-Sphere gap</b>	<b>69</b>
Introduction	69
Applying Positive DC to the Finial	69
Applying Negative DC to the Sphere	70
Applying DC to the Finial, and impulse to the sphere	71
Time to Breakdown	76
<b>4.4 Modelling the Experimental Set Up</b>	<b>78</b>
Introduction	78
Setting up the Finite Element Mesh	78
Calculations	79
<b>4.5 Tests on the artificial ESE device</b>	<b>85</b>
Corona Inception Times of the finial under its own excitation	85
Time to Breakdown	87
<b>5. CONCLUSIONS</b>	<b>94</b>
<b>6. APPENDIX</b>	<b>96</b>
<b>6.1 Main Impulse Generator Calibration Sheet</b>	<b>97</b>
<b>6.2 Small Impulse Generator Calibration Sheets</b>	<b>98</b>
<b>6.3 Substitute Impulse Generator Calibration Sheet</b>	<b>100</b>
<b>6.4 Results for calculation of V50% for finial-sphere gap</b>	<b>101</b>
<b>6.5 References</b>	<b>102</b>

# 1. Introduction

## 1.1 Background

One of the most effective methods of protecting buildings and other large objects against direct lightning strikes is by the installation of lightning rods. The traditional lightning rod (or finial) is a simple spiked conductor which is solidly earthed via a conductor capable of carrying the peak lightning current. The finials are placed at critical points on the building to attract lightning strokes away from terminating on the building. This method of protecting buildings has remained largely unchanged since its use was first developed by Franklin in 1752.

A common lightning protection arrangement for a simple cuboid building is to have a lightning finial connected at each of the top four corners. This is shown in figure 1.1.1a (note that none of the down-conductors are shown).

Quite recently it has been reported and indeed commercially exploited, that by energising the lightning finial a greater area of attraction is attained over the usual passive finial. Thus it has also been claimed that one single energised finial can replace an entire passive network as in figure 1.1.1b.

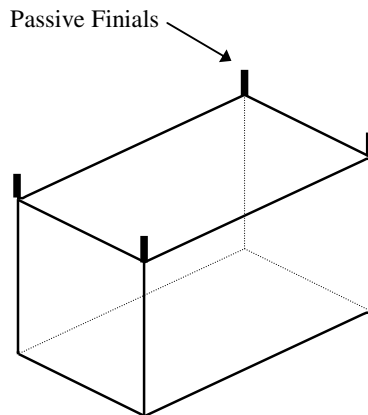


**Figure 1.1.1a:** Typical passive finial arrangement.

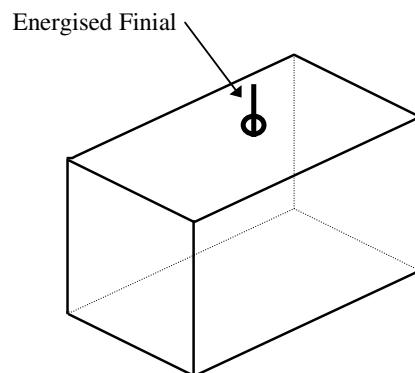


**Figure 1.1.1b:** Proposed active finial arrangement.

One of the main reasons for wanting to reduce the number of finials and down conductors is for purely aesthetic purposes. For example, the protection of old buildings

of architectural significance. The area of 'active lightning protection' is a topic of much debate and a number of companies have begun marketing active devices making claims of enhanced performance.

The research to be conducted will seek to determine by how much an active finial is an improvement on a conventional passive finial.

## **1.2 Theory**

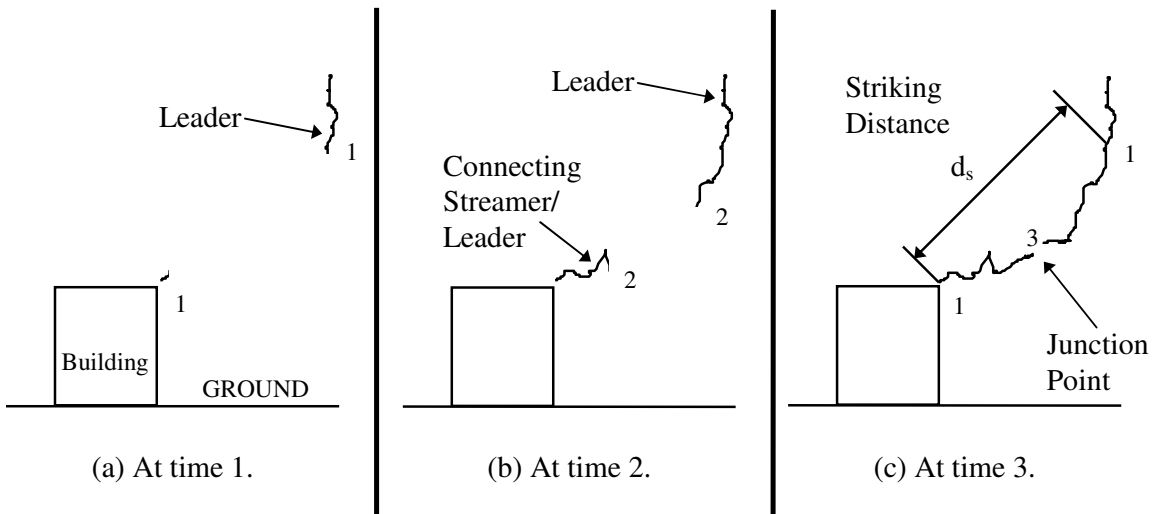
It is important to have an understanding of the processes involved in the build up to a lightning strike in order to understand how a lightning conductor works and how an active device might improve on it.

The process begins with the development of large pockets of charge in the thunder cloud by a phenomenon that is not fully understood. These charge pockets continue to grow until the electric field becomes great enough to initiate a breakdown process. Most often this is between two pockets of charge in the cloud but of more importance to us are the strikes to earth. Lightning strikes to earth are always in almost all cases negative in polarity.

The basic physics of lightning strikes can be found in many text books, so only a brief summary will be given here. A downward leader propagates from the thunder cloud towards earth, as it makes its way down an upwards leader from earth is initiated. The two leaders propagate towards each other and when they meet the two ionised channels form a conducting path from ground to cloud and a large discharge current occurs as the charge pocket in the cloud flows to earth. This violent discharge is called the return stroke. The mechanism leading up to the return stroke is called the attachment process.

A lightning rod is an air termination, this term refers to any metallic object with an electrical connection to earth to which a lightning strike may attach. The attachment process starts when the first downward leader from the cloud reaches a point about 100m to 200m above the ground. The time taken for the downward leader to travel from

the cloud to this point is in the order of 10 to 40ms. The leader takes the form of a charged channel progressing towards earth. When the leader channel reaches the point above earth described, the electric field in the region of any nearby “sharp” objects on the ground becomes high enough for corona discharge to take place. As the downward leader progresses further the electric field strength increases further and the coronaing objects on the ground start to produce upward streamers. This situation is shown in figure 1.2.2a below.



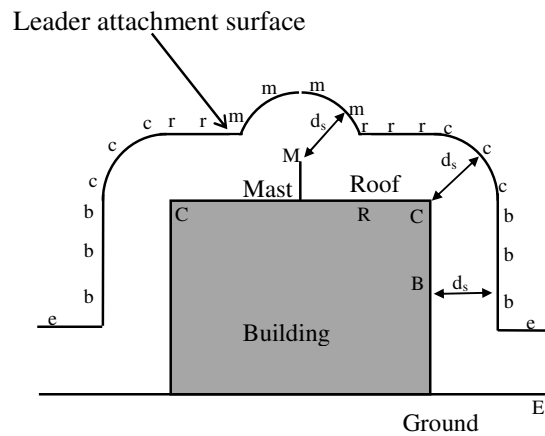
**Figure 1.2.2:** Stages in the lightning attachment process.

Figure 1.2.2b shows the situation shortly after as the upward (connecting) leader progresses further toward the downwards leader. At time 3, shown in figure 1.2.2c, the two leaders meet and a large current flows (the return stroke).

The striking distance,  $d_s$  for the corner of the building in figure 1.2.2, is defined as the distance at which the down coming leader is away from the corner of the building, when a upwards streamer is initiated.

In real life it will be very probable that a number of other streamers will be initiated from other objects nearby (even blades of grass). However only one streamer will attach to the main downward streamer.

The striking distance can be used to obtain a “leader attachment surface” for the building to be protected. The leader attachment surface is generated using the rolling sphere method, where a sphere of diameter  $d_s$  is rolled over the surface of the building. The surface generated *should* indicate which part of the building will be struck when a downward leader reaches the surface. An example of a leader attachment surface for a simple building with a mast on the roof is shown in figure 1.2.3.



**Figure 1.2.3:** Lightning attachment surface for a building.

For example if a downward leader reaches the surface at one of the points marked ‘c’, then a upward leader will start to propagate upwards from the corner of the building to meet the downward leader.

Lightning finials also have an associated leader attachment surface, figure 1.2.4a shows the surface for a passive finial of height  $h$ . A building can therefore be protected by lightning rods by placing them at critical points on the building, in such a way that the attachment surface for the rod is at a higher level than the attachment surface for the building. Thus a down coming leader will reach the rods attachment surface first, and the lightning will strike the rod as opposed to the building.

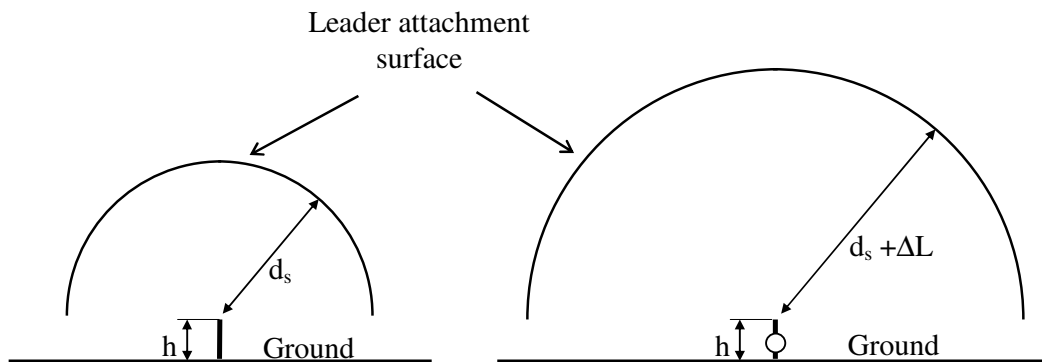


**Figure 1.2.4a:** Protective radius for a passive finial.

**Figure 1.2.4b:** Protective radius for a ESE finial.

### The Active Device

Up until this point only the passive finial has been discussed. The active finial is simply a lightning rod that attempts to improve on a standard device by some active property. The basic aim of active devices is to improve the development of a leader from the tip of the rod. Various methods of doing so have been proposed, such as using a radioactive source, but the method studied in this report is **Early Streamer Emission (ESE)**. Active finials that use this principle are termed ESE devices. As its name suggests it is a device which is capable of initiating an upwards streamer at a point in time earlier than the passive finial. The argument is that because the ESE device sends up a streamer when the downward streamer is a greater distance away the attachment surface radius is greater, as is shown in figure 1.2.4b.

The claim of greater area of attraction is based on the assumption of constant propagation speed of upward leader [5], i.e. if you start first and go at the same speed you will get there first. The simple assumption that the early streamer will continue to propagate after initiation is also made. However the electric field in which the early leader is produced is much weaker so it is possible that an early leader could peter out since it may propagate into a field too weak for its continued propagation.

Method of operation

The ESE device is able to launch streamers at an earlier time by applying voltage pulses (of the opposite polarity to the downward leader) to the tip of the air termination. This has an effect of increasing the electric field strength at the tip and thus allowing the terminal to emit a streamer at an earlier time than it would otherwise. Downward leaders are invariably negative in polarity.

Lightning strikes an ‘average’ building only about 2 or 3 times per century, it obviously therefore not feasible to continuously apply voltage impulses to the ESE device. The device must therefore only operate when a leader is approaching. An ESE device has been developed that needs no external power supply, its exact method of operation is not known. However it is obvious that it must draw its energy from the electric field of the downward leader. A possible circuit that may achieve this is shown in figure 1.2.5.

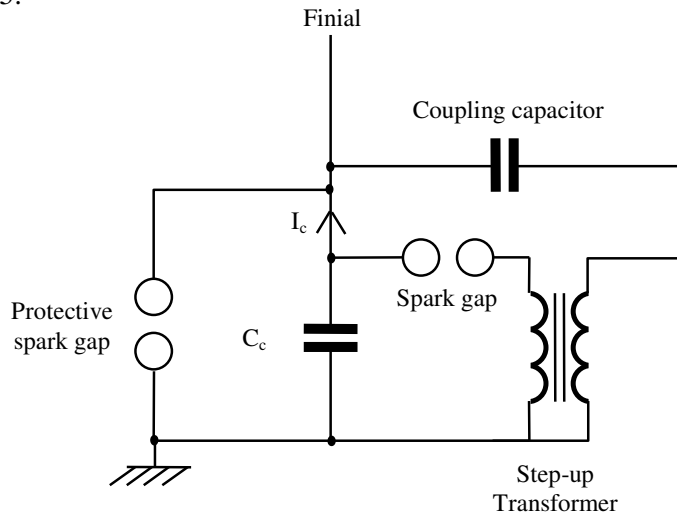


**Figure 1.2.5:** Possible ESE circuit.

The circuit works on the fact that corona discharge occurs before streamer emission. As the electric field increases as the downward leader approaches, the finial starts to draw a corona current,  $I_c$  as the finial partially discharges in the air. This current charges the capacitor,  $C_c$ , and when the voltage across the capacitor becomes high

enough the sphere gap breaks down and the discharging current oscillates around the LC circuit created by the capacitor and the transformer winding. The high voltage winding of the transformer is capacitively coupled back to the finial. Thus generating high voltage pulses to on the finial.

Thus it is theoretically possible to have an ESE device that has no external power supply. However it is not this point which is investigated in this report but the actual claims that applying a voltage pulse to a finial will result in a greater area of attraction.

### **1.3 Objectives**

The overall aim of this project is to examine the efficacy of the Early Streamer Emission device as compared with the conventional passive device.

### **1.4 Summary of Work Conducted**

Previous experiments have been conducted on specific ESE devices comparing them to a passive finial. This project seeks to establish the *effectiveness* of the *principle* behind ESE, i.e. in what way does (or can) the application of a voltage to a finial increase its 'protective radius' over a passive finial.

Apparatus had to be designed that would mimic the mode of operation of an ESE device. Simulating an ESE device rather than using a particular device allowed accurate and repeatable variations to be easily made to all possible parameters involved. The design construction of this apparatus took up a major part of the project time.

The behaviour of the passive finial had to be first investigated to allow comparison with the active case. A number of experiments were devised to achieve this:

The nature of the discharges from the finial were analysed using a photo-multiplier. The time to breakdown was also studied.

Experiments were devised to give a true measure of performance under lightning conditions. The set up had to (as closely as possible) simulate the conditions experienced by a lightning finial during a lightning strike. The field conditions simulated were analysed theoretically to check the validity of the experimental approach.

Finally the work built up to an experiment using the artificial ESE device where the effect the time delay before the application of the pulse to the finial was investigated.

This report is divided into chapters, this is the end of the first introductory chapter. Chapter 2, describes the development of the experimental set up and details the apparatus used. Chapter 3, documents the development, construction and testing of the apparatus used to simulate the effect of an ESE device. The experiments conducted are detailed in chapter 4, included in this chapter are the experimental results and discussions of the results obtained. The conclusions reached are given in chapter 5.

## **2. Apparatus**

### **2.1 Introduction**

This chapter describes the development of the experimental set up and the apparatus required to examine the efficacy of applying a voltage pulse to a lightning finial.

The main objective of the laboratory work was to perform experiments which gave a true measure of performance under lightning conditions. To do this the electric field conditions experienced during a lightning strike would have to be simulated.

### **2. 2 Development of the Experimental Set up**

#### ***Electric field at ground level***

The natural electric field at ground level during a lightning strike is made up of two components: 'permanent' and 'impulse'.

- The permanent field is the field strength in the minutes prior to the lightning strike, it is caused by charge separation in the thunder cloud in the early stages of the lightning mechanism. At ground level this field strength can reach values in the order of 20kV/m, before the lightning strike [5].
- The impulse field, which is superimposed on the permanent field, is caused by the down-coming leader. The downward leader is effectively a charged path approaching ground, thus the field at ground level will rise rapidly as the head of the leader nears earth.

A very important point to make is that both the permanent and the impulse field can vary greatly in magnitude for every lightning strike.

### *Electric Field Simulation in the Laboratory*

A method was required to generate the field experienced at ground level in the laboratory. There are two distinctly different methods of achieving this: a) where a downward leader is initiated and, b) where no downward leader is initiated, but the field generated by a down-coming leader is simulated.

Method a) (with down-coming leader) could be achieved using a rod as an upper electrode supported a distance above the lightning finial. When a HV impulse wave is applied to the upper rod it would produce streamers and in theory a down-coming leader. This method was employed, with limited success, by an undergraduate at UMIST in a final year project.

Method b) (with no down-coming leader) is similar to the experimental procedure used by Berger in the Les Renardieres experiments [5]. Their set up consisted of a very large (15m×20m) metal sheet suspended some 13m above the lightning finial. This sheet was used to represent the ‘cloud’. The cloud is large enough create a uniform field over the gap length. A DC voltage and a superimposed impulse was then applied to the sheet, no downward leaders are produced. The impulse voltage reproduces the field generated by a downward leader. From measurements taken from natural strikes Berger suggests a rise time between 200 and 1200 $\mu$ s for the impulse voltage wave. The Renardieres approach is good at reproducing the field created when the leader is at high altitudes, however in the final stages of the leaders decent the field becomes increasingly less uniform.

Due to the previous lack of success with downward leader generation it was decided that a set up where no upward leader is generated was the best route to take. The scale of the Renardieres experiments was not possible to re-create in the UMIST High Voltage laboratory so a slightly different approach was required.

The approach adopted involved using a large sphere instead of a huge sheet above the finial. DC and impulse voltages would then be applied to the sphere. The electric field directly beneath the sphere will be relatively uniform. However it will become increasingly less uniform away from the centre region, as would the field generated by an actual downward leader.

The impulse applied to the sphere was a 250/2500 $\mu$ s wave i.e. an impulse voltage wave with a 250 $\mu$ s front time and a 2500 $\mu$ s tail time. This wave shape was chosen because it has a rise time within the range of values proposed by Berger, and it is a standard switching impulse wave shape that is commonly used in the High Voltage laboratory.

As was stated previously lightning strikes are invariably negative in polarity, thus experiments will be limited to using negative voltages (DC and Impulse) on the sphere.

### ESE Device Simulation

To allow examination of the effect of energising a lightning finial a controllable method of applying voltages to the rod was required. The voltage pulse applied to commercially available ESE devices is claimed to be damped oscillatory in nature (this fits in with the possible ESE circuit diagram shown in figure 1.2.5).

Rather than having the finial energised with a oscillatory voltage pulse an impulse voltage was used instead. The magnitude of the applied impulse could then be easily varied. It is also known that ESE devices energise the finial when the electric field at the tip of the finial reaches a certain value. Thus it can be said that the ESE device energises the finial a certain time after the onset of a downward leader. To simulate this feature of an ESE device the impulse applied to the finial should be delayed for a certain time after the application of the main impulse to simulate the down-coming leader. The time to finial energization should be within the rise time of the main lightning simulation impulse, i.e. 250 $\mu$ s.

If the time delay between the application of the 250/2500 $\mu$ s wave and the finial impulse is to be variable between 0 and 250 $\mu$ s, then the finial impulse itself must be short compared to the main impulse. A fast rise time in the order of 1 $\mu$ s is suitable, an obvious choice is the standard 1.2/50 $\mu$ s wave (a voltage wave with a 1.2 $\mu$ s front time and a 50 $\mu$ s tail time). Figure 2.2.1 summarises the operation of the artificial ESE device.

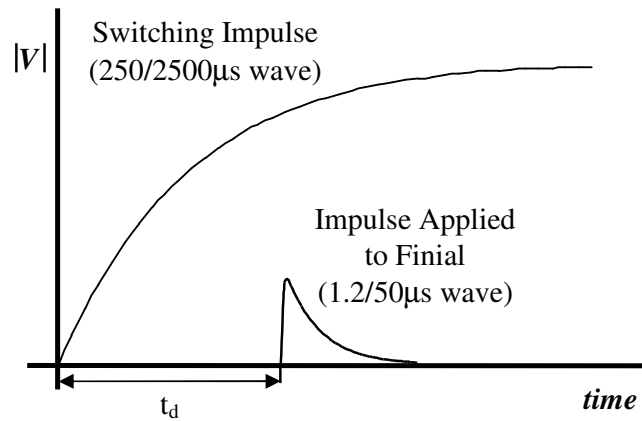


**Figure 2.2.1** : Chart showing proposed operation of the artificial ESE device.

The development of the apparatus required to generate the delayed impulse applied to the finial is described in the next chapter.

### Experiments

To understand what area the experiments should focus on it is first necessary to have some knowledge of the detailed processes involved in the development of a leader from a lightning finial.

In these experiments a negative voltage will be applied to the sphere, the finial is thus positive relative to the sphere and so a positive leader will develop from its tip.

The leader development process starts when free electrons in the air are accelerated by the intense electric field near sharp finial tip and collide with neutral gas atoms. If the field is strong enough, some of the collisions may be ionising. One ionising collision produces a positive ion and another free electron. The two electrons are again accelerated in the high electric field and go on to cause further ionising collisions thus generating more positive ions and free electrons. The positive ions will drift slowly away towards the negative electrode (the sphere). The ionising process continues rapidly setting up an avalanche. Groups of avalanches often link together to form branched channels, known as streamers, which generally travel in the direction of the applied field. Streamers have been shown to propagate at velocities in excess of  $10^5 \text{ms}^{-1}$ .

The transition from streamer to leader is by a process of ohmic heating within resistive streamer channel. The rise in temperature results in an increase in ionisation and a hot arc-like channel, termed the leader develops. The leader itself is much slower than the preceding streamers and has been shown to propagate with velocities in the order of  $10^4\text{ms}^{-1}$ .

Since the formation of the leader is dependant on the streamers that precede it, an experiment which looks at streamer discharge would be useful for examining lightning finials.

One method to detect discharge from the finial is to measure the flow of current through the finial, from ground to the corona discharge. This could be achieved using a resistor placed in series with the finial, flow of current through the finial would generate a voltage across the resistor which could be measured using an oscilloscope. The problem here being that the measuring equipment would not be electrically isolated from high voltage in the event of breakdown.

Another method, and the one used in this project, is to detect the light given out from the corona discharge. Corona is the general term for luminous discharges such as leaders and steamers. Light produced in the visible range is minimal, however corona are rich in ultra violet that can easily be detected with a photo-multiplier.

A photo-multiplier is a device which converts the light into a voltage which can be viewed on an oscilloscope. The beauty of this method is that it involves no electrical connection to the test arrangement.

## 2.3 Laboratory set up

The general experimental set up used is shown below:

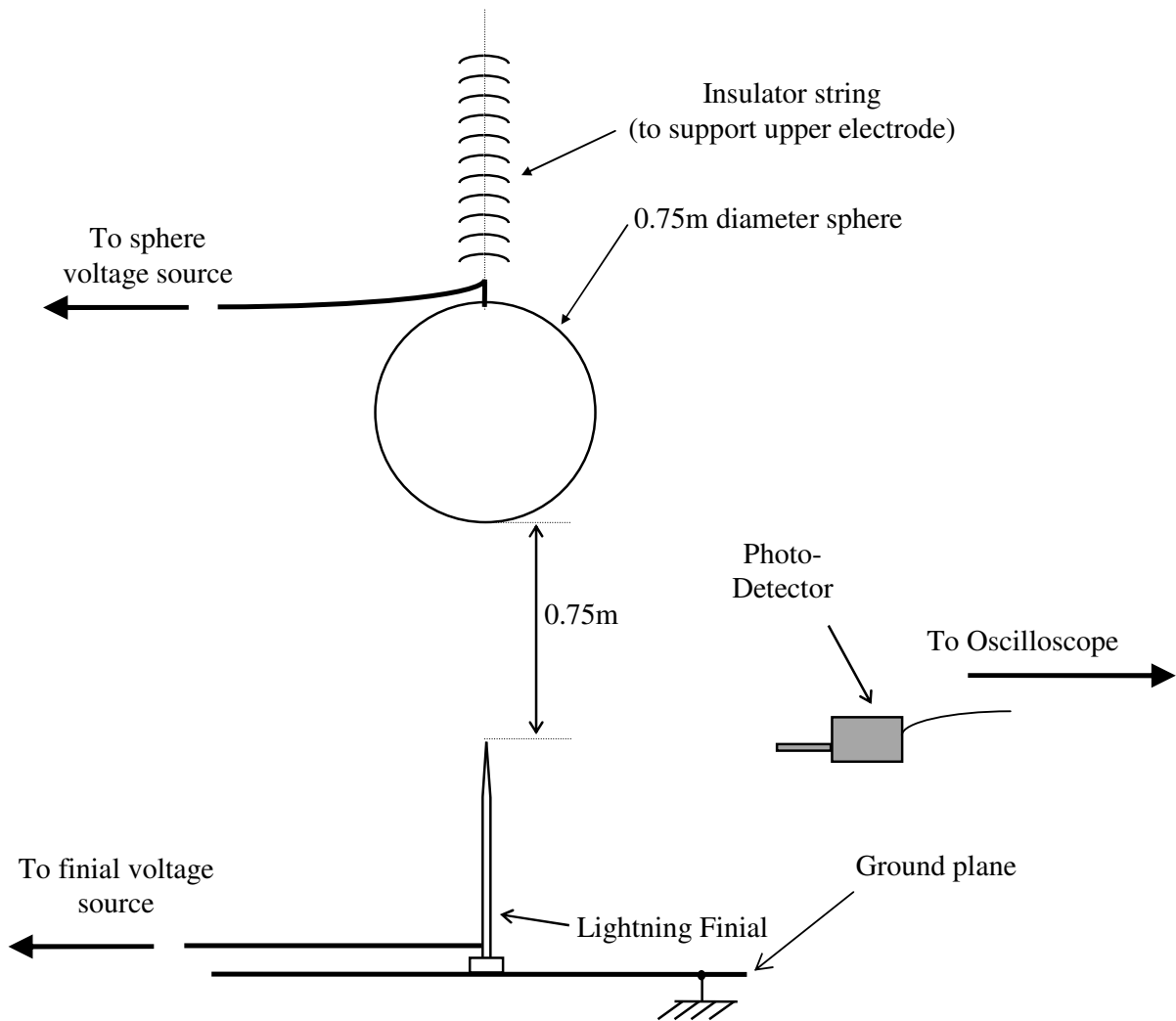


**Figure 2.3.1:** The Experimental set up.

The following is a description of the apparatus used in the experiments:

**Lightning Finial:** The dimensions of the lightning finial used for all the experiments is shown in figure 2.3.2. The rod was constructed from hollow copper tubing and mounted on an insulating base of synthetic resin bonded paper.

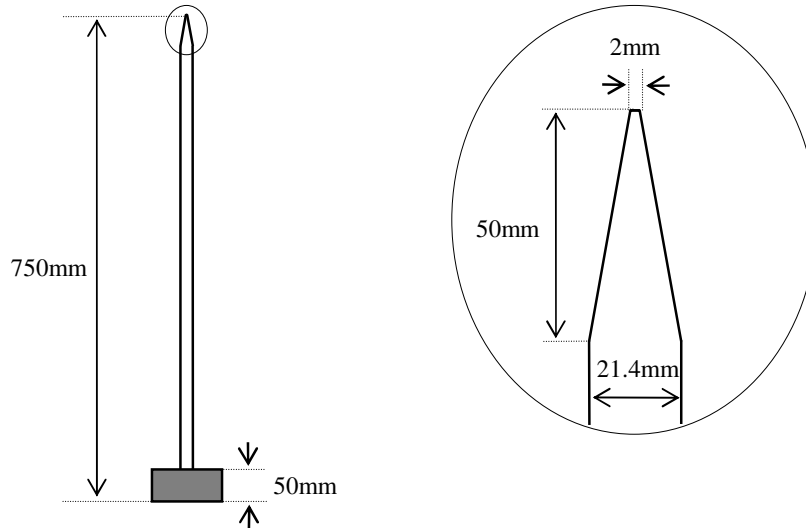


**Figure 2.3.2 :** The lightning finial used in the experiments.

**Ground Plane:** To create a good earth plane for finial to stand on, a steel sheet (1m × 2m) was placed on the laboratory floor and strongly bonded to an earth point.

**Photo-multiplier:** A sensitive device which can measure low levels of light and give an analogue output voltage that is proportional to the intensity of the light. The device used was particularly sensitive to light in the UV part of the spectrum. It works on the principle of photo-emission of primary electrons, these primary electrons are accelerated and multiplied using a strong electric field generated by a series of electrodes. The primary electrons are amplified by a factor of about  $10^9$ .

The photo-multiplier used has a very narrow aperture so its vertical field of view is very narrow. Hence it is capable of looking at a very small region (1cm) from a distance of about 2m, e.g. the area just above the tip of the finial. This will allow corona discharges from the finial tip to be observed from a “safe” distance.

Power supply for the multiplier is from a 12V battery with a DC-DC converter to increase the voltage to 200V DC. Using the photo-multiplier the corona from the tip can be measured indirectly, thus achieving electrical isolation from the test circuit.

**Storage oscilloscope:** To record the transient signal from the photo-multiplier an analogue storage oscilloscope was used.

**DC generator:** In some of the experiments a DC source was required. A portable Brandenburg generator was used for this purpose. It was capable of generating up to 50kV DC of either polarity.

## 2.4 The Main Generator

The impulse generator used for the main impulse to simulate the down-coming leader was a Ferranti 10 stage generator based on the Marx principle. It is capable of generating up to 2MV. Only six stages were used in this investigation, the other stages were shorted together. The generator was configured to produce the standard switching impulse (250/2500 $\mu$ s) wave.

### Circuit diagram

The impulse generator circuit diagram for the 250/2500 $\mu$ s wave is shown in figure 2.4.1. The generator has a stage capacitance of 0.14 $\mu$ F and 6 internal 38k $\Omega$  wave tail resistors. The wave front capacitance is provided by the capacitive voltage divider used to measure the impulse voltage wave shape. The capacitive voltage divider has calculated ratio of 5500:1.

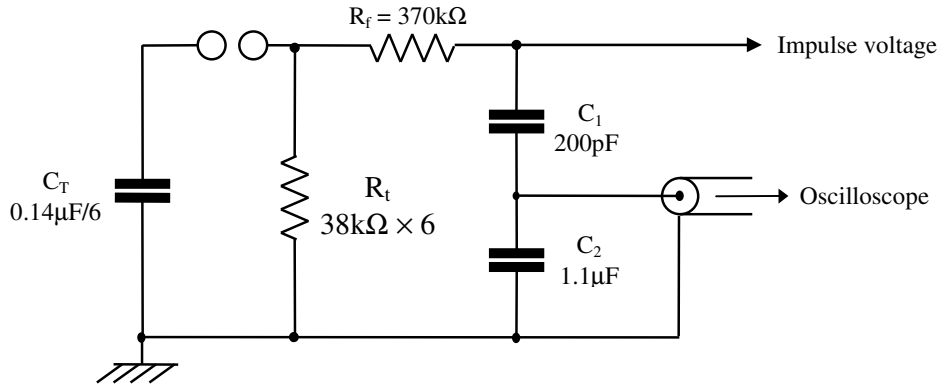


**Figure 2.4.1** : Main impulse generator equivalent circuit diagram.

### Wave shape

To allow meaningful discussion of the results the exact wave shape generated needed to be known. Figure 2.4.2 shows the output of the capacitive voltage divider for a  $-375\text{kVp}$  impulse applied to the sphere.

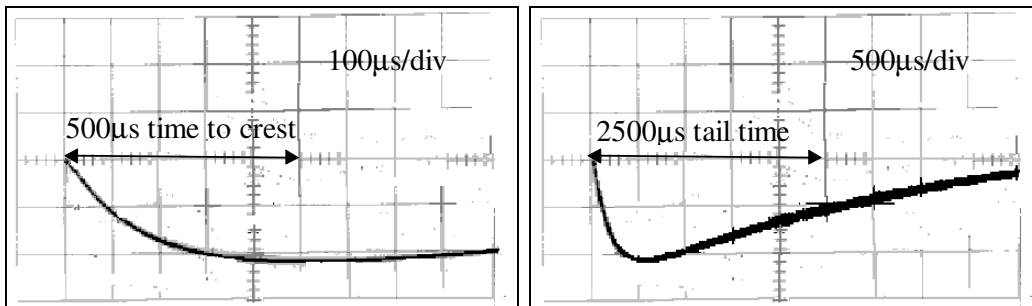


**Figure 2.4.2a:** Front time of main generator. **Figure 2.4.2b:** Tail time of main generator.

The impulse wave has a slightly longer front time than the standard 250/2500  $\mu\text{s}$  wave, however this front time is ideal for the purposes of this investigation.

## Voltage Calibration

A calibration factor was required to allow the peak impulse voltage applied to be calculated from the stage charging voltage. The stage charging voltage is measured directly and can be read from a meter on the control panel of the main impulse generator.

The measurement of the peak impulse voltage was carried out using standard sphere gaps. Tables of the breakdown voltages for spheres of certain sizes and separations are well established. The tables give the peak impulse voltage that give a 50% probability of breakdown. With a certain sphere gap setting, the stage voltage reading that caused the spheres to spark over was found using the “up down method”.

In the “up down method” the impulse voltage is set to just to a value just below the expected breakdown voltage of the sphere gap. The applied impulse voltage is then increased in small steps (in this case the stage voltage was increased in 1kV steps), until the sphere gap breaks down. The impulse voltage is then decreased by one step. The following process is then repeated; if the gap does not breakdown then the voltage is **increased** by one step, if the gap does breakdown then the voltage is **decreased** by one step. This process of increasing and decreasing the voltage is continued until at least 20 impulses have been applied after the first breakdown. The average of the meter readings is the stage voltage reading at which the gap breaks down.

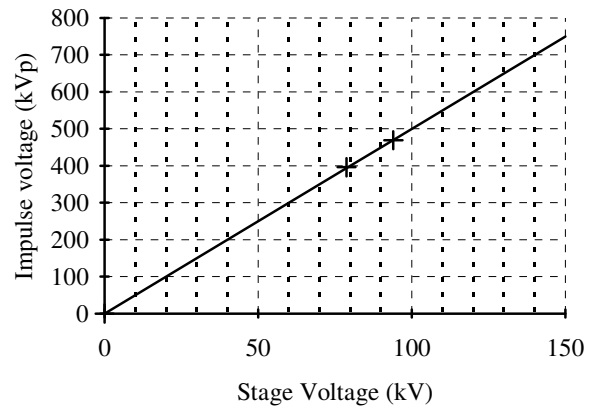
The breakdown voltage of the sphere gap used is then found from a standard table. The table gives the breakdown voltage for standard conditions, so a correction factor is calculated to find the gap breakdown voltage for the conditions in the laboratory.

Two calibration measurements were taken, a copy of the up down results table is shown in the appendix. The results of the voltage calibration are shown on the next page.

**Voltage Calibration Summary:**

Stage Meter (kV)	Impulse (kVp)
0	0
78.8	395.9
94.1	468.9

∴ Average Generator Efficiency = 83.3%



Thus: Peak Impulse voltage (kVp) =  $6 \times 0.833 \times$  Stage voltage = **4.998 × Stage voltage**

## **3. The Artificial ESE device**

### **3.1 Introduction**

In this chapter the design, construction and testing of the equipment required to generate the delayed impulse voltage is described. This part of the apparatus proved to be much harder to set up than had been previously imagined and it took up a large amount of the total project time. A systems approach was adopted for the design and development process. The modifications involved with each component of the system as it was developed and problems arisen are detailed.

### **3.2 System requirements**

The purpose of this part of the apparatus is to generate an impulse voltage wave to be applied to the lighting finial. The impulse should be applied a specified time after the application of the main impulse voltage applied to the gap.

Since the main impulse voltage will be a 250/2500 $\mu$ s wave the time delay required will have to be *variable* over the range of 0-250 $\mu$ s. This will allow the onset of the impulse applied to the finial to be moved within the rise-time of the main impulse voltage.

The wave shape applied to the finial should approximate a 1.2/50 $\mu$ s wave, (this impulse wave shape is short enough to be moved within the 250 $\mu$ s rise time). The exact shape of the finial impulse is not critical because there are no standards for this type of test, and the wave shape of the voltage generated on commercial ESE devices is not accurately known.

The finial impulse generator should be capable of applying impulses of differing magnitude to the rod.

When the main impulse generator fires the electric field in the vicinity of the generator will rise very quickly. The large electromagnetic pulse generated may interfere

with other apparatus, thus the system should not be susceptible to interference that may cause misfiring of the final impulse generator.

### 3.3 System design overview

The triggering signal for the delayed impulse will be derived from the pulse feed unit (the circuit that provides the high voltage pulse required to breakdown the triggered gap on the main impulse generator in the UMIST High Voltage Laboratory). This signal will then be sent to a delay unit and then on to another smaller impulse generator that will apply the voltage to the final.

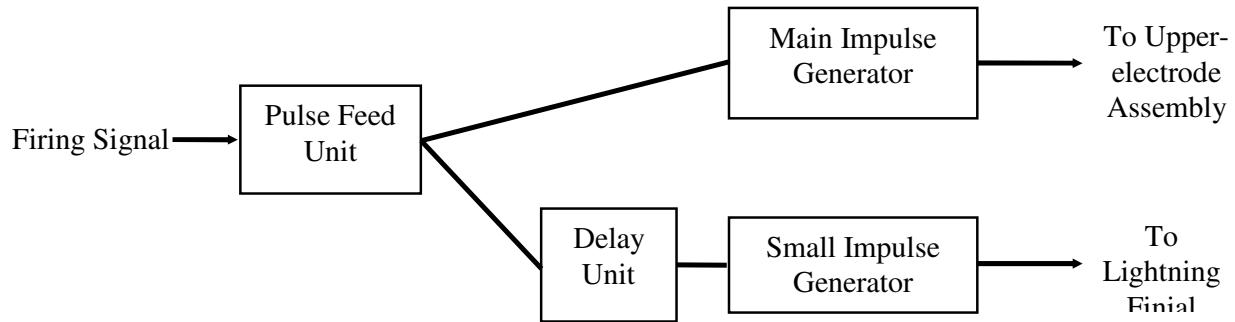


**Figure 3.3.1:** System design overview for delayed impulse apparatus.

To prevent misfiring of the *Small Impulse Generator* (SIG) the connection between the delay unit and the SIG must not be susceptible to interference. An obvious choice for this connection is an optical link.

The high voltage step-wave from the pulse feed unit will need to be stepped down to a voltage low enough to be controlled by the delay unit. A capacitive voltage divider was used for this purpose.

The capacitor divider used was first tested to find its divider ratio. The measured divider capacitance's were 91.5nF and 179.4pF this gives a divider ratio of 511 to 1. To check this value a 6V sinusoidal signal was put across the divider, this gave an output of 7.5mV thus giving a ratio of 800 to 1. The output of the pulse feed unit was known to be

about 15KV a divider ratio of around 600 to 1 would provide a triggering signal of around 25V. When tested with the pulse feed unit the output of the divider circuit was actually exactly 25V. This voltage is low enough to put through a simple resistive voltage divider to fine tune the signal down to a level that the delay unit can operate at.

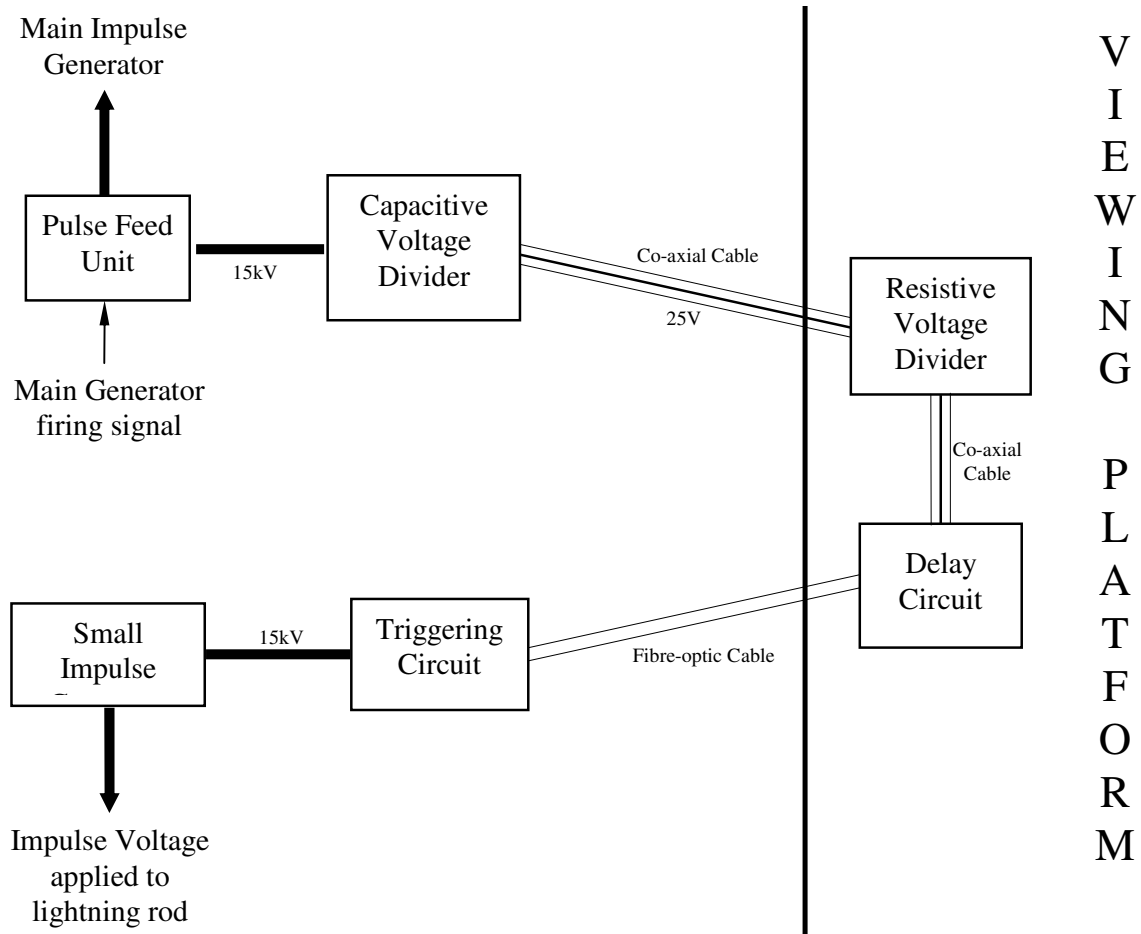


**Figure 3.3.2:** Schematic diagram of proposed delayed impulse apparatus.

### 3.4 Delay Unit

#### Requirements:

- The incoming triggering signal should be delayed for a length of time then transmitted in the form of an optical pulse.
- The delay should be variable over the range of 0-250 $\mu$ s.
- Once set the delay should be stable and provide an accurately repeatable delay time.

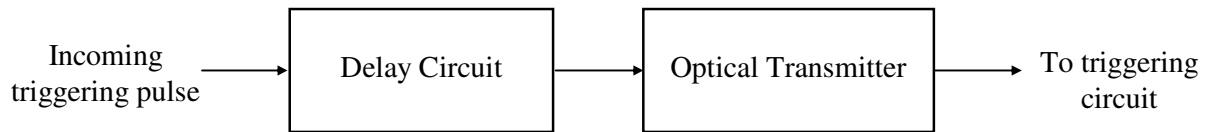


**Figure 3.4.1:** Outline of initial design - solution to delay unit requirements.

#### Delay Circuit - design options

This forms the basis of the delay unit, the delay circuit must be an electronic circuit that is capable of providing a variable delay over 0-250 $\mu$ s. The two options considered were:

- *Operational Amplifier*- Configured to integrate the incoming triggering pulse, hence producing a rising signal. When this signal reaches a threshold level the output triggers and sends the delayed triggering signal. The rise time of the signal can be varied by changing the value of the circuits RC time constant, thus allowing variable delays to be produced.
- *Monostable Circuit*- A monostable latch is a circuit that when triggered, its output will turn on and then turn off after a certain time period defined by the value of an RC time constant. Using two monostable connected in series a delayed pulse of arbitrary width could be produced. The first monostable would provide the delay time and the second the output pulse width.

### Monostable delay circuit design

The monostable delay circuit was chosen, because it was capable of producing a reliable and variable, delay and output pulse width. Monostable latches are also cheap and readily available in IC packages.

The output high time for a monostable latch is set by an external RC connection. The delay time is given approximately by:  $t_w \approx RC$

The type of package chosen for this project was a type LS221 chip. The chip contains two monostables and is available from various manufacturers. This IC is not powerful enough to drive the optical transmitter circuit, so an output buffer is also required. The output buffer used was an LS7404 Hex inverter, this chip is also available from several manufacturers and contains 6 inverting buffers (only one of which was needed). The two monostable latches and the inverting buffer were connected as shown in figure 3.4.2.

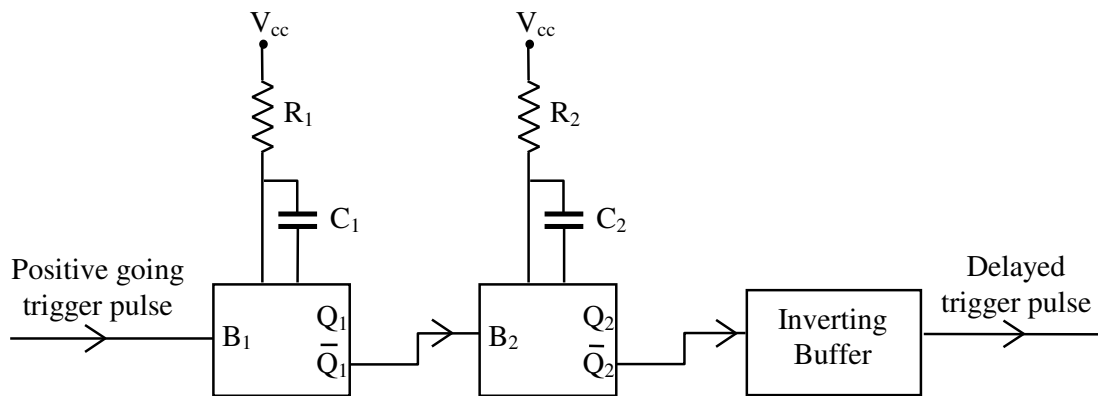


**Figure 3.4.2:** Using two monostable latches to produce a delayed pulse

The supply voltage for the IC's was +5V. When a positive going 5V pulse arrives at the input of the first monostable (B<sub>1</sub>), its inverting output drops to 0V, then  $R_1C_1$  seconds later returns to 5V, this generates the positive going 5V pulse required to trigger the second monostable. The inverting output of the second monostable then drops to 0V for a time  $R_2C_2$  then back to 5V. Thus the output of the inverting buffer generates a positive pulse as shown in figure 3.4.3. The two monostable RC times are  $t_{w1}$

and  $t_{w2}$ . Hence, the delay time is given by  $R_1C_1$ , and the output pulse width is given by  $R_2C_2$ .

The pulse width  $t_{w2}$  is not critical it just has to be long enough to trigger the optical transmitter. Arbitrary values of  $R_2 = 1k\Omega$  and  $C_2 = 1\mu F$  were chosen to give a pulse width in the region of 1ms.

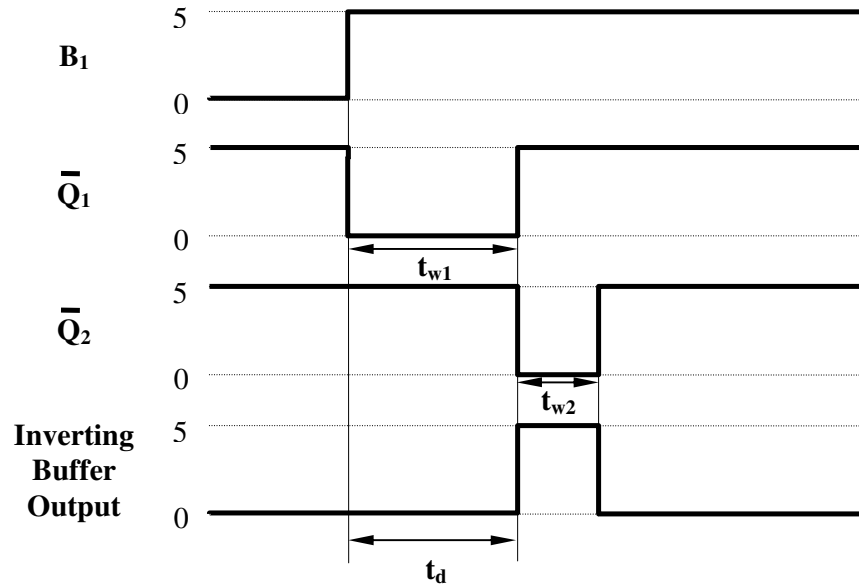


**Figure3.4.3:** Timing diagram for delay circuit.

Since a variable delay was required the product  $R_1C_1$  must be controllable, this can be achieved by varying  $R_1$ ,  $C_1$  or both of them. A delay from 0 to 250 $\mu s$  is required so an obvious initial choice was to have  $C_1$  fixed at 1 $\mu F$  and have  $R_1$  as a 250 $\Omega$  variable resistor.

### Resistive Voltage Divider

To step down the 25V triggering pulse from the capacitive voltage divider attached to the pulse feed unit a simple resistive voltage divider was used. A triggering signal of 5V was required, so a divider ratio of 1:5 was required. To achieve this a divider made up of a 1k $\Omega$  resistance and a 250 $\Omega$  resistance was used.

### Optical Transmitter Design

The purpose of the optical transmitter is to convert the electrical pulse from the output of the buffer to an optical pulse to be transmitted down an optical fibre to the impulse generator firing circuit.

The design of the optical transmitter was based on an available optical emitter. An optical emitter is basically an LED and can be treated exactly as one when it comes to circuit design. The available opto-emitter was a universal SMA emitter from FEC (order code 179-128).

A simple transistor switch was used to drive the emitter as shown in figure 3.4.4. The only design parameter was the emitter maximum forward current rating of 50mA. If a 5V supply was used this current could be limited by placing a resistor in series with the emitter. Using  $R = V/I$  gives  $R = 5/50 \times 10^{-3} = 100\Omega$ , since the turn-on resistance of the transistor is not known a variable resistor was used to fine tune the current to the emitter.

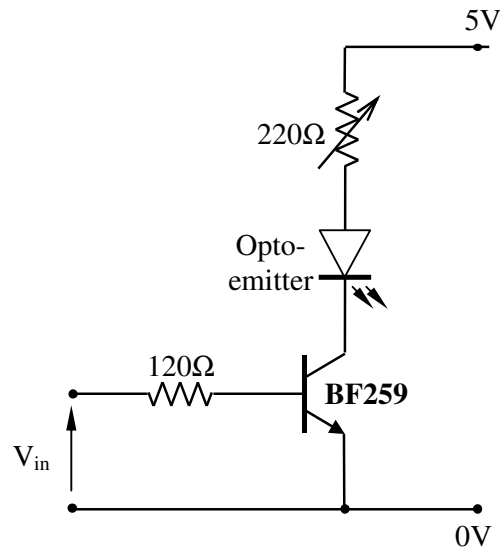


**Figure 3.4.4:** Optical transmitter circuit diagram.

### Delay Unit Construction

The LS221 chip comes with logic gates on the inputs of the two monostable latches and clear latch connections, as is shown in the chip pin-out in figure 3.4.5. These features of the chip are not required for the purpose of the delay circuit so they need to be by-passed.

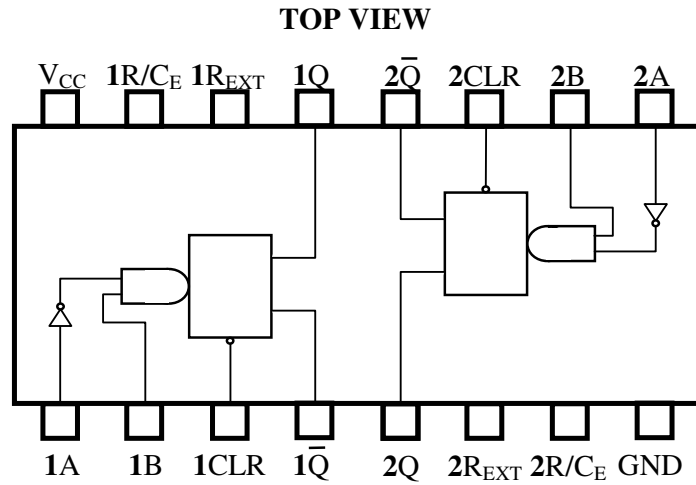


**Figure 3.4.5:** LS221 pin-out.

The  $R/C_{EXT}$  and  $R_{EXT}$  connections are where the resistor and capacitor that define the length of the delay are connected. The truth table for each monostable is shown in figure 3.4.6. By holding clear high, and input A low, the input B will become the input to the monostable. (This corresponds to the second from last line of the truth table)

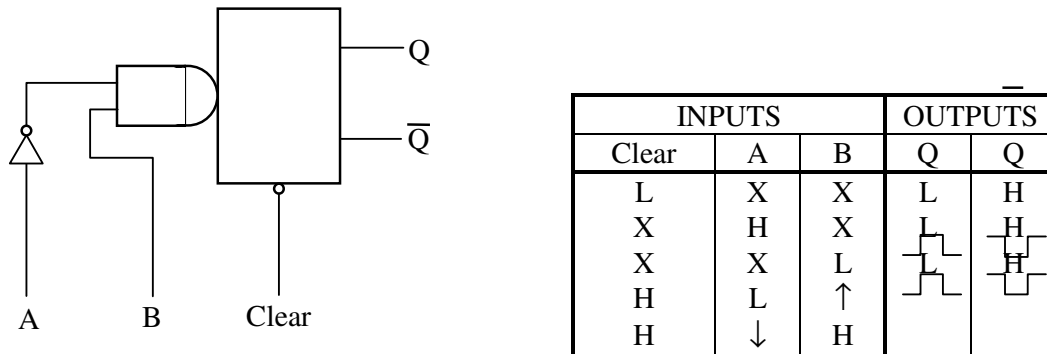


**Figure 3.4.6:** Truth table for monostable latch.

If pin 1B is made the input then pin  $\bar{1Q}$  should be connected to pin 2B, this makes pin  $\bar{2Q}$  is the output of the delay. This pin is connected to one of the six inverting buffers in the LS7404. The output of this buffer will drive the optical transmitter.

The delay circuit was constructed on prototyping board, using the RC values specified in the design section. Using a function generator a 5V square wave was applied to the input of the circuit, the input and output of the circuit were then observed on an oscilloscope as shown in figure 3.4.7. The output pulse width  $t_{w2}$  was found to be 0.6ms, this time was set by  $R = 1k\Omega$ , and  $C = 1\mu F$ , (giving  $RC = 1ms$ ). Thus the equation for output pulse width,  $t_w = RC$  is only an approximate relationship.

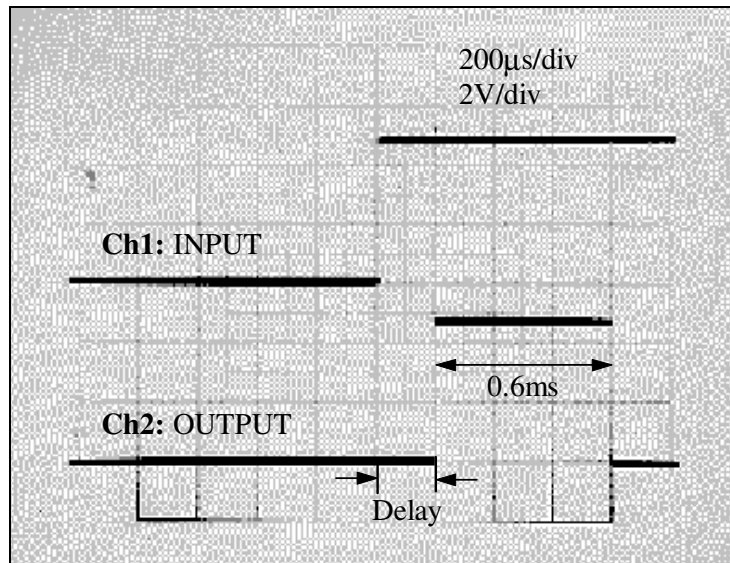


**Figure 3.4.7:** Delay circuit input and output waveforms.

The variable delay was set using a  $1\mu F$  capacitor and a  $250\Omega$  variable resistor. However the delay became unstable for resistances less than  $200\Omega$ , to prevent delay instability a fixed resistance of  $250\Omega$  was placed in series with the variable resistance. This gave delays variable from  $120\mu s$  to  $280\mu s$ . In order to achieve delays less than  $120\mu s$  the capacitance would have to be reduced. Using a smaller value of capacitance would produce shorter delays variable over a smaller range. Thus the delay would be set

with a variable resistor and a range switch, that would switch the between two capacitors. After a process of trial and error the following values for R and C were chosen:

$$R = 250\Omega \rightarrow 1250\Omega \quad C_{\text{short}} = 47\text{nF} \quad C_{\text{long}} = 0.32\mu\text{F}$$

This gave the following range of time delays:

$$\text{Short} = 25\mu\text{s} \rightarrow 64\mu\text{s} \quad \text{Long} = 60\mu\text{s} \rightarrow 280\mu\text{s}$$

The working delay circuit and the designed optical transmitter circuit were then combined and constructed on strip-board. The delay unit circuit diagram is shown in figure 3.4.8. Power for the circuit was provided from an external 5V power supply.

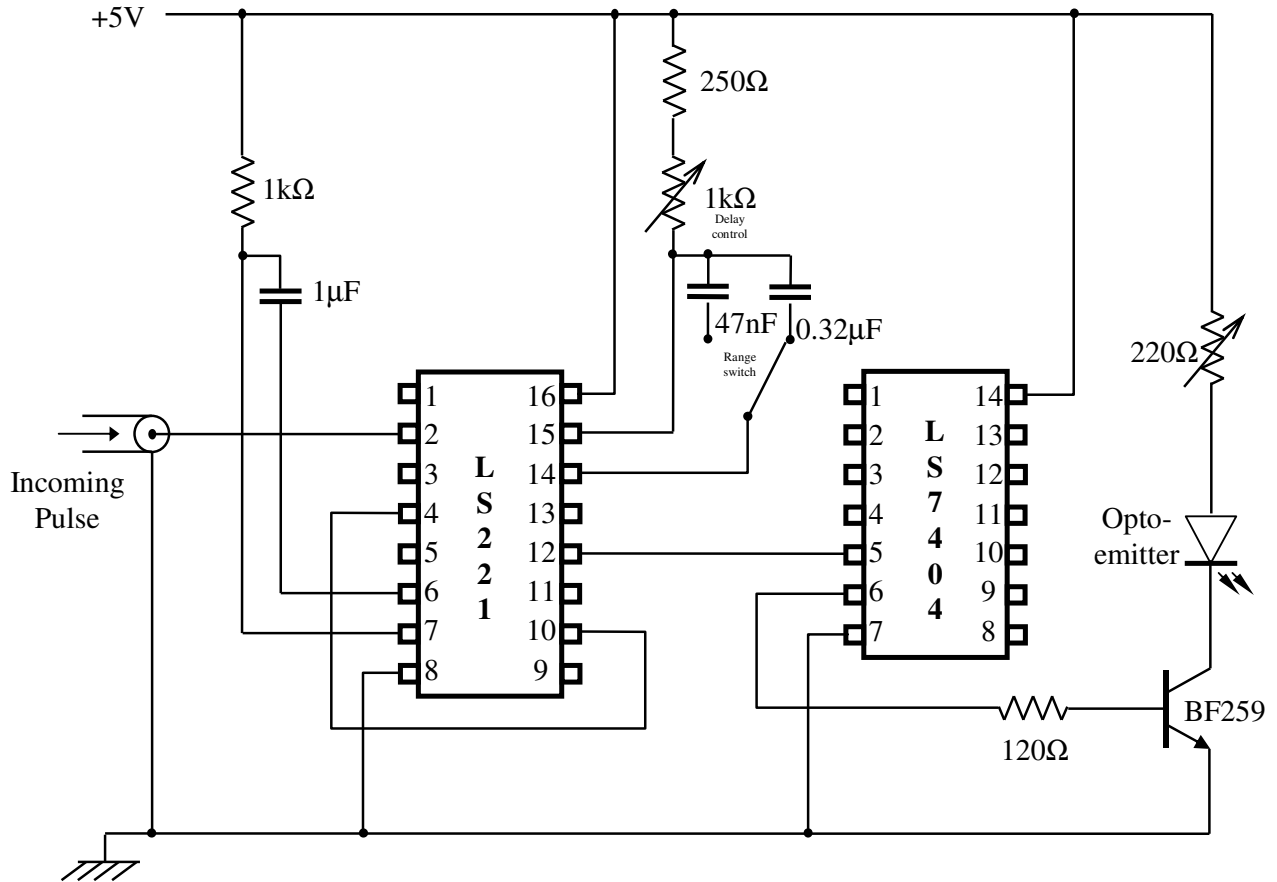


**Figure 3.4.8:** Delay unit circuit diagram.

### Delay Unit Modifications

The delay unit is one component in the delayed impulse apparatus. When the unit was integrated into the rest of the system a number of modifications were required to get the system working as a whole.

### **Optical Emitter- Output Power:**

The launch power of the optical emitter was not great enough to reliably trigger the optical detector in the electronic firing circuit of the impulse generator (*see section on Impulse Generator Firing*).

This problem was overcome by replacing the opto-emitter with a high power opto-emitter. The emitter used was a High Power SMA Emitter (PCB mount) available from FEC (stock no. 179-144). This higher power emitter not only has a greater launch power but also emits in the near infra-red, which the opto-detector in the receiver is also more sensitive to. The high power emitter has a higher current rating (100mA as opposed to 50mA), this meant that the setting of the 220 $\Omega$  variable resistor in the transmitter circuit had to be reduced.

### **Input Spike Protection:**

When the circuit was connected to the pulse feed unit (via the capacitive and resistive divider circuit) after several shots the delay unit stopped working. On investigation it was found that the monostable latch chip (LS221) had been destroyed.

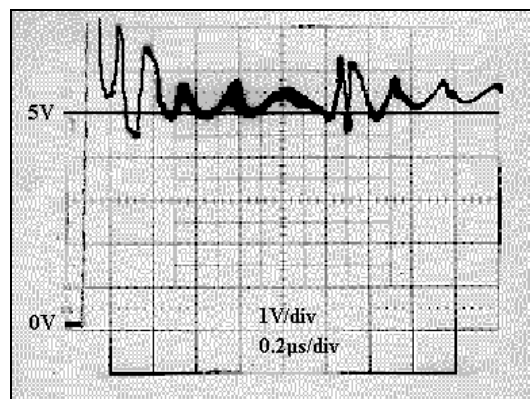


**Figure 3.4.9:** Delay unit input triggering wave form.

The reason for this was that the 5V triggering pulse from the divider had a large oscillation superimposed on it, see figure 3.4.9, and it was probably this spike that was to blame for the destruction of the chip.

The solution to this problem was to limit the voltage that could reach the delay circuit. A simple method of doing this is shown in figure 3.4.10.

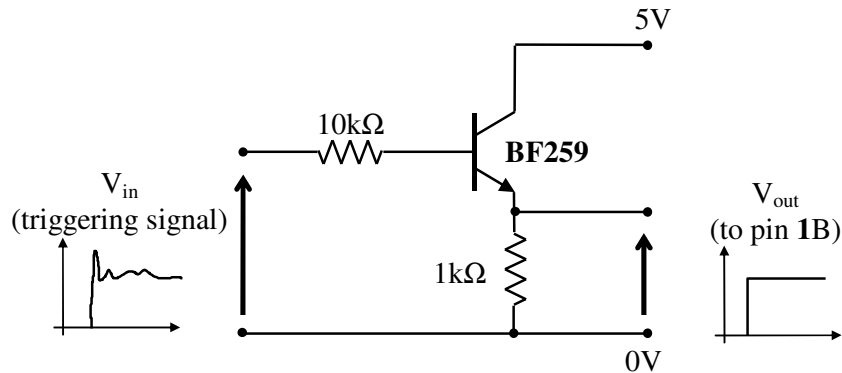


**Figure 3.4.10** Delay circuit, input spike protection.

When  $V_{in} = 0V$  the transistor is off, thus  $V_E = V_{out} = 0V$ . When  $V_{in} = 5V$  the transistor becomes conducting and  $V_{out} = 5V$ . The BF259 transistor is capable of withstanding any spikes on the triggering signal and because the supply voltage is 5V it is impossible for  $V_E$  to rise above 5V, thus the input to the delay circuit is protected.

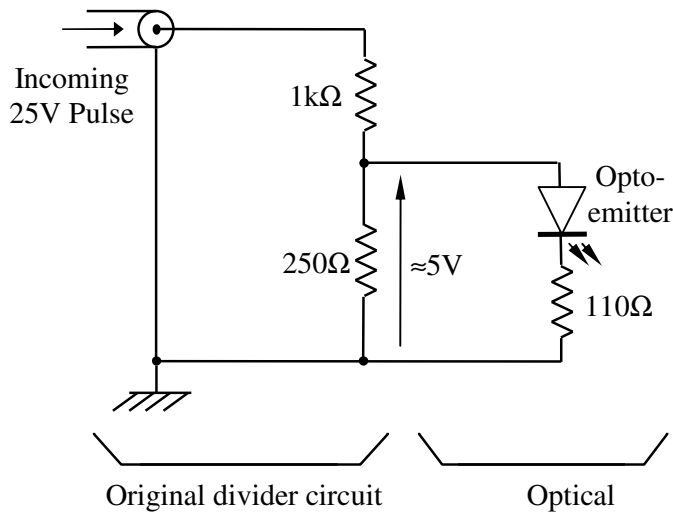
This circuit was added to the delay unit and no further problems were caused by the shape of the triggering signal.

### **Isolation from ground:**

In the development stage of the apparatus the triggering signal from the pulse feed unit was used on its own, i.e. without any stage voltage on the main impulse generator. When it came to putting volts on the main generator, the small generator invariably fired instantaneously no matter what the delay setting. Initially the problem was thought to be the small impulse generator firing circuit picking up the high voltage electromagnetic pulse caused when the main generator fired. However the small generator did not fire when power for the delay unit was removed, thus the problem was not with the firing circuit but with the delay unit itself.

When the main impulse generator fires the earth potential may rise slightly, and because the pulse feed unit earth is bonded to the same point as the impulse generator earth the earth voltage of the capacitive voltage divider attached to it may rise slightly also. The earth of the capacitive voltage divider is connected via a length of co-axial cable to the delay unit. A sudden rise of just a couple of volts would be enough to trigger the optical transmitter in the delay unit, thus causing the delay circuit to be bypassed and the small impulse generator to fire instantaneously. The fact that sometimes the delay worked can be explained because the rise in earth potential may not always be great enough to trigger the optical transmitter.

To solve this problem the delay unit must be isolated from the impulse generator earth. The only way to really do this is by the addition of a second optical link between the capacitive voltage divider and the delay unit. The first part of the link, the optical transmitter at the capacitive voltage divider, was very simply constructed. Another high power emitter was purchased and connected to directly across the output of the resistive voltage divider as shown in figure 3.4.11.



*Diode current limiting resistor:*

$$I_{max} = 100mA$$

$$V = 5V$$

$$\therefore R_{min} = 50\Omega$$

*Choose 110Ω to be sure to protect diode even if spike on trigger wave is 10V.*

**Figure 3.4.11:** Optical transmitter attached to resistive divider output.

The second part of the optical link, the receiver was constructed on the same piece of strip-board as the delay circuit. The optical receiver would have to convert the light pulse into a 5V triggering pulse. The detector used was a Universal SMA detector available from FEC (order code 179-132). This detector is a PIN photo-diode, when reverse biased the reverse leakage current is dependant on the incident light intensity. A simple test was carried out and the reverse current through the diode when illuminated was  $10\mu\text{A}$  (note that this value is independent of applied voltage). When the diode was not illuminated a negligible current flowed. A current of  $10\mu\text{A}$  with a 5V supply would be equivalent to a  $500\text{k}\Omega$  resistor.

A Darlington pair made up of two BF259 transistors was used to amplify the small current signal. A  $470\text{k}\Omega$  resistor and the opto-detector were used to bias the base of the Darlington pair with a 5V power supply. A  $1\text{k}\Omega$  resistor attached to the emitter of the Darlington pair made the transistors act like a switch: the voltage at the emitter was 5V when the diode was illuminated and 0V when not.

This optical receiver circuit was added to the delay unit circuit as is shown in figure 3.4.12. Note that the input spike protection transistor is no longer required and the output of the optical receiver circuit is connected directly to the input of the monostable delay circuit.

#### **Electrical Interference pick up:**

The modified system worked perfectly well, triggering from the pulse feed unit without any volts on the main generator. However when the delay was tried with volts on the main generator, the delay once more became temperamental, firing instantaneously most of the time.

The cause of the problem this time was found to be with the external leads connecting the delay to its power supply. They were acting like aerials, picking up a voltage from the large electromagnetic pulse created when the main impulse generator fired. The sudden increase in supply voltage caused the biasing in the optical transmitter to change thus causing it to send a firing pulse without the delay. This problem was solved by removing the external power supply and powering the delay unit from an internal 5V regulator attached to a 9V battery. The voltage regulator used was a

LM7805CT from RS. This regulator comes in a three pin package ( $V_{\text{supply}}$ , common and  $V_{\text{out}} = 5\text{V}$ ) and as a 1A output, offering internal overload, thermal and short circuit protection. Its supply voltage can range 7 to 35V.

The delay unit and power supply were then housed in one box, with the input and the output for the optical fibres as the only external connections to the delay unit. The delay unit was now completely self contained and was basically now an *optical delay*. The circuit was now completely electrically isolated, and under testing worked perfectly well. The completed delay unit circuit diagram is shown below.

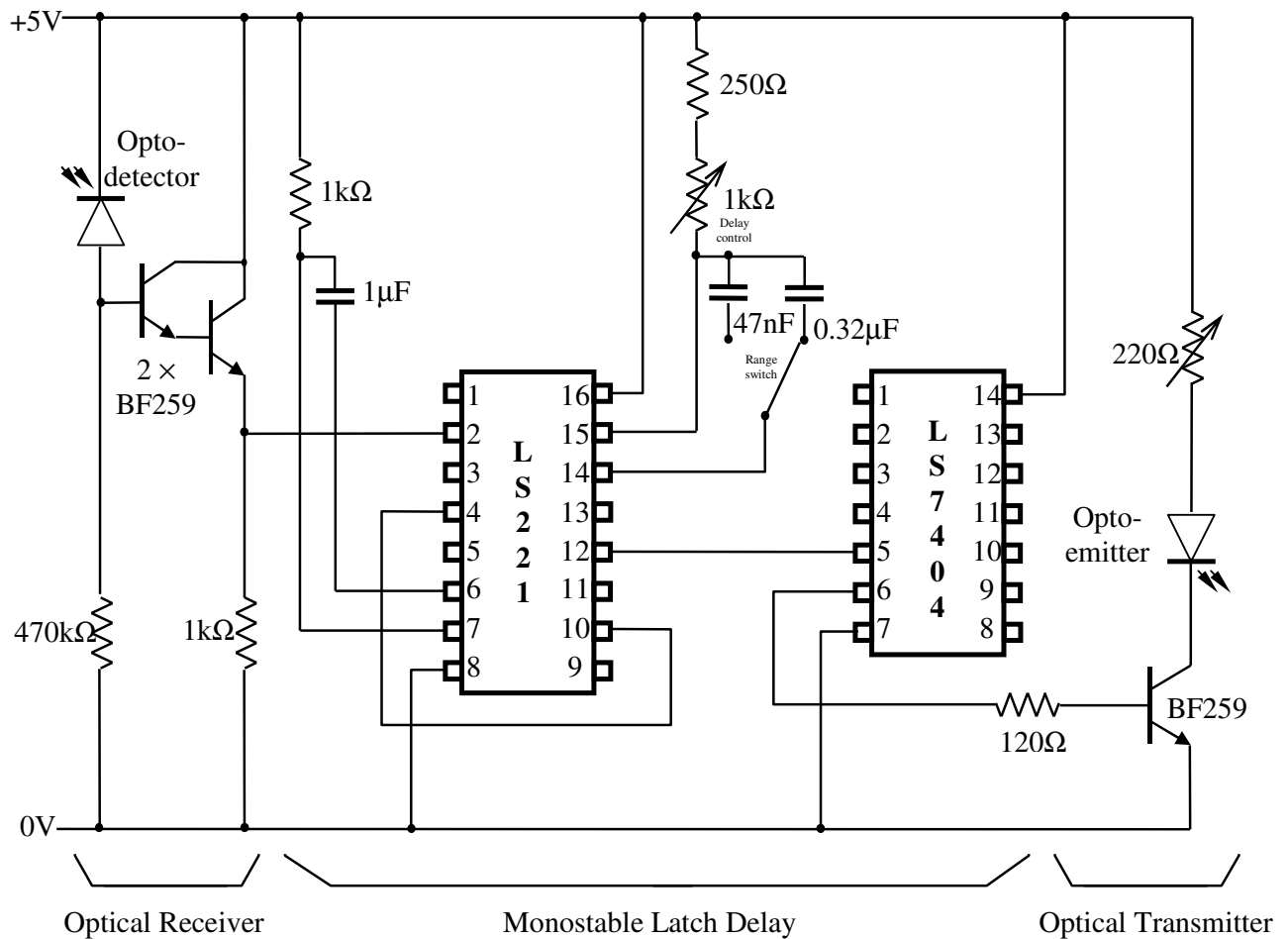


**Figure 3.4.12:** Final delay unit circuit diagram.

**Figure 3.4.13 :** The completed delay unit.

## 3.5 The Small Impulse Generator

### Introduction

An impulse generator provides a convenient method of applying a transient voltage to the lightning finial. The basic method of operation of an impulse generator is as follows: A certain number ( $n$ ) of capacitors are charged in *parallel* to a specific voltage ( $V$ ), then using spark gaps the capacitors are discharged in *series* to produce an impulse voltage of magnitude approximately equal to  $n \times V$ . The wave shape of the impulse voltage is controlled by a simple network of resistors and capacitors.

### Wave Shape

As mentioned previously, this smaller impulse has to be applied to the finial whilst the voltage simulating the down-coming leader is still increasing. The main impulse voltage has a rise time of  $250\mu\text{s}$ ,  $\therefore$  the finial impulse must be short enough to be applied within this time. A fast fronted wave is therefore required, say with around a  $1\mu\text{s}$  rise time, an obvious choice is the standard lightning impulse wave; the  $1.2/50\mu\text{s}$  wave.

In order to be effective the impulse applied to the finial should cause the localised field around the tip of the rod to increase, this can be done by applying an impulse of opposite polarity to that of the surrounding field. Since the down-coming leader is being simulated by a negative impulse, then the finial impulse should be of positive polarity with respect to ground.

Having defined the type of impulse wave to be used the wave shaping components required to generate such a wave are required. To calculate these it is necessary to look at the simplified generator circuit diagram shown in figure 3.5.1.

The capacitor  $C_t$  represents the stage capacitors in the generator, this equivalent capacitor is charged to a voltage  $V_c$ . The other components  $R_T$ ,  $R_F$  and  $C_F$  can be varied to change the shape of the voltage wave, labelled  $V$ .

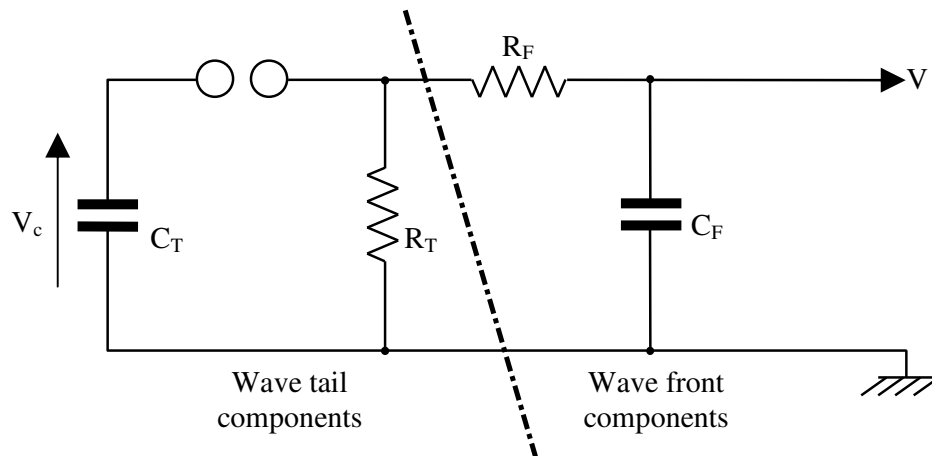


**Figure 3.5.1 :** Equivalent impulse generator diagram

What follows is a simple analysis of the above circuit to find how the output voltage wave shape depends on the wave shaping components.

An impulse wave can be considered to be a double exponential, i.e. a curve that is made up of two exponential curves ( $V_1$  and  $V_2$  in the diagram below) subtracted from each other.

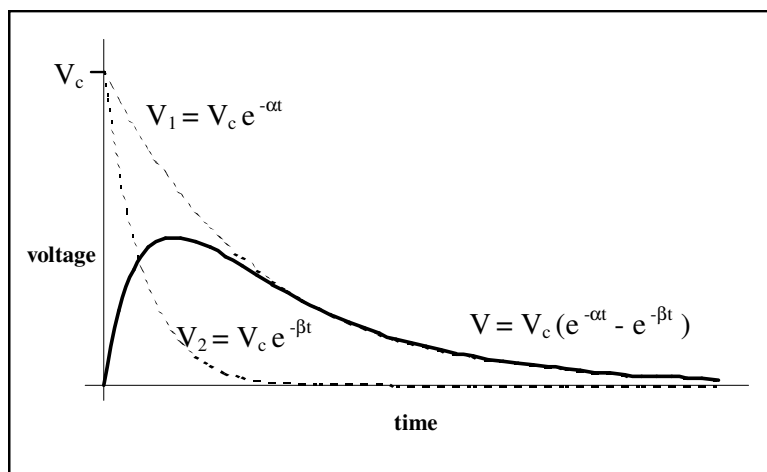


**Figure 3.5.2:** The impulse wave represented as a double exponential

The three points that can be used to specify an impulse wave are; peak impulse voltage, front time and tail time. The definitions of each of these terms can be found in the main impulse generator section in the chapter on apparatus. The peak impulse voltage is determined by  $V_c$  and the generators efficiency, the front time is defined by the values of  $R_F$  and  $C_F$ , and the tail time is defined by the values of  $R_T$  and  $C_T$ .

From figure 3.5.2 on the previous page it can be seen that after the peak impulse voltage has occurred the wave shape is mainly defined by  $V_1$ . Thus to find the tail time only  $V_1$  needs to be obtained. This can easily be done by neglecting the front components and reducing the generator circuit diagram to the one shown below in figure 3.5.3.

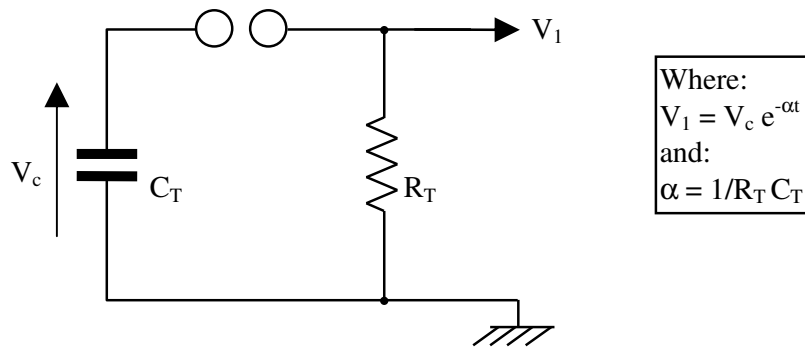


**Figure 3.5.3** : Simplified generator circuit diagram for tail time calculation.

The tail time of the wave is defined as the time for the voltage to decay to 50% of the peak voltage. The peak voltage can be obtained from the stage voltage thus:

$$\text{Peak voltage} = \text{Stage voltage} \times \text{Number of stages} \times \text{Generator efficiency}(\eta)$$

In this theoretical case the generator has only one stage, so the 50% value of the voltage is given by:  $V_c \eta / 2$ . So to find the tail time this voltage must be equated with the equation for  $V_1$  and rearranged thus:

$$\begin{aligned} V_c \eta / 2 &= V_c e^{-\alpha t} \\ \Rightarrow \ln(\eta/2) &= -\alpha t \\ \therefore t_{\text{TAIL}} &= -C_T R_T \ln(\eta/2) \end{aligned}$$

The wave front time can be found by assuming the wave tail resistor  $R_T$  can be neglected during the fast initial period. The equivalent circuit then becomes:

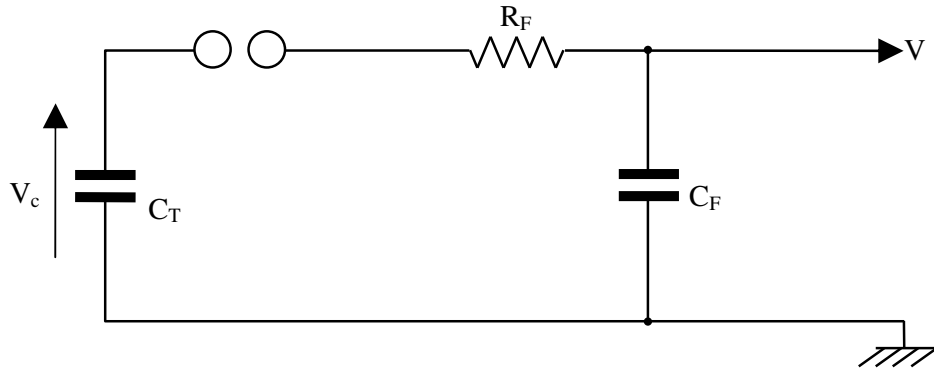


**Figure 3.5.4 :** Simplified generator circuit diagram for front time calculation.

If the capacitor  $C_F$  is initially uncharged, then the voltage  $V$  can be shown to be:

$$V = V_c \frac{C_T}{C_T + C_F} \left( 1 - e^{-\left( \frac{C_T + C_F}{C_T C_F R_F} \right) t} \right)$$

This shows that  $V$  rises to its asymptotic value of  $V_c \frac{C_T}{C_T + C_F}$  with a time constant

$\frac{C_T C_F R_F}{C_F + C_T}$ . After 3 time constants the voltage will have risen to within 5% of its final

value. If we say this period is equal to the wave front time then:

$$t_{\text{FRONT}} = \frac{3C_T C_F R_F}{C_F + C_T}$$

The two equations obtained for  $t_{\text{FRONT}}$  and  $t_{\text{TAIL}}$  will be used later in this section.

### Available Impulse generator

A small 8-stage impulse generator was already available, however some of the stage capacitors had broken down and those that remained were not of the correct voltage rating. The whole generator required rebuilding, this however allowed the generator to be redesigned and purpose built for this job.

Nominal Voltage Rating

The nominal output voltage of an impulse generator is the stage charging voltage  $V_s$  multiplied by the number of stages in the generator. The peak impulse voltage is obviously less than this because the generator's voltage efficiency is less than 100% due to resistance and inductance of the generator test circuit. The stage charging circuitry for the existing generator was still operational and was used for the new generator.

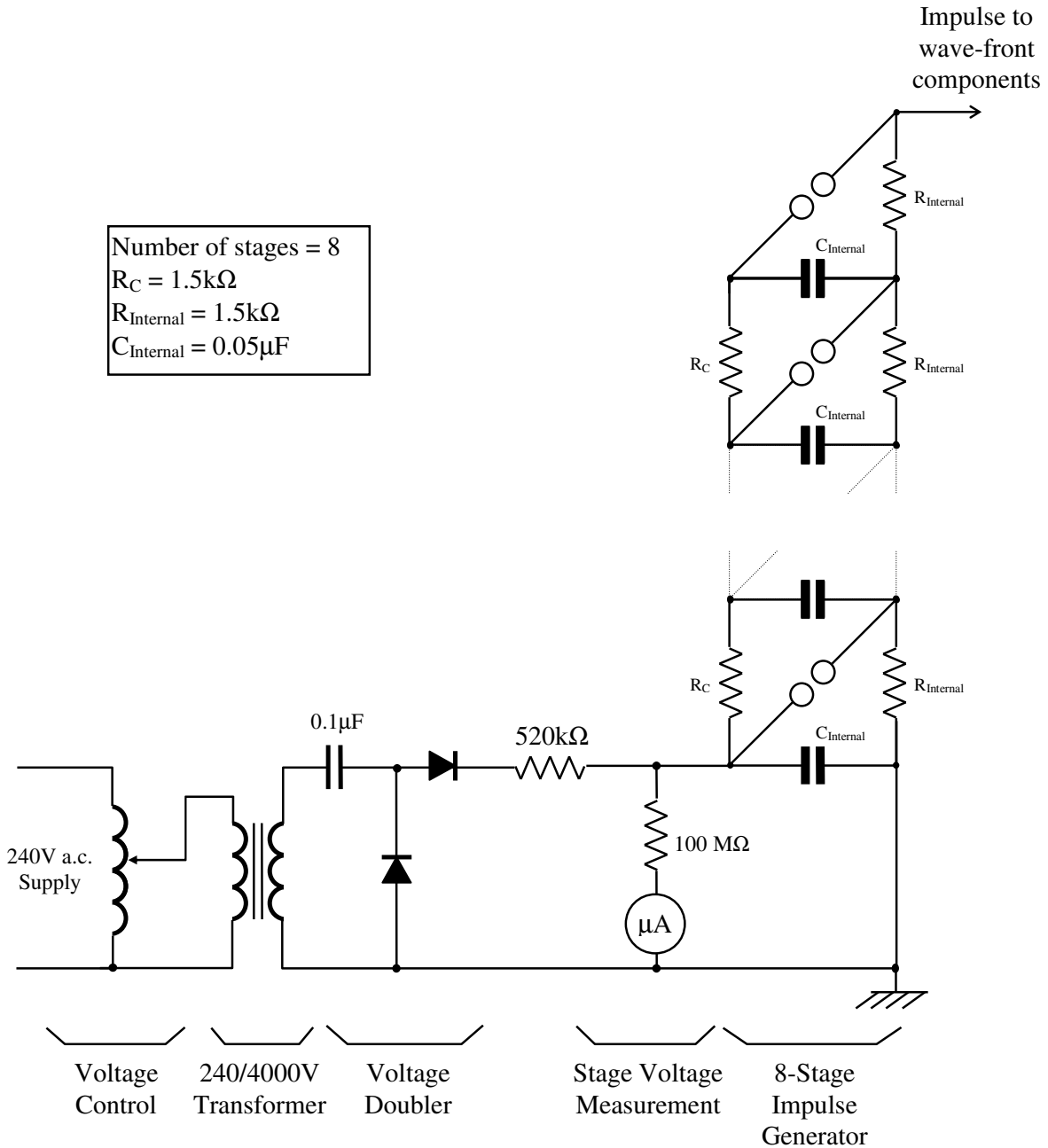


**Figure 3.5.5:** Impulse Generator circuit diagram.

The stage charging circuit consists of a voltage doubling circuit supplied from a 240/4000V transformer. The charging voltage is controlled using a variac. The internal capacitance makes up the other half of the voltage doubling circuit. The charging voltage wave shapes are shown in figure 3.5.6. The wave shapes were measured using a 1000× probe.

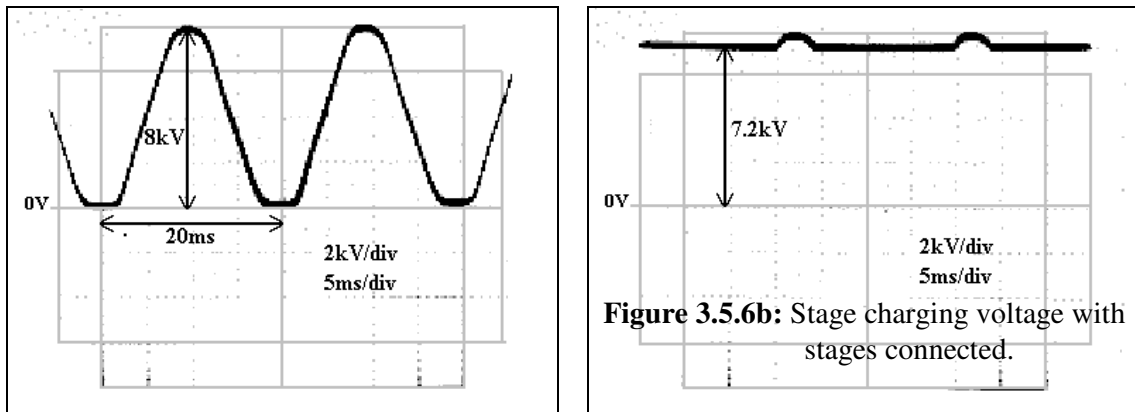


**Figure 3.5.6a:** Stage charging voltage without stages connected.

As can be seen in figure 3.5.6 the stages need to be connected to complete the voltage doubling circuit. It can also be seen that an input of 8kVpk-pk, provides a DC stage charging voltage of 7.2kV. Using this piece of information it is possible to work out the maximum stage charging voltage obtainable.

$$\text{Maximum input voltage} = 4000\text{V}_{\text{rms}} = 5657\text{V}_{\text{peak}} = 11.31\text{kV}_{\text{pk-pk}}$$

∴ If 8kVpk-pk gives 7.2kV dc

then: 11.31kVpk-pk gives **10.2kV dc**

This value defines the minimum voltage rating of the stage capacitors. Previously the stage capacitors were rated at 7kV, it is therefore not surprising that some of the had short circuited. Eight 15kV 0.05μF capacitors were available and these were installed in the old generator. The chassis of the generator had to be substantially rebuilt to house the larger, higher rated voltage, stage capacitors.

The stage capacitors were not connected directly to the charging circuit, a protective resistance of  $520\text{k}\Omega$  was placed between them. This is to prevent heavy oscillations appearing on the front of the impulse wave and to damp out any impulses reflected back from the generator into the charging circuit.

### Number of Stages

The generator is capable of working with up to eight stages this will provide a maximum impulse voltage of around  $80\text{kV}$ , however for lower impulse voltages only four stages will be used. The reason for this is that at lower stage charging voltages it is harder to get all eight stages of the generator to fire accurately, this is due to the small spark gap settings required.

### Nominal Capacitance

The nominal generator capacitance is the capacitance per stage,  $C_{\text{Internal}}$  divided by the number of stages. If eight stages are used this would give the small generator a nominal capacitance of  $6.25\text{nF}$ . This capacitance is also the value of  $C_T$  as used in the equation for the impulse wave tail time. A nominal capacitance of at least five times the capacitance of the test object is required as, otherwise, the voltage efficiency is low. In the case of these experiments the test object is a rod-sphere gap created by the finial and the upper electrode, this arrangement will have a capacitance in the order of a few picofarads, so there will be no problems with voltage efficiency. An efficiency of around 80% is expected.

Enough information is now available to calculate the expected tail time for the generator. The tail resistance is internal to the generator and is made up of the eight  $1.5\text{k}\Omega$  resistors producing  $R_T = 8 \times 1.5\text{k} = 12\text{k}\Omega$ . Using  $t_{\text{TAIL}} = -C_T R_T \ln(\eta/2)$  gives a tail time of around  $60\mu\text{s}$ , this around the correct value for a  $1.2/50\mu\text{s}$  wave.

### Nominal Energy

The nominal energy of the generator is denoted by its maximum stored energy and is given by  $\frac{1}{2}nC_{\text{Internal}}V^2$ . For this generator using all eight stages, with the maximum stage charging voltage the nominal energy is 20.8J. This is quite a low energy for an impulse generator however it is a very small generator and this value is adequate for the purposes of this project.

### Sphere Gaps

The sphere gaps were mounted horizontally one above each other in the generator chassis, the first gap being at the bottom. 2cm diameter spheres were used for the spark gaps. To vary the impulse voltage the sphere gap settings would have to be variable. This was achieved by solidly mounting the high voltage spheres to the chassis by means of threaded brass rods. The grounded (through the internal resistors) spheres were mounted through an insulating rod as shown in figure 3.5.7.

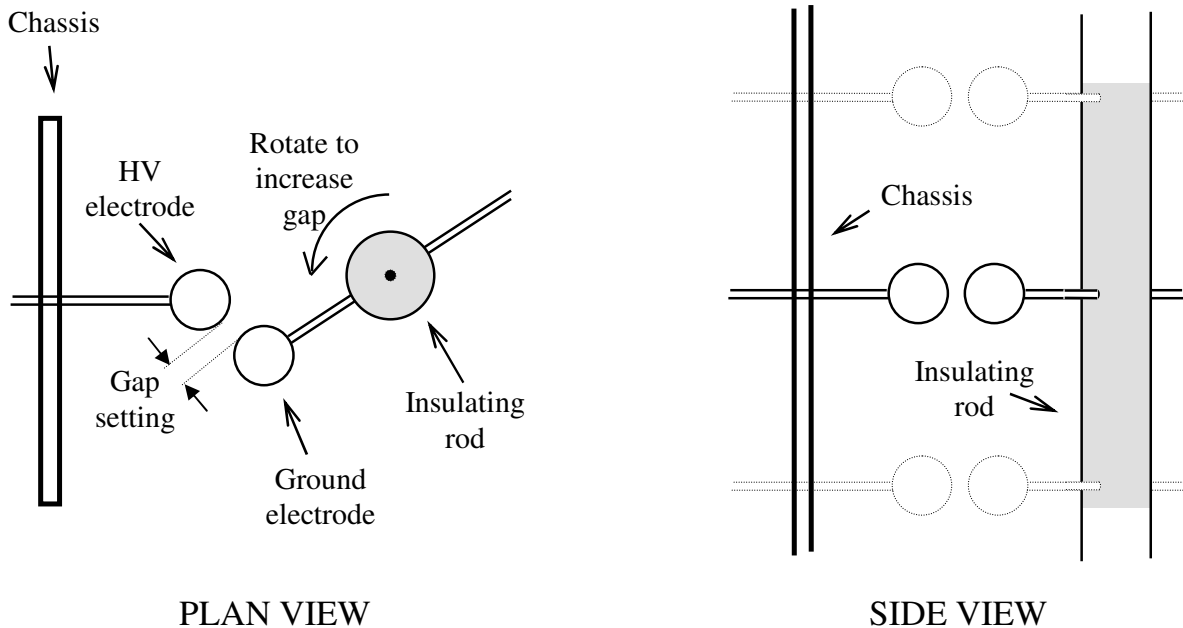


**Figure 3.5.7:** Sphere gap arrangement

The insulating rod was mounted vertically to allow rotation on its axis. Rotating the insulating rod through a few degrees would open all eight of the spark gaps at the same time by the same amount, thus enabling a higher stage voltage to be used.

The question was how to control the spark gap setting, i.e. what method was to be used to rotate the insulating rod accurately and controllably through only about 30°.

Three alternatives were investigated:

- DC Drive: Using a DC Drive with a gear box, attached to a crank arm, attached to the insulating rod would allow the rod to be rotated in both directions, depending on the polarity of the supply to the motor. A small DC motor was available, initial tests showed that it was not strong enough to turn the insulating rod, a larger motor was required. If a larger motor was purchased this method would work, however the angular position of the rod would need to be measured using some form of angular transducer. A simple transducer would be a variable resistor that could make up an arm of a potential divider. The voltage output of the divider would then give a measurement of angular position and thus could be calibrated to show gap setting.
- Stepper Motor: Using a stepper motor through a gearbox, the insulating rod could be moved very accurately. Stepper motors require a control board, using the control board the gap setting could be changed in very small steps (depending on the step size of the motor and the ratio of the gearbox) by sending trains of pulses to the control board. No position transducer would be necessary because the position of the motor is obtained from the number of pulses sent to the board. No stepper motor was available so one would have to purchase, however a controller could be borrowed for the duration of the project.
- Manual Control: By far the simplest method of changing the gap setting. By adding an arm perpendicular to the axis of the insulating rod, the rod can be rotated by moving the arm. If the arm has a pointer on it and a scale is put on the stationary chassis of the generator, the sphere gap setting can be simply and accurately changed.

The only problem with this method is that it does not allow remote setting of the gaps as the two previous methods did.

The simplest choice of manual operation was chosen, because it was very quick and simple to get working. The other two alternatives could be looked at as a project in themselves, and would be costly and time consuming. The method of opening and closing sphere gaps is not essential to this project.

### Spark Gap Setting

As well as all the gaps having to open and close for different test voltages the gaps have to be precisely set to fire accurately and in the correct order. When the impulse generator fires the first (lowest) gap should break down first, that causes the voltage to double at the second gap thus causing that gap to break down. The voltage at the third gap is then tripled, which breaks down and so on. To make sure the gaps break down in the correct order the gap setting should get slightly larger further up the generator. In other words the gap settings should be graduated in a tapered manner. Poorly graduated sphere gaps either produce; a stepped front wave due to gaps firing in the wrong order, or a smaller overall wave because not all of the stages fire.

Sphere gap graduation was achieved by fixing the distance between the grounded spheres and the insulated rod (see figure 3.5.7) and slightly varying the distance between the high voltage spheres and the generator chassis. The adjustment involved was very fine (around a quarter of a turn on the threaded rod supporting the HV spheres) and required some patience to achieve.

### Earthing and Safety

All points of the generator circuit that required earthing were connected to one point on the generator chassis, that point was then solidly bonded to the laboratory high voltage earth.

Extra care and attention to safety was required when operating the generator because it was not possible to arrange an automatic earthing system to short out the stage

capacitors when the charging voltage was removed. An earthing stick was used to earth down the capacitors, and it was essential to remember to attach the earth stick before approaching the generator.

### External Wave Front Components

The components that shape the front of the wave are internal to the generator however external components are required to shape the front of the wave. These consist of a front resistor  $R_F$  and a front capacitance  $C_F$  they are connected to the generator as shown in figure 3.5.1.

The front capacitance used was a capacitive voltage divider to allow measurement of the wave shape. The divider had a nominal capacitance of 99pF and a divider ratio of approximately 3500:1. With  $C_F$  set this only left  $R_F$  to be defined, for a 1.2 $\mu$ s front time and using the equation:  $t_{FRONT} = \frac{3C_T C_F R_F}{C_F + C_T}$ .  $R_F$  worked out to be 4k $\Omega$ .

In the actual generator this value gave slightly too long a front time, so the front resistance was reduced to a 3k $\Omega$  resistor.

### Wave Shape Measurement

Before any experiments could be conducted the generator had to be fully tested and calibrated. The front and tail times of the small generator were found using the oscillograms shown in figure 3.5.8.

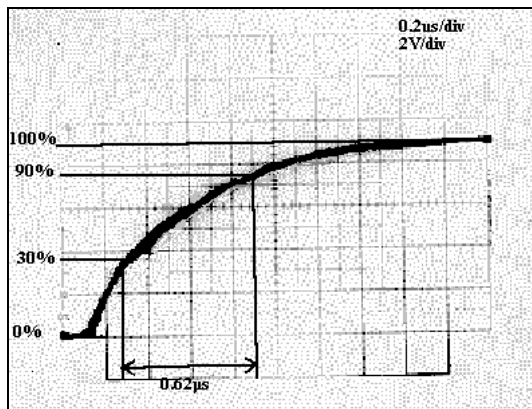


**Figure 3.5.8a** : Small Impulse Generator front time measurement.

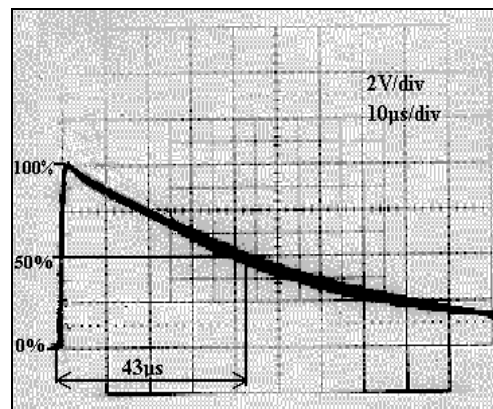


**Figure 3.5.8b** : Small Impulse Generator tail time measurement.

From figure 3.5.8a the front time of the wave was found to be:  $0.62\mu\text{s} / 0.6 = 1.03\mu\text{s}$ . From figure 3.5.8b the impulse tail time was found to be  $43\mu\text{s}$ . Both these values are within the tolerances of accepted standards for the lightning impulse wave. However it would not particularly matter if the wave was not standard because there is no standard wave for this type of investigation.

### Voltage Calibration

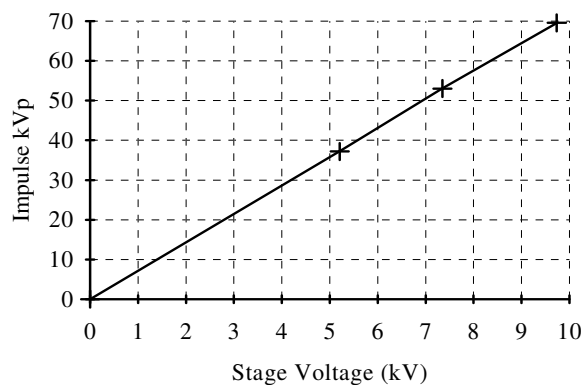
A method was required to conveniently measure the peak impulse voltage generated, to do this a circuit parameter that could easily be measured would need to be calibrated against peak impulse voltage. The usual measurand is the generator stage charging voltage.

The stage charging voltage in the generator was obtained by measuring the current through a  $100\text{M}\Omega$  resistor as shown in the generator circuit diagram (figure 3.5.5). A meter with a  $100\mu\text{A}$  full scale deflection was used. A current of  $100\mu\text{A}$  through a  $100\text{M}\Omega$  resistor corresponds to a voltage of  $10\text{kV}$ . The meter scale went from 0 to  $30\text{kV}$ , so to convert to stage kV the meter scale reading had to be divided by 3.

Calibration of the generator was conducted using the up-down method, copies of the calibration sheets are shown in the appendix. Calibration had to be carried out for operation with both 4 and 8 stages. A summary of the calibration is shown below.

#### **8 stages:**

Stage Meter	Stage kV	Peak kV
0	0	0
15.6	5.20	37.2
22.05	7.35	53.1
29.2	9.73	69.5



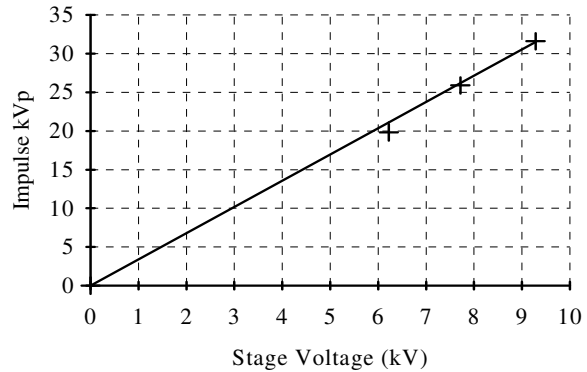
Average generator efficiency 89.5%.

Thus: Peak Impulse voltage (kVp) =  $8 \times 0.895 \times \text{Stage meter} / 3 = 2.37 \times \text{Stage Meter}$

#### 4 stages:

Stage Meter	Stage kV	Peak kV
0	0	0
18.65	6.22	19.8
23.15	7.72	25.9
27.85	9.28	31.6

Average generator efficiency 84.5%



Thus: Peak Impulse voltage (kVp) =  $4 \times 0.845 \times \text{Stage meter} / 3 = 1.13 \times \text{Stage Meter}$

#### Contingency Impulse Generator

Due to circumstances beyond the control of the UMIST high voltage department the small impulse generator described in the previous section had to be replaced by an alternative impulse generator half way through the experimental work. A direct substitution was made.

The replacement generator was a five stage generator, with motorised sphere gap control and an external wave tail resistance.

The generator was set up with following nominal values for its wave shape components:

$$C_{\text{stage}} = 0.05\mu\text{F} \quad C_{\text{front}} = 2160\text{pF}$$

$$R_{\text{tail}} = 2.9\text{k}\Omega \quad R_{\text{front}} = 306\Omega$$

The wave front capacitance was made up of a 2000pF capacitor in parallel with a potential divider (160pF nominal capacitance) for measuring the wave shape.

The front and tail times of the new generator were found using the oscillograms shown in figure 3.5.9.

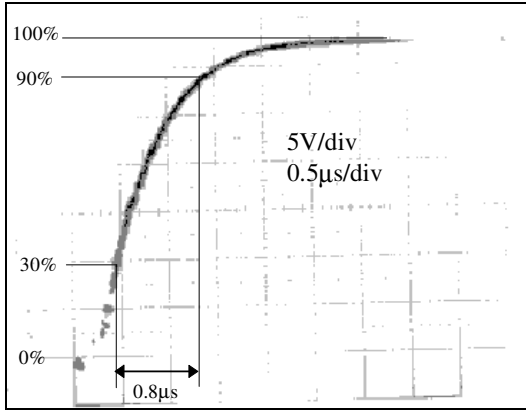


**Figure 3.5.9a** : Wave shape for tail time calculation.

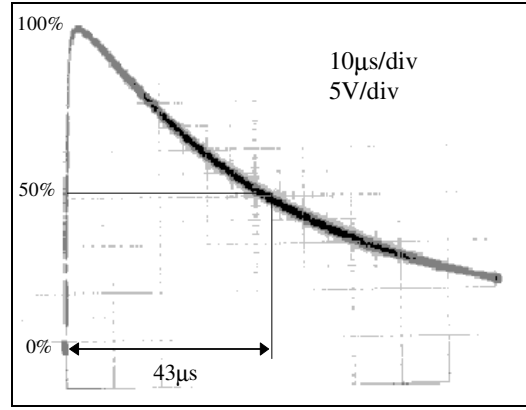


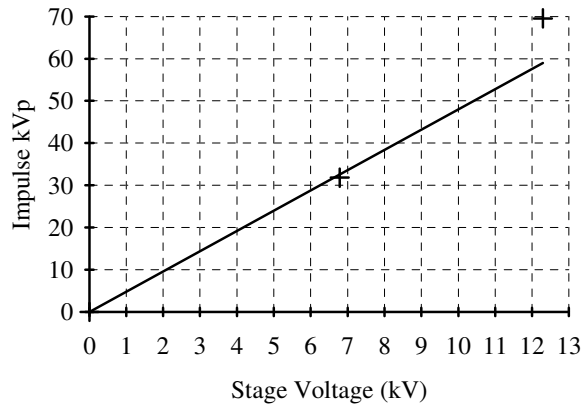
**Figure 3.5.9b** : Wave shape for tail time calculation.

From figure 3.5.9a the new front time of the wave was found to be:  $0.8\mu\text{s} / 0.6 = 1.33\mu\text{s}$ . From figure 3.5.9b the impulse tail time was found to be  $43\mu\text{s}$  the same as before.

The new generator also required voltage calibration. A stage voltage meter was already in place on the generator control panel. The stage charging voltage was measured directly using a high voltage meter. The stage voltage meter reading was found to be half the actual measured stage kV. Using the control panel reading the new generator was calibrated using standard sphere gaps and the up-down method as before. The results of the calibration are shown in the appendix, the summary of the calibration is shown below.

Stage Meter	Stage kV	Peak kV
0	0	0
3.39	6.78	31.8
6.15	12.3	69.5

Average generator efficiency 96%



Thus: Peak Impulse voltage (kVp) =  $5 \times 0.96 \times \text{Stage meter} \times 2 = 9.6 \times \text{Stage Meter}$

## 3.6 Firing The Small Impulse Generator

### Introduction

The triggering pulse from the delay unit is in the form of an optical pulse. This optical pulse must first be converted back into an electrical triggering signal, which is then used to trigger a pulse feed unit, i.e. a device that generates a high voltage triggering pulse that fires the small generator.

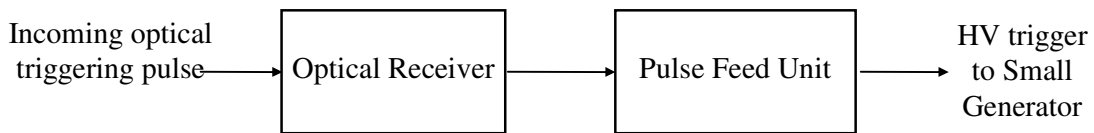


**Figure 3.6.1:** Outline of small generator firing unit.

The diagram above shows the outline design of the small impulse generator firing unit. This part of the apparatus was designed and constructed backwards, i.e. first a method of firing the generator was found, then the pulse feed unit was constructed and finally the optical receiver was added.

### Triggering the generator

To make the impulse generator fire the first stage spark gap must be made to breakdown. This is done using a *triggered gap*, the simplest form of which is a three ball gap as shown in figure 3.6.2.

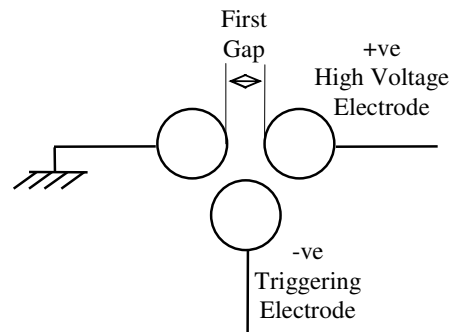


**Figure 3.6.2:** Three ball gap triggering arrangement.

The first gap will already have the stage charging voltage across it, the gap spacing will be set so that the stage voltage is below the breakdown voltage of the gap. When a trigger pulse of opposite polarity to the stage voltage, of the order of -20kV, is applied to the third electrode it causes a breakdown between the high voltage electrode and the triggering electrode. This creates a copious amount of charge in the region of the electrodes, furthermore the electric field in the first gap is enhanced because the trigger pulse is of the opposite polarity to the charging voltage across the gap. This combination of space charge and enhanced field secures a controllable breakdown of the first gap.

### Pulse Feed Unit

To generate the high voltage triggering pulse a pulse feed circuit was required. This circuit would be triggered by a low voltage pulse. The circuit used is shown in figure 3.6.3. A 250V DC supply was used to charge up a  $0.47\mu\text{F}$  capacitor via a  $1\text{M}\Omega$  resistor. When a voltage was applied across the gate and cathode of the thyristor, the thyristor becomes conducting and brings the positively charged end of the capacitor down to ground. This causes the voltage at the top of the low voltage winding of the transformer to jump to -250V. The charge on the capacitor oscillates around the winding and capacitor decaying away at a frequency equal to  $LC$ , where  $L$  is the inductance of the low voltage winding. The free-wheeling diode allows the current to flow in both directions. The oscillations in the low voltage winding induce high voltage oscillations in the high voltage winding. The high voltage winding is connected to the triggering electrode in the three ball electrode arrangement.

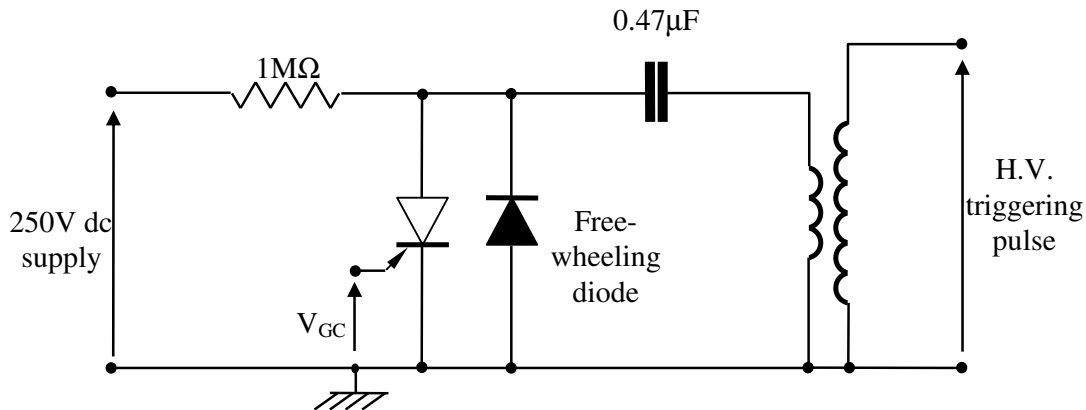


**Figure 3.6.3:** Firing circuit for impulse generator.

### Optical Receiver

An optical receiver was required to convert the incoming optical triggering pulse to an electrical triggering signal for the pulse feed circuit. The detector used was a Universal SMA detector available from FEC (order code 179-132). This detector is a PIN photo-diode, when reverse biased the reverse leakage current is dependant on the incident light intensity. A simple test was carried out and the reverse current through the diode when illuminated was  $10\mu\text{A}$  (note that this value is independent of applied voltage). When the diode was not illuminated a negligible current flowed.

The diagram below shows the circuit used to generate a 9V triggering pulse to drive the gate of the thyristor in the pulse feed circuit.

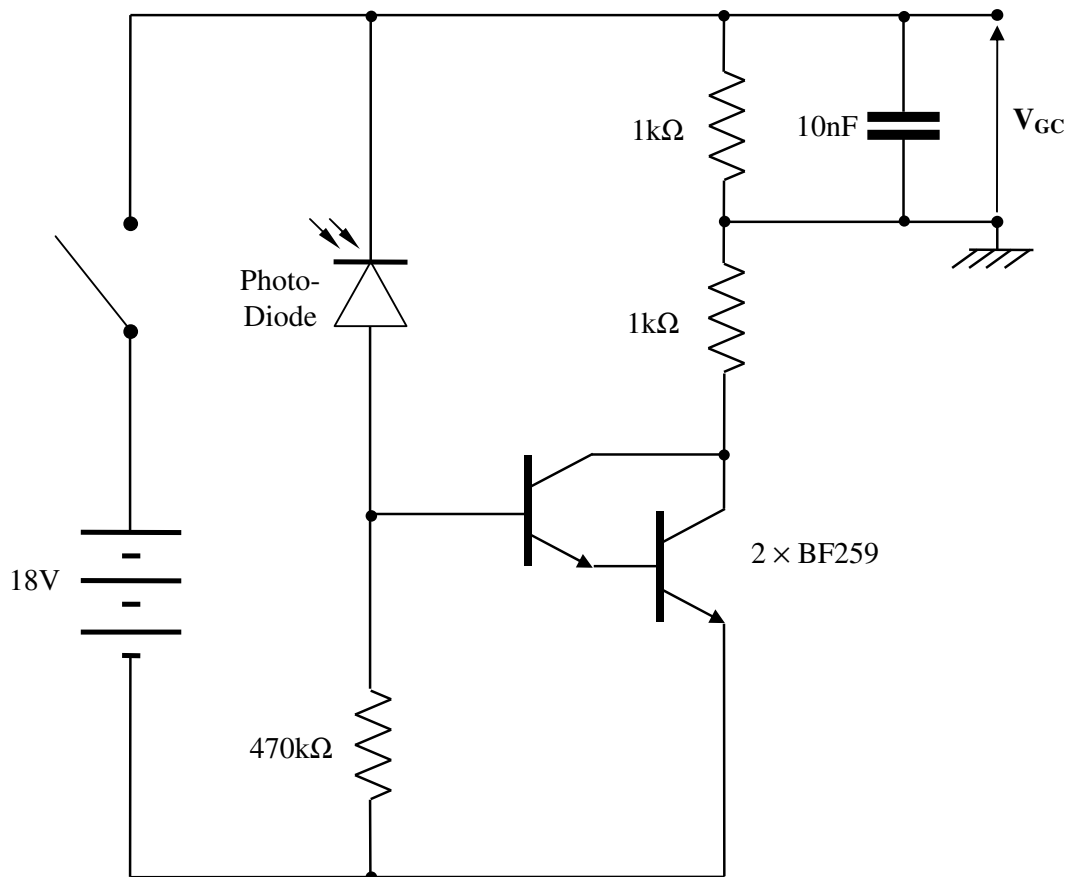


**Figure 3.6.4:** Optical receiver circuit diagram.

A Darlington pair made up of two BF259 transistors was used to amplify the small current signal. A  $470\text{k}\Omega$  resistor and the opto-detector were used to bias the base of the Darlington pair with a 18V power supply. The two  $1\text{k}\Omega$  resistors attached to the collector of the Darlington pair made the transistors act like a switch:  $V_{GC} \approx 9\text{V}$  when the diode was illuminated and  $V_{GC} \approx 0\text{V}$  when the diode was not illuminated.

### Construction of the Firing Unit

The coil used for the pulse feed circuit was a LOCUS car ignition coil, this coil had a very large turns ratio, so a high voltage was produced when the current oscillated in its low voltage windings. The 250V DC source used to charge the capacitor was adapted from a camera photo-flash, this proved to be a very convenient, compact and reliable DC source. The photo-flash ran on  $4 \times 1.5\text{V}$  batteries.

Both the pulse feed circuit and the optical receiver were constructed on a piece of strip board, the 18V power supply for the optical receiver was provided by two 9V batteries. The power supplies, circuits and the coil were then all mounted inside a specially constructed box. The completed firing unit is shown in figure 3.6.5.

**Figure 3.6.5 :** The small impulse generator firing unit.

## Testing The Firing Unit

The completed firing unit was tested first on its own to check the shape of the HV triggering pulse, a  $\times 1000$  probe was used to observe the wave shape. The traces obtained are shown below.

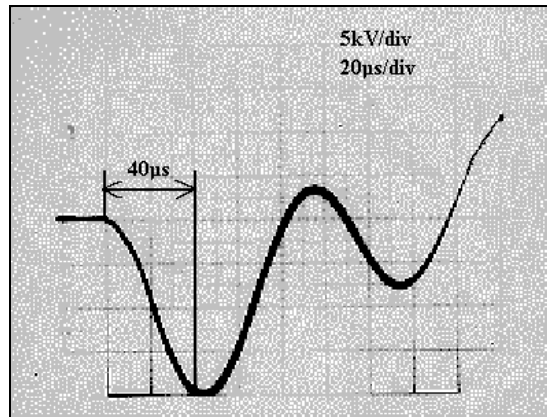
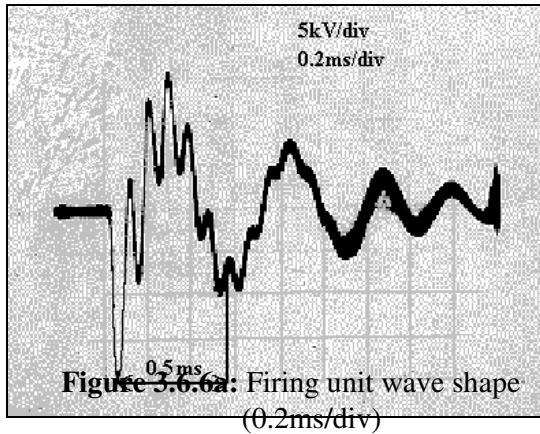


**Figure 3.6.6b:** Firing unit wave shape (20µs/div)

From the traces it can be seen that the triggering pulse is a decaying sinusoid with a higher frequency oscillation superimposed on top. The important part of the firing pulse is its initial rise, this is shown in figure 3.6.6b. The voltage rises to -20kV in 40µs, this is quite a slow fronted triggering pulse so there concern was raised as to the time to breakdown of the triggered gap.

The firing unit was attached to the triggered gap on the small impulse generator and the time between application of the optical pulse to the firing unit and the triggering of the small generator recorded for 50 shots.

A mean time to firing of 7.5µs with a standard deviation of 1.7µs was obtained. The mean time to firing is un-important because the delay to firing could just be added to the total time delay generated by the delay unit. The stability of the firing time *is* important because the experiments to be conducted later would have to be accurately repeatable. However the range of delay time settings that will be used later are in the

order of  $100\mu\text{s}$  so a standard deviation of  $1.7\mu\text{s}$  corresponds to a variation of only around 1% in the total delay time which is quite acceptable.

Attempts were made to increase firing stability even further by irradiating the triggered gap with UV light, however this met with only limited success and so was abandoned.

Although not mentioned earlier the variation in total delay time caused by the delay unit itself is negligible. The main contribution to total delay time jitter is from the firing unit and triggered gap.

### *Firing the Contingency Impulse Generator*

When the small impulse generator had to be replaced the same firing unit was used to trigger the generator. The replacement impulse generator was already fitted with a triggertron gap as the first sphere gap. The earthed sphere in the triggertron gap was provided with a small hole through which an insulated metal rod was mounted with an annular clearance of about 1mm. When the HV trigger pulse from the firing unit was applied to the rod it caused a discharge between the rod and the earthed sphere, this generated a large amount of charge at the surface of the sphere thus causing breakdown of the first gap.

### 3.7 Linking The Small Generator to the Finial

#### Protecting the Small Impulse Generator

The small impulse generator could obviously not be connected directly to the finial because in the event of flashover of the main gap the small generator would provide the connection to earth and would most probably be damaged.

To protect the small generator a  $8k\Omega$  resistor and a protective spark gap were connected as shown in figure 3.7.1.

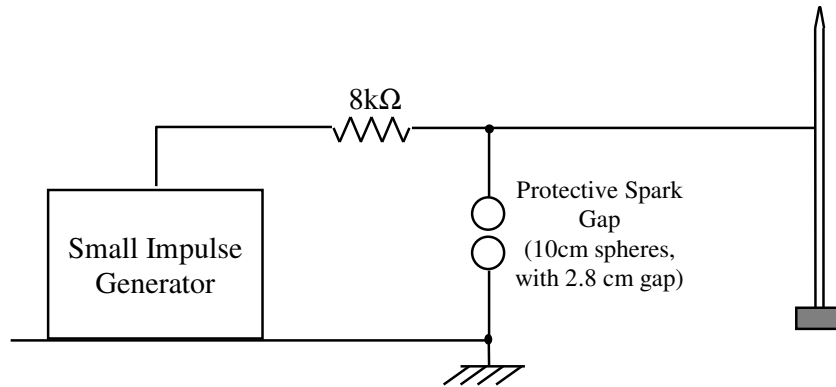


**Figure 3.7.1 :** Method of protecting the small impulse generator.

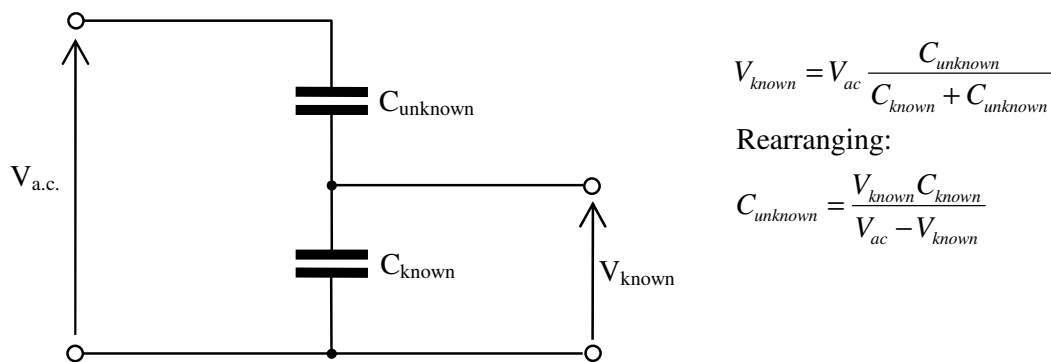
The spark gap was set using calibration tables to have a 50% flashover voltage of 80.5kVp. This value is above the maximum voltage applied to the finial, thus the protective gap will not break down under impulses applied by the small generator. However in the event of the main finial-sphere gap breaking down the voltage at the finial will rapidly rise, until the protective gap breaks down. Thus the voltage on the small generator is limited by the protective spark gap. The  $8k\Omega$  resistor provides further protection is so far as it makes up an RC time constant with the capacitance of the protective gap, thus also limiting the rise time of the voltage appearing at the small generator.

### Gap Capacitance measurements

Not only will the RC time constant created by the 8kΩ resistor and the protective spark gap limit the rise time of the voltage at the generator it will also alter the front time of the impulse applied to the finial. To find out by how much the front time of the finial impulse is lengthened the capacitance of the protective gap is required.

Another point to note is that the main finial-sphere gap will also have a capacitance. The consequence of this is that the finial-sphere capacitance and the protective gap capacitance will act as a capacitive voltage divider. Therefore the main impulse voltage applied to the sphere will divide across the two capacitance's, resulting in the fact that only a certain percentage of the main impulse voltage will occur across the main finial sphere gap. To find out by how much the voltage across the finial-sphere gap is reduced from the case were the finial is grounded, the gap capacitance's are required.

To measure the gap capacitance's the capacitive voltage divider method was used. In this method the gap under test is connected in series with a known capacitance. An a.c. voltage is applied across the two capacitance's and the voltage appearing across the known capacitance is measured. From the two voltage readings and the known capacitance the value of the unknown capacitance can be found as follows:



$$V_{known} = V_{ac} \frac{C_{unknown}}{C_{known} + C_{unknown}}$$

Rearranging:

$$C_{unknown} = \frac{V_{known} C_{known}}{V_{ac} - V_{known}}$$

**Figure 3.7.2 :** Capacitance measurement using the voltage divider method.

The unknown gap capacitance will be in the order of a few pico-farads. If  $V_{ac}$  is set to 10kV then to get a easily measurable voltage across the known capacitance it must have a value of about 1000 times the expected gap capacitance. A nominal value of 50nF was therefore chosen for the measuring capacitance.

Using a step-up transformer and a variac  $V_{ac}$  was set to 10kV rms (measured using a high voltage meter).  $V_{known}$  was measured using an oscilloscope and its rms value calculated.  $C_{known}$  was accurately measured using an LCR bridge and was found to be 49.6nF. The results for the two different gaps are shown below.

Finial-Sphere gap:  $V_{known} = 0.262V \text{ rms} \Rightarrow C_{unknown} = \mathbf{1.3pF}$   
Protective gap:  $V_{known} = 0.721V \text{ rms} \Rightarrow C_{unknown} = \mathbf{12.0pF}$

From these values the protection RC time constant works out to:

$$8 \times 10^3 \times 12.0 \times 10^{-12} = \mathbf{0.1\mu s}$$

This value is small enough so as not to affect the shape of the wave shape from the small impulse generator. However it is large enough to slow down the rise time of the voltage occurring at the generator in the event of main gap breakdown.

The capacitive voltage divider set up by the two gaps means that around 90% of the test voltage will occur across the main finial-sphere gap. This factor may have to be taken into account if a very quantitative analysis of the results is required, however this is unlikely because most observations will be of a qualitative nature.

### 3.8 Overall Artificial ESE Device Apparatus

The diagram below shows the final arrangement of the apparatus used to simulate the ESE device in the laboratory. The apparatus had been thoroughly tested and was working reliably, this allowed the experimental work detailed in the next section to move on and study the effect of energising the lightning finial.

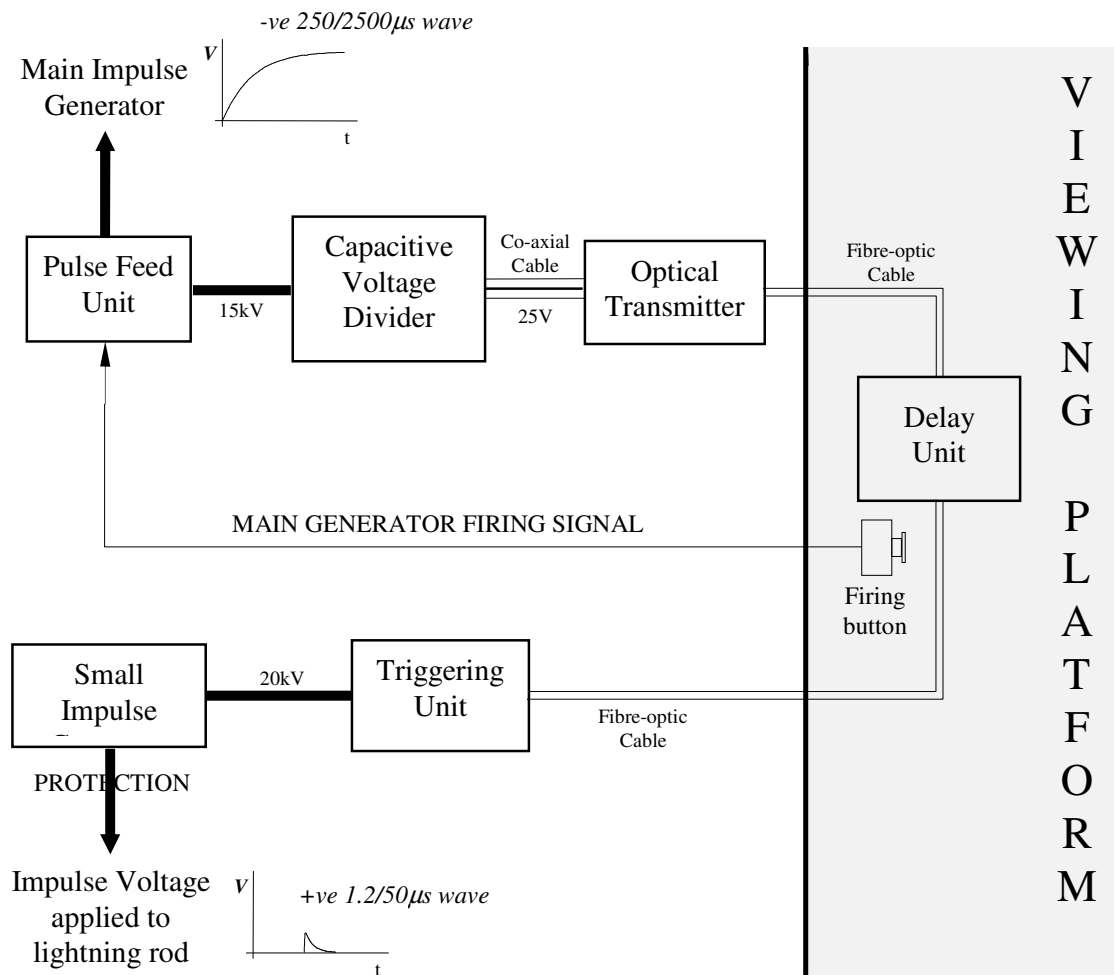


**Figure 3.8.1 :** Schematic diagram of artificial ESE device apparatus.

## 4. Experiments

### 4.1 Introduction

This chapter documents all the experiments carried out at various points throughout the project. Each section contains descriptions and results of the experiments conducted, and is followed by a discussion of the results obtained.

First the passive finial was investigated i.e. with the rod grounded. A theoretical examination of the electric field in the main finial-sphere gap was also conducted. The effect of pre-stressing the gap was examined before moving on to test the artificial ESE device documented in the previous chapter.

### 4.2 Preliminary Experiments- The Passive Finial

#### V50% for Finial-Sphere Gap

It was first essential to examine the passive case, this would form a base reference to allow comparison between the active and the passive finial.

The first experiment conducted was to find the impulse breakdown voltage of the finial-sphere gap. This would provide a valuable reference and define the range of voltages to be considered for the rest of the experiments.

The 50% breakdown voltage is a common statistical definition used in high voltage testing and is defined as the impulse voltage at which half of all impulses applied result in flashover.

To obtain the 50% breakdown voltage the *up-down* method was employed. A description of this method has already been given in the section on impulse generator calibration. A copy of the laboratory *up-down* sheet is shown in the appendix, this gave a average stage meter voltage of 98.3kV.

**Using:** Impulse kVp = Number of stages × Stage kV × Generator Efficiency

**Gives:** Impulse kVp =  $6 \times 98.3 \times 0.833 = 491.3\text{kVp}$

Thus the 50% breakdown voltage for the 75cm finial-sphere gap is **491.3kVp**.

### Corona Inception Times

The second line of investigation into the passive case involved looking at the corona discharges from the finial tip when impulses were applied *below* the 50% breakdown voltage were applied to the sphere.

#### **Method:**

The lightning finial was grounded and the main impulse generator was used to apply negative 250/2500 $\mu$ s impulses of various magnitudes to the sphere to simulate the effect of the down-coming leader. A photo-multiplier was used to look at corona from the tip of the rod and a storage oscilloscope was used to record the photo-multiplier output.

#### **Results:**

The long front time of the impulse applied to the sphere allowed multiple corona discharges to occur from the tip of the finial. Figure 4.2.1 shows the typical corona discharges observed from the finial when a -250kVp impulse was applied to the sphere. A method was required to record and document the corona discharge patterns, a choice was made to record the time to first corona, time to second corona, time to last corona and number of corona at each application of the impulse. Twenty impulses were applied at each test level and the average of the 4 measuring parameters stated above were found.

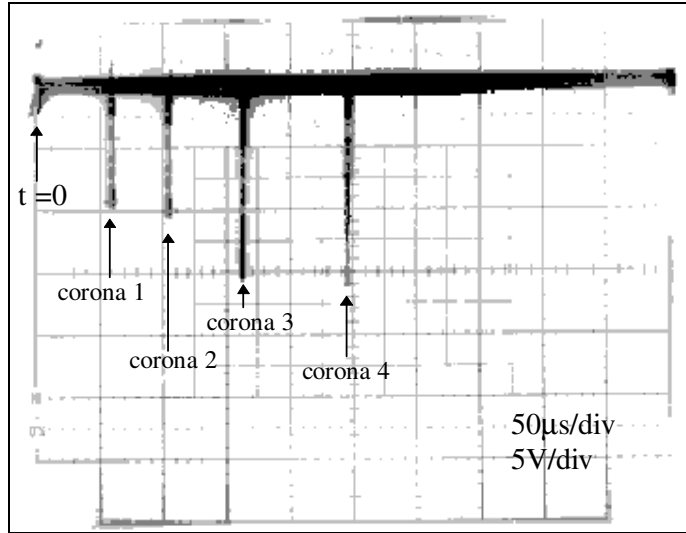


**Figure 4.2.1 :** Typical corona observed from the tip of the passive finial with a -250kVp impulse applied to the sphere.

Confidence limits are required to allow analysis of the results obtained, the usual confidence limits employed are the 95% limits. These are two values either side of the mean value between which there is a 95% certainty that the ‘true’ value lies. For a data sample from a population with a normal distribution the 95% confidence limits are defined as:

$$\text{Upper limit} = \text{mean} + 3\sigma$$

$$\text{Lower limit} = \text{mean} - 3\sigma$$

Where  $\sigma$  is the standard deviation of the sample population.

For the 95% limits to be applied the data population must be approximately normal. To see if this is the case 30 shots were taken at 300kVp and the time to last corona discharge recorded. The distribution obtained is shown in figure 4.2.2.

A normal curve with the same mean and standard deviation as the sample data is also shown in figure 4.2.2. From this it can be seen that the data is distributed approximately normally and thus  $\pm 3\sigma$  can be used as the 95% confidence limits.

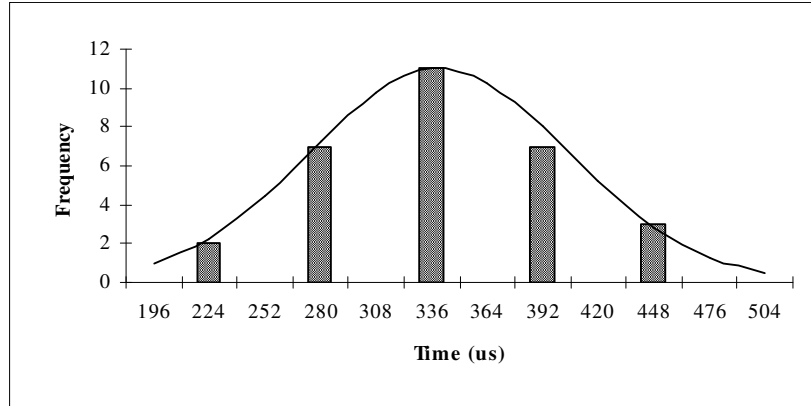
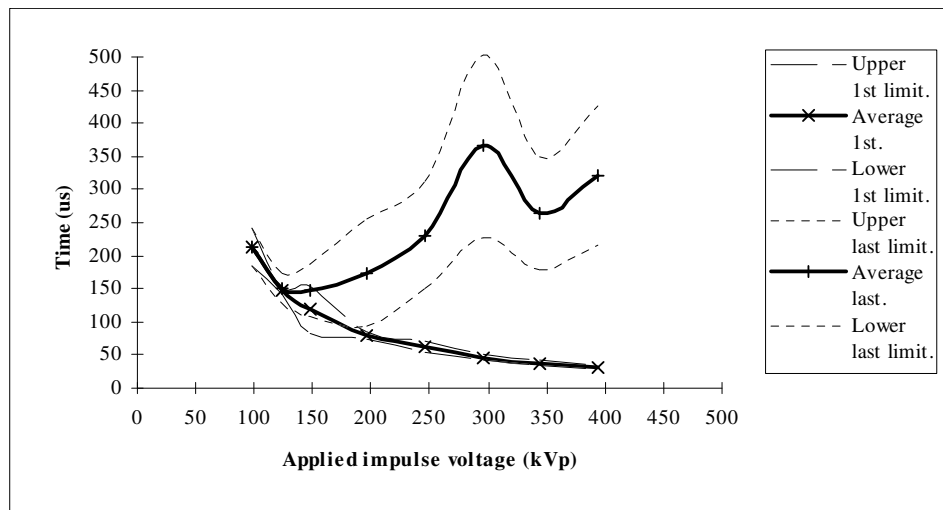


**Figure 4.2.2 :** Distribution of time to last corona at -300kVp.

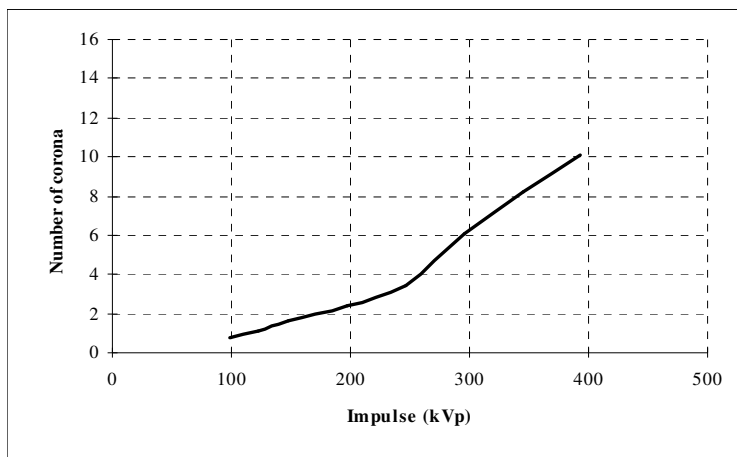
The 95% confidence limits for the data are shown as thin lines in the following graphs.

Figure 4.2.3 shows the average time to 1st corona and average time to last corona vs. impulse voltage. It thus shows the envelope of times within which the corona discharges occur. Below -130kVp the 1st and last corona lines converge, this means that only one corona discharge was detected below this voltage.

Figure 4.2.4 shows the average number of corona detected vs. impulse voltage, and thus the number of corona in the envelope defined by figure 4.2.3.



**Figure 4.2.3 :** Range of corona inception times for passive finial.



**Figure 4.2.4 :** Average number of corona for passive finial.

The corona were not equally spaced over the range in which they occurred, as can be seen from the oscilloscope photograph shown in figure 4.2.1. It was unfeasible to record the position of each corona for each applied impulse, but figure 4.2.5 showing the time to first and second corona gives an idea of the positioning of the corona.

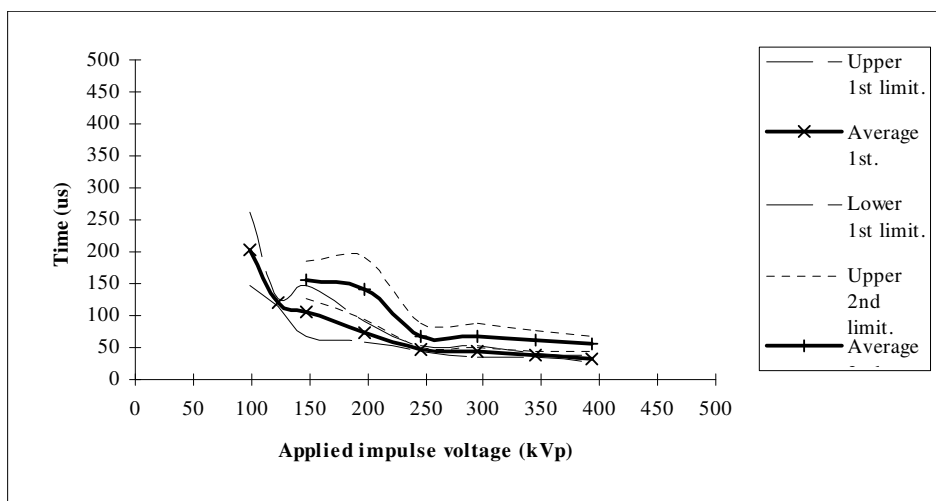


**Figure 4.2.5 :** Average time to first and second corona for passive finial

## Discussion

Corona pulses are observable for impulses as low as 20% of the gap flashover voltage i.e. at only around 100kVp. Thus there will be lots of corona activity in the gap before breakdown takes place.

Figure 4.2.6 shows the shape of the applied impulse, the wave takes 500 $\mu$ s to reach its peak value. All the corona observed occurred on the front of the wave, none were observed after peak, this is quite a surprising result because the long flat top of the impulse wave should allow corona to continue later. Therefore a space charge mechanism is probably at work; the initial corona discharges set up a space charge around the tip of the rod, thus inhibiting further corona.

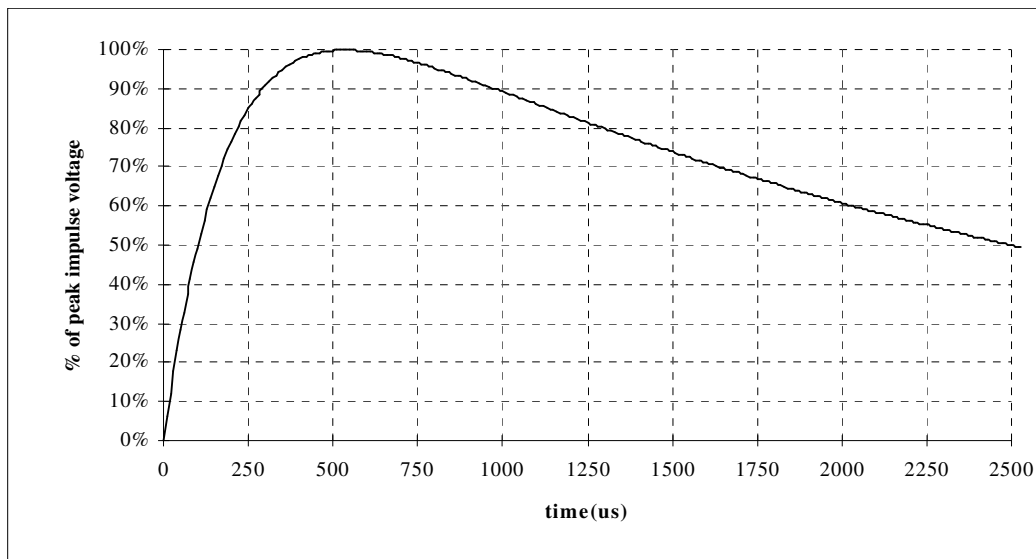


**Figure 4.2.6 :** The shape of the applied impulse wave.

The time between individual corona is in the order of 50 $\mu$ s. It is hard to interpret this result because two factors are involved, the decreasing  $dV/dt$  of the voltage on the front and the mobility of the charge carriers (i.e. the time for the charge generated by one corona to disperse enough to allow the creation of another corona).

The large variation in time to last corona indicates the statistical nature of corona, the small variation in time to first corona can be explained, by the fact that the initial voltage on the front of the wave is increasing very rapidly.

### Time to Breakdown

Having studied the corona distribution at voltages below  $V_{50\%}$  the next step was to see what was happening when voltages **above**  $V_{50\%}$  were applied.

The breakdown process in the gap will involve the generation of a positive leader from the finial, so recording the time to breakdown will give an indication of the time to initiation of a positive leader from the tip of the finial.

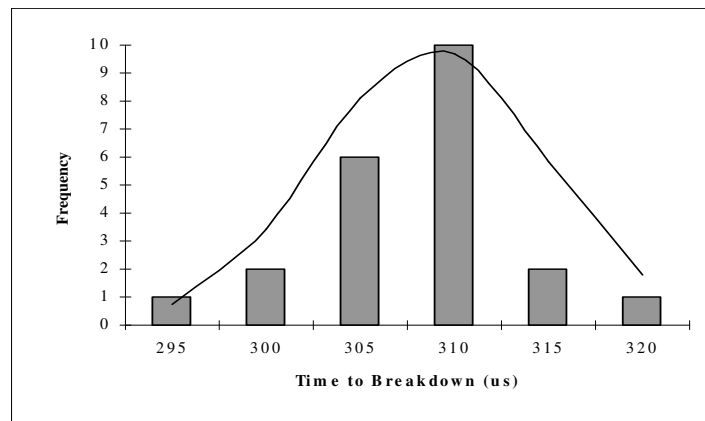
The time to leader formation is critical to this investigation because under natural lightning conditions the generation of a leader from the finial is the start of the attachment process for a lightning strike.

### **Method:**

With the finial grounded, impulses of increasing magnitude were applied to the sphere. The time to breakdown was recorded for 20 impulses at each voltage level. A photo-multiplier was used to observe the discharge from the tip of the rod.

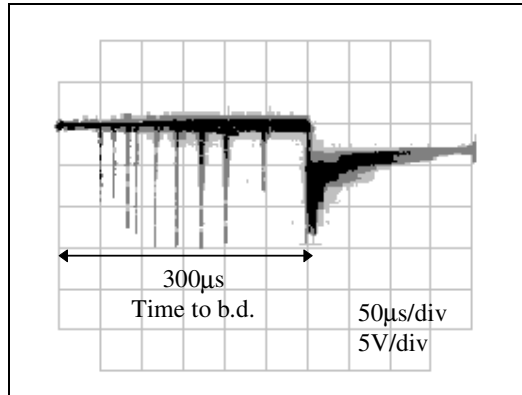
### **Results:**

Again confidence limits would be required to allow reliable discussion of the results. Figure 4.2.7 shows the distribution of times to breakdown at  $-725\text{kVp}$ , the distribution of times approximates to the normal curve (also shown) and thus the  $\pm 3\sigma$  method of obtaining the 95% confidence limits can be used.



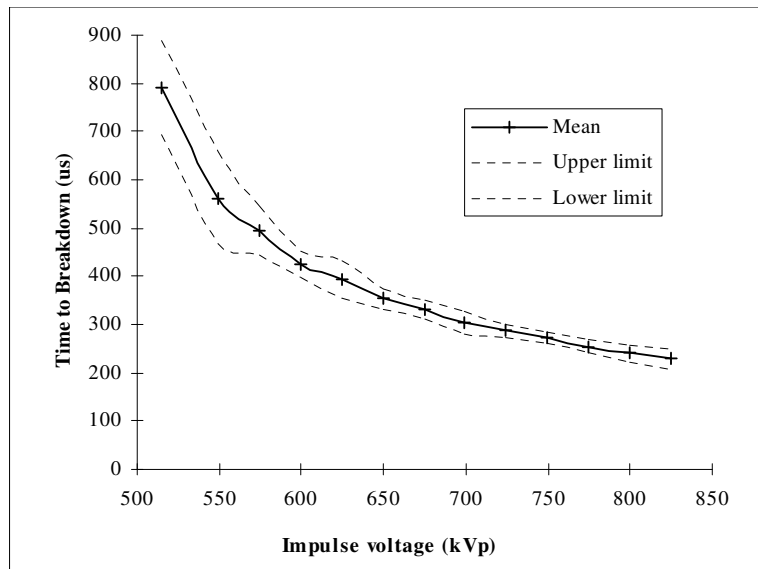
**Figure 4.2.7** : Distribution of time to breakdown for a 725kVp impulse.

Figure 4.2.7 shows a typical photo-multiplier recording, a number of corona discharges occur before breakdown of the gap. The large pulse then a constant off-set signifies breakdown of the gap.



**Figure 4.2.8 :** Typical photo-multiplier measurements for -725kVp impulse.

Figure 4.2.9 shows time to breakdown vs. applied impulse voltage for the final-sphere gap. Note that the origin of the graph is 500kVp (approximately  $V_{50\%}$  for the gap). The thin lines show the 95% confidence limits for the data.



**Figure 4.2.9 :** Time to breakdown for increasing impulse voltage.

**Discussion:**

Above -600kVp breakdown occurs before 500 $\mu$ s and i.e. on the front of the wave. As the peak impulse breakdown voltage is increased the time to breakdown decreases as does the range of scatter. This is due to the increasing value of  $dV/dt$ , thus the statistical variation in breakdown voltage will have a smaller effect on  $t$ .

The characteristic should continue to decrease slowly as the peak impulse voltage is increased further, the minimum obtainable time to breakdown will eventually be limited by the physical processes involved in breakdown.

Figure 4.2.8 shows a typical photo-multiplier measurement, no positive leader was detectable. A positive leader is much slower than the corona discharges, and would be visible as a constant output from the photo-multiplier just prior to the breakdown pulse.

An explanation for not being able to detect a leader comes from the *possible* breakdown mechanism in the gap: A leader is a hot slow moving path of ionised gas molecules, it can be considered as an extension of the tip of the finial. The leader propagates by emitting further corona style discharges or streamers from its tip. Since laboratory gap is quite short it is possible that the streamers from the head of the slow moving positive leader, may reach the sphere before the leader has propagated very far into the gap. This causes the gap to breakdown faster than the gap transit time for a leader. Thus the leader that is formed is only there for a very short while before breakdown occurs and thus is not detectable with the photo-multiplier.

A second possible reason for not being able to detect a leader is because of the poor resolution obtainable with the storage oscilloscope.

## 4.3 Pre-stressing the Finial-Sphere gap

### Introduction

Due to limitations on time and apparatus it was not possible to combine both DC and impulse voltages on the sphere. This meant that the exact electric field conditions experienced during a lightning strike could not be simulated, however it was possible to apply a DC voltage to the finial.

Applying a positive DC voltage to the finial will have approximately the same effect as applying a negative DC voltage to the sphere, in so far as they will both intensify the electric field at the tip of the finial and they will both cause corona discharge to occur (if the voltage is high enough) and thus set up space charge at the tip. However caution must be used because the situation is *not* fully reversible, due to the effect of the ground plane (see section 4.4).

### Applying Positive DC to the Finial

#### **Method:**

A positive high voltage DC generator (Brandenburg generator) was attached to the finial. A high voltage volt meter was used to measure the applied voltage.

The sphere was grounded through a 500k $\Omega$  resistance so that any current flowing from the gap to earth would create a voltage across the grounding resistor. The voltage across the resistor was observed on an oscilloscope.

#### **Results:**

The positive DC voltage was slowly increased from zero until at +14.8kV intermittent current pulses were observed on the oscilloscope. As the voltage was increased further the current pulses became more and more frequent. An audible corona hiss could be heard from the finial. When the DC voltage reached +28.7kV the current pulses and the audible corona stopped abruptly.

The voltage was increased up to 50kV (the limit of the generator) and no further corona could be detected, however the current through the grounding resistor continued to increase steadily after the corona had ceased.

**Discussion:**

The explanation for the observed phenomenon is available in many high voltage texts [9,11]. Below +14.8 kV the field strength at the finial tip is not high enough to produce corona, between +14.8kV and +28.7kV regular corona pulses are observed known as Trichel (1939) pulses, as the voltage is increased in this range the partial discharges are produced at a faster and faster rate. At +28.7kV the space charge set up by the corona discharges reaches a critical value and ‘shuts off’ further corona pulses, setting up a *glow* discharge mechanism. This is observed as steady current that increases as field strength increases.

*Applying Negative DC to the Sphere*

**Method:**

The DC generator was attached to the sphere and the finial was grounded through the 500k $\Omega$  resistor. The same method as before was used to measure corona discharges from the finial.

**Results:**

The negative DC voltage applied to sphere was steadily increased from 0kV until at -21.1kV intermittent current pulses were observed on the scope. As the voltage was increased further the current pulses became more and more frequent. Again an audible corona hiss could be heard from the finial. The applied voltage was increased to -50kV with no great change in the corona discharge pattern.

**Discussion:**

Exactly the same explanation as before can be called upon because both cases result in positive corona from the finial tip. It was not possible to generate a glow discharge in this configuration. The different corona inception voltages for the two configurations are investigated in section 4.4.

### Applying DC to the Finial, and impulse to the sphere

The lightning finial under natural conditions will experience a DC pre-stress followed by an impulse field. From the previous DC experiments three different regions in the pre-stress characteristics of the finial have been observed; below corona inception voltage (no discharge activity), intermittent corona discharge, and glow discharge. Thus applying pre-stress in each of these regions before impulse may give an insight into the effect of the permanent field prior to the lightning strike.

#### **Method:**

The same DC set was used as above but with a sparkgap in parallel to protect the DC generator in the event of breakdown, as is shown in figure 4.3.1.

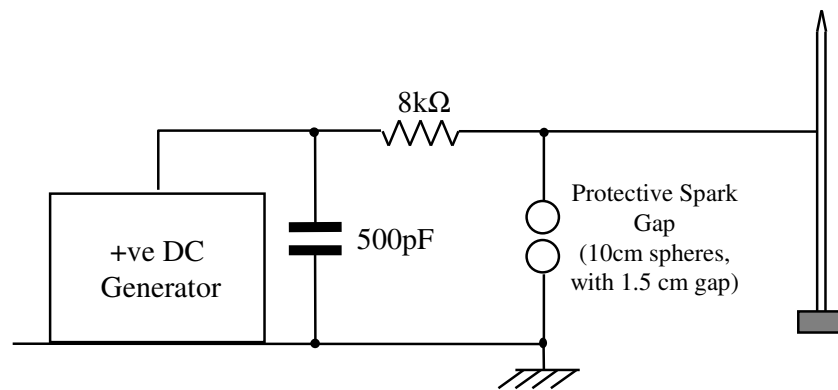


**Figure 4.3.1 :** Method of protecting the DC generator.

The  $8\text{k}\Omega$  resistor and the  $500\text{pF}$  capacitor have an RC time constant of  $5\mu\text{s}$ , this was used to limit the rise time of the voltage occurring at the DC generator in the event of breakdown.

The same method of recording the corona discharge patterns as the passive rod was used, i.e. time to 1st,2nd,last and average number of corona. This experiment was repeated for three different DC voltages on the finial: +10kV, +20kV and +30kV. The results are summarised below, the 95% confidence limits are shown as broken lines.

**Results: +10kV on finial**

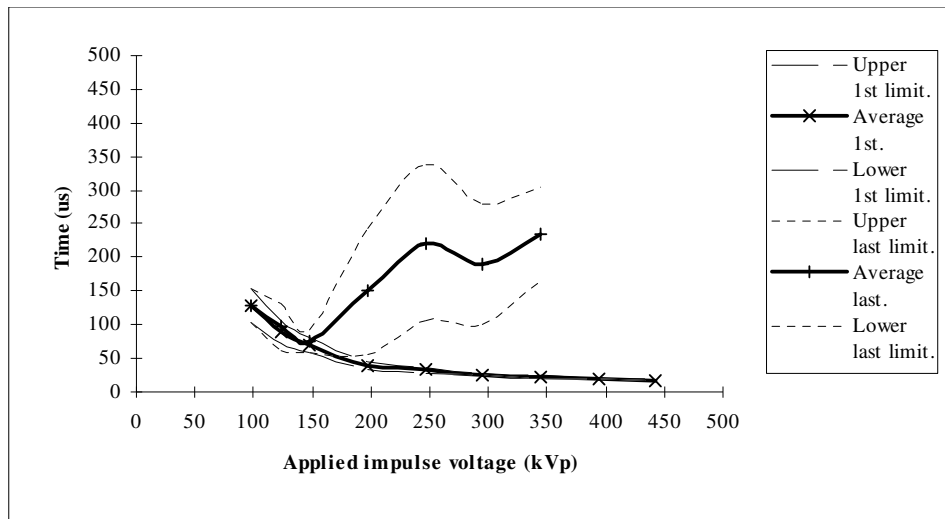


**Figure 4.3.2 : Range of corona inception times for 10kV on finial.**

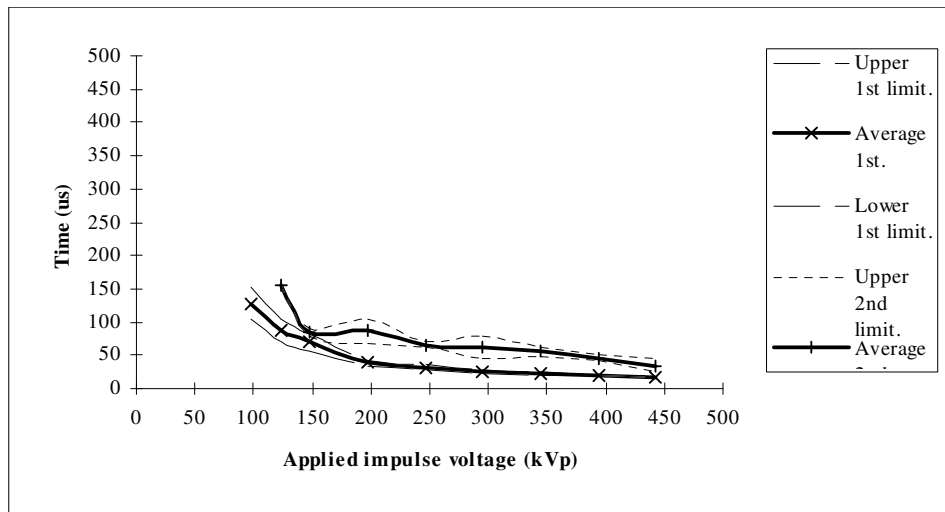


**Figure 4.3.3 : Average time to first and second corona for 10kV on finial.**

**Results: +20kV on finial**

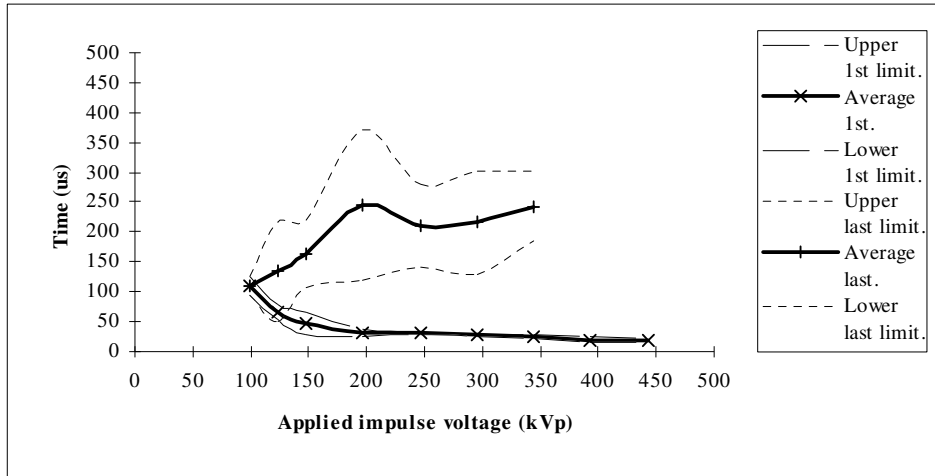


**Figure 4.3.4 :** Range of corona inception times for 20kV on finial.

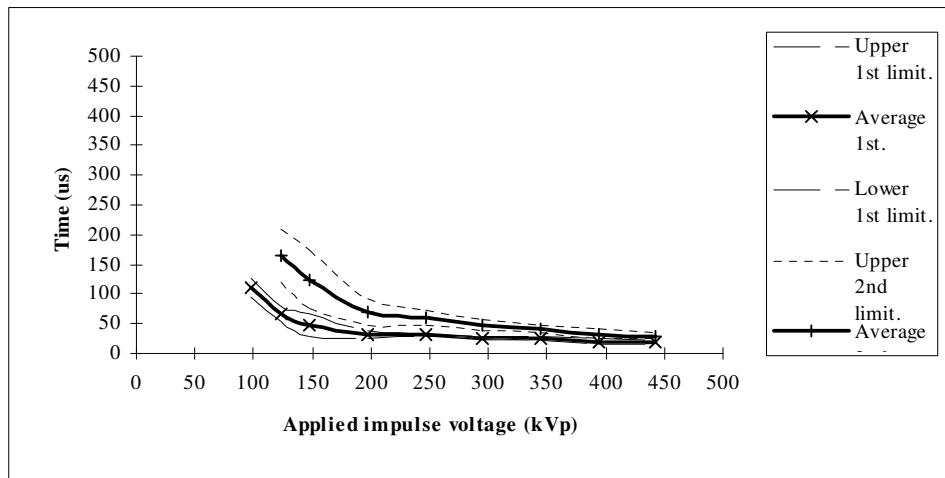


**Figure 4.3.5:** Average time to first and second corona for 20kV on finial.

**Results: +30kV on finial**

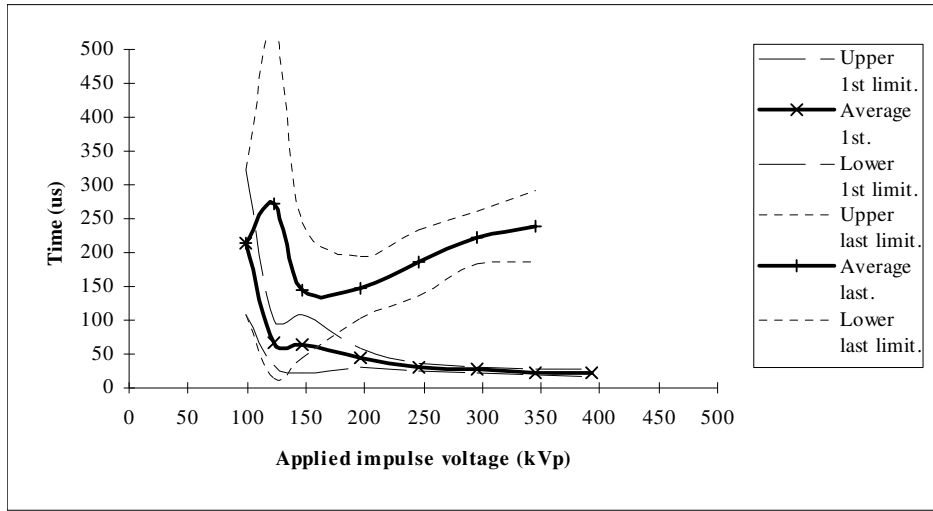


**Figure 4.3.6 :**Range of corona inception times for 30kV on finial.

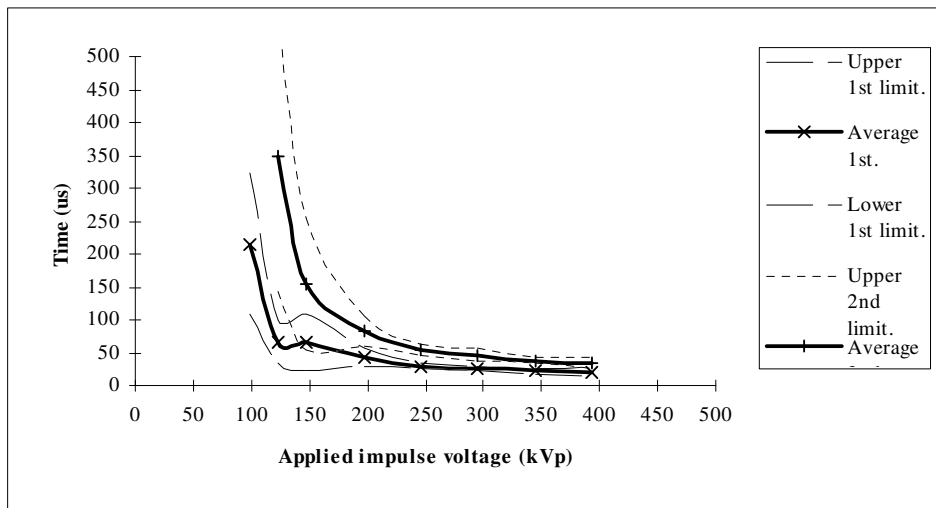


**Figure 4.3.7 :** Average time to first and second corona for 30kV on finial.

**Discussion:**

10kV pre-stress:- No partial discharge activity from finial prior to impulse, ∴ there will be no space charge at the tip of the finial. The only effect will be to increase the field strength at the finial. Figure 4.3.2 is very similar to the passive case (figure 4.2.3), the time to first corona is brought forwards by about 30μs, because there is already a voltage on the finial.

20kV pre-stress:- Finial will already be producing corona, ∴ some space charge will be present. The main effect is still to increase the field strength at the tip. The time to first corona is brought further forwards than the 10kV case, although for higher impulse voltages the time to first corona in both the 10kV and 20kV cases are very similar. Multiple corona are observed for slightly lower impulse voltages.

30kV pre-stress:- Finial will be in the glow state, ∴ Large amount of space charge around the finial tip, it will have already “sealed itself off”. At lower impulse voltages (below -250kVp) the time to first corona is later than in the previous two cases. The space charge has deterred further corona discharge.

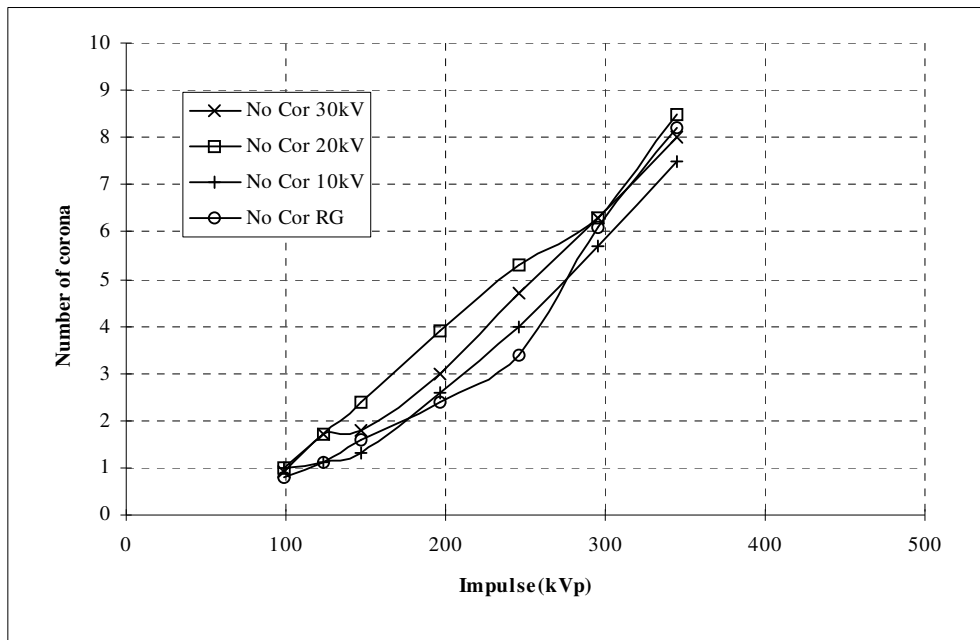


**Figure 4.3.8 :** Comparison of average number of corona.

Figure 4.3.8 shows the average number of corona observed at each test level for the three different pre-stress cases and for the passive case. The only observation that can be made from this graph is that there is no significant change in the number of corona for the pre-stressed case.

Typical photo-multiplier observations of the corona for the three pre-stress cases were also very similar to the passive case, (in so far as the nature of the corona appeared the same).

Pre-stress only appears to have a significant effect on the corona distributions for low (smaller than -250kVp) impulses.

### Time to Breakdown

The effect that pre-stress had on the time to breakdown curve was investigated.

#### **Method:**

The same DC generator and protective circuit as shown in figure 4.3.1 was used to apply +10 and +30kV to the finial. The time to breakdown curves were found for each case.

#### **Results:**

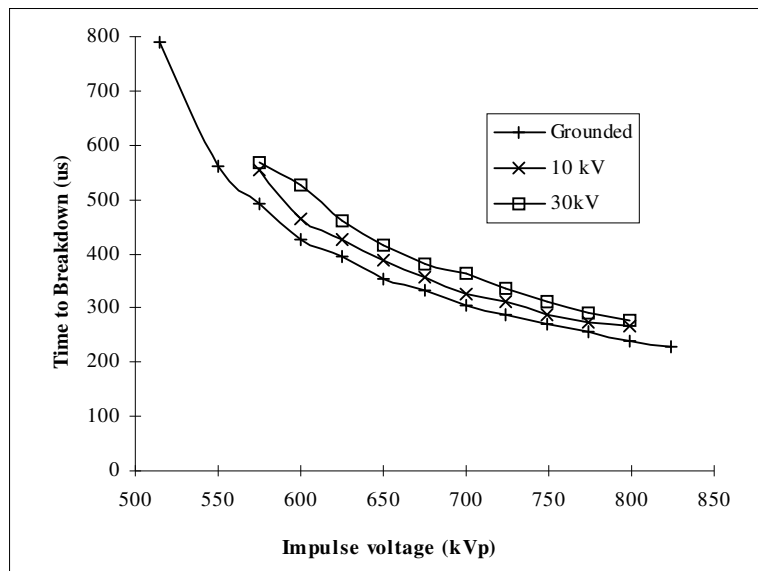


**Figure 4.3.9 :** Time to breakdown for the pre-stressed finial-sphere gap.

**Discussion:**

Average time to breakdown appears to be increased by pre-stressing the gap. The change in time to breakdown for the 10kV case is small and within the 95% confidence limits for the passive case and so may not be significant. However for 30kV pre-stress the time to breakdown is about 50 $\mu$ s later than the passive case, this is probably significant.

Investigations into the effect of pre-stressing conductor-rod gaps [2,3] have been carried out, with the conclusion that pre-stressing the gap causes an *increase* in flashover voltage due to space charge set up prior to application of impulse voltage. This fits in with the observations made of longer time to breakdown in the pre-stressed cases.

## 4.4 Modelling the Experimental Set Up

### Introduction

Running in parallel with the experimental work was a computer simulation study. The aim of the study was to model the experimental set-up to allow examination of the electric field in the finial-sphere gap.

A 2-dimensional electromagnetic CAD software package called SLIM was used in this project. SLIM is an integrated set of software modules providing facilities for generating finite-element meshes, solving electromagnetic field problems and the analysis of solutions. For the purpose of this project only electrostatic static studies were required, although SLIM is capable of doing a number of other types of electromagnetic studies. The SLIM software was run on the Sun Systems on A-floor in the Main Building at UMIST.

### Setting up the Finite Element Mesh

The first task was to input a 2-dimensional representation of the set up into the mesh generator program module. The finial-sphere gap has axial symmetry, so the 2-dimensional model will give a realistic field plot (this would not be the case if the arrangement had no axial symmetry.)

The dimensions of the sphere and the finial (including the exact measurements of the tip) were used to create the mesh shown on the next page in figure 4.4.1a. The mesh is made up of triangular elements, the vertices of triangles are called nodes. The size of the elements in the mesh correspond to the accuracy of the model. SLIM is capable of working with meshes made up of elements of different sizes, thus where more detail is required in the model (around the tip of the finial) the elements are made smaller. Figure 4.4.1b shows the outline defined by the mesh.

In SLIM nodes can be constrained to certain values this corresponds to putting a fixed voltage on them. Constraint nodes were added to the mesh for the sphere, finial and ground plane.

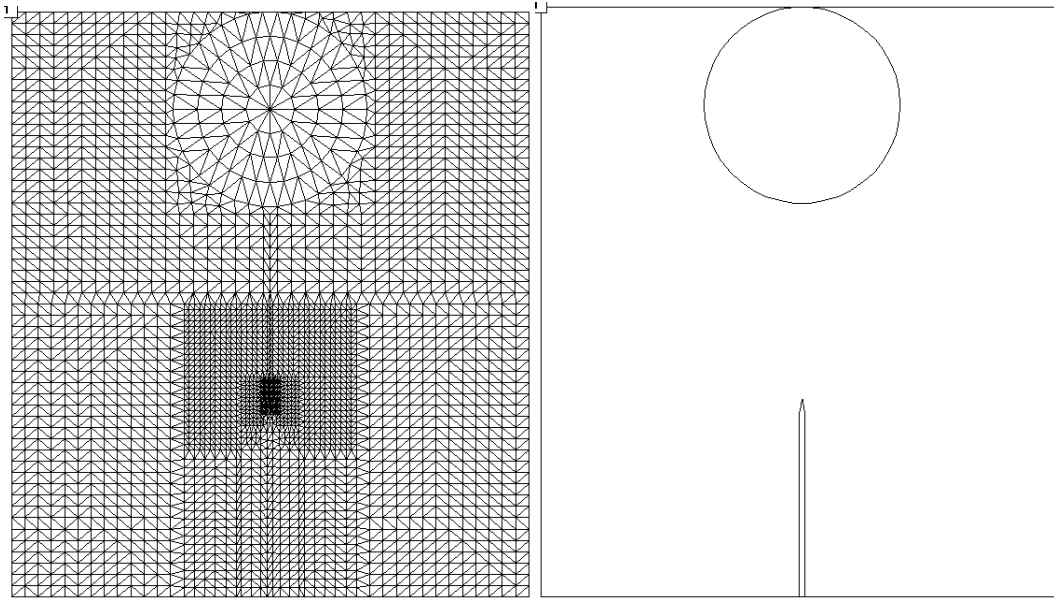


**Figure 4.4.1a** : The finite element mesh. **Figure 4.4.1b** : Outline defined by mesh.

### Calculations

SLIM needed to know the relative permittivities of the material that each element in the model was simulating. There were only two different types of element; air or metal, their relative permittivities were set to  $\epsilon_r = 1$ , and  $\epsilon_r = 100\,000$ , respectively. The exact value for metal is not required because the electric field inside the finial and the sphere is of no significance to this work, besides all the nodes on the surface of the finial and sphere have been constrained to a certain value.

Two different situations were modelled:

1. The finial grounded and the voltage on the sphere set to **-21.1kV**, the measured finial corona inception voltage for this configuration. The field plot is shown in figure 4.4.2.
2. The sphere grounded and the voltage on the finial set to **+14.8kV**, the measured finial corona inception voltage for this configuration. The field plot is shown in figure 4.4.3.

In both plots the lines shown are equipotential lines and they are separated by an interval of 5%, i.e. there are 20 equipotential lines, (N.B. the finial sits on a ground plane at the bottom of each model).

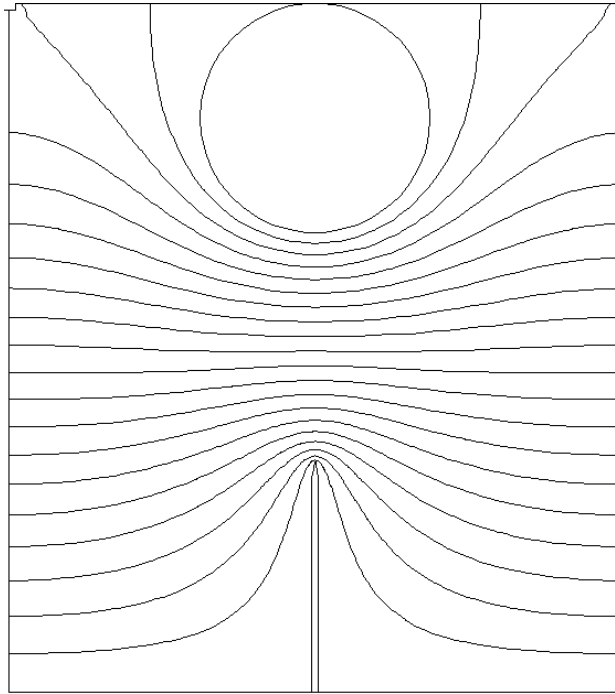


**Figure 4.4.2 :** Equipotential lines for  $-21.1\text{kV}$  applied to the sphere, finial grounded.

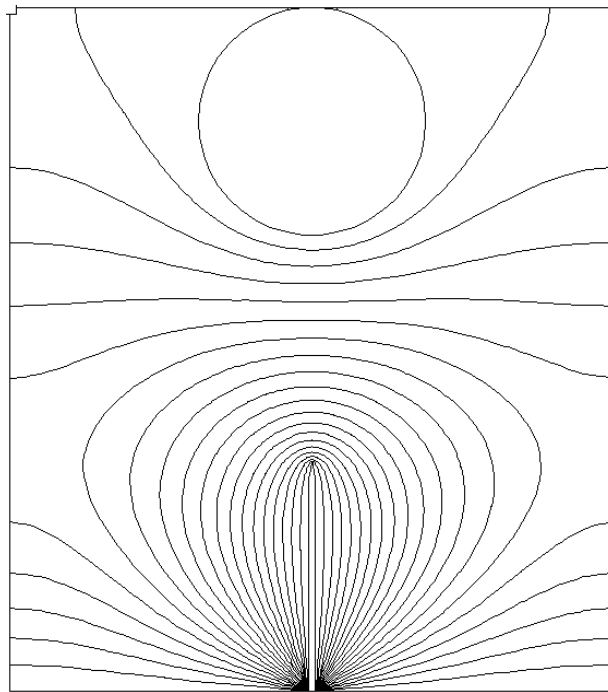


**Figure 4.4.3 :** Equipotential lines for  $+14.8\text{kV}$  applied to the finial, sphere grounded.

SLIM was capable of plotting the electric field strength between two points, this allowed investigation of the electric field set up between the tip of the finial and the sphere. The path defined over which SLIM calculated the electric field strength is shown in figure 4.4.4.

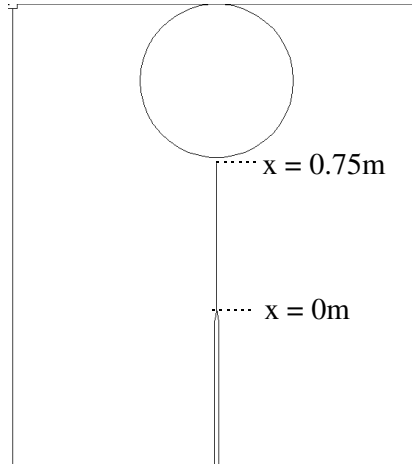


**Figure 4.4.4 :** Path over which SLIM calculated the field strength.

The electric field strength is defined as:  $E = -\frac{dV}{dx}$ . The electric field strength was calculated for the two situations modelled. The results are shown in figures 4.4.5 and 4.4.6.

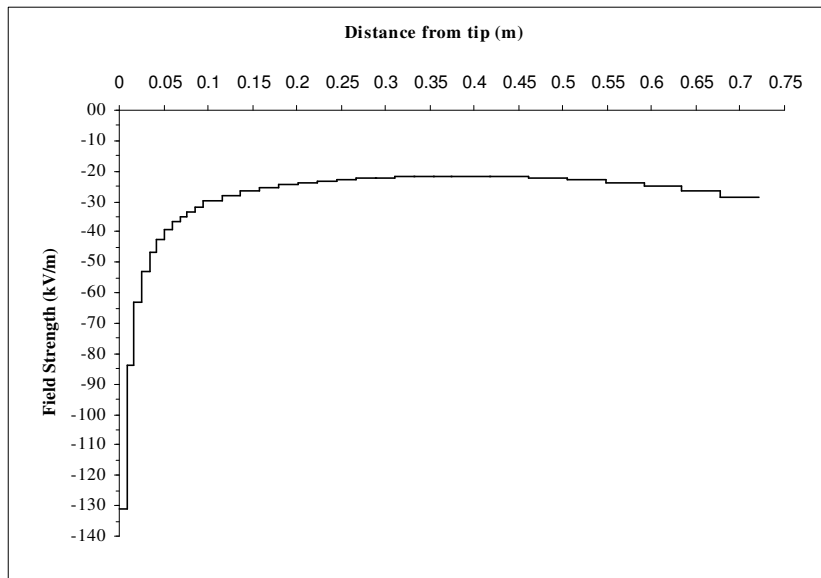


**Figure 4.4.5 :** Electric field strength in gap for rod grounded.

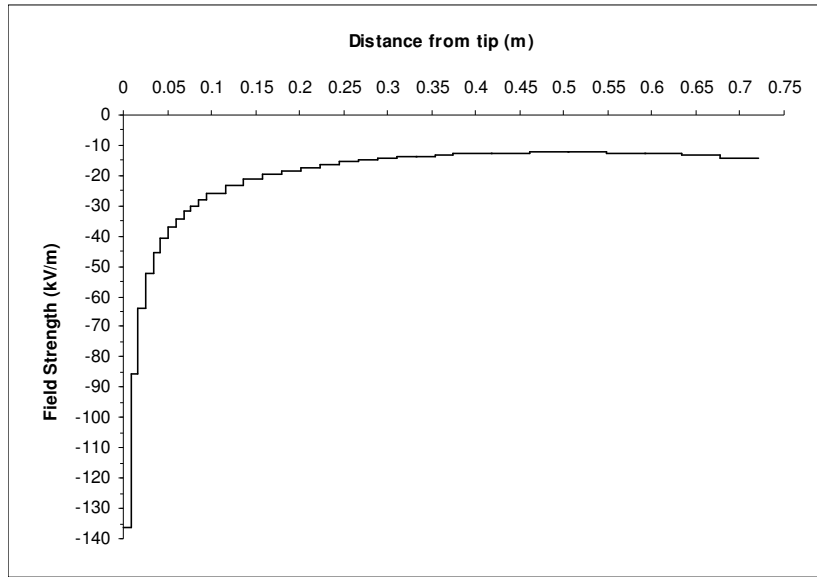


**Figure 4.4.6 :** Electric field strength in gap for sphere grounded.

**Discussion:**

The first observation to make is that the electric field strength is greatly enhanced at the tip of the finial. For both situations modelled the electric field strength in the middle of the gap is around  $20\text{kVm}^{-1}$ , this is in the region of the values observed in nature for the permanent field prior to lightning strike at ground level [5]. The field strength at the tip of the finial is around  $130\text{kVm}^{-1}$ . The small radius of curvature at the tip causes the electric field to be increased by a factor of about 6.

In both situations modelled the voltages applied to the sphere are the experimental DC corona inception voltages for that configuration. The electric field strengths calculated at the tip of the finial for each arrangement are therefore the corona inception field strengths. Since both situations use the inception voltages for *positive* corona from the tip of the finial, then the electric field strengths at the tip should be the same. In fact the field strength at the tip for the inception voltage on the finial is  $131\text{kVm}^{-1}$  (see figure 4.4.5) and for the inception voltage on the sphere it is  $136\text{kVm}^{-1}$  (see figure 4.4.6). The two values compare very well.

The theoretical critical field strength  $E_c$ , at which ionisation begins for dry air at the tip of a **rounded** rod is given by:

$$E_c = 300m\rho \left[ 1 + \frac{0.3}{\sqrt{r\rho}} \right] \text{ kVm}^{-1} \quad [1]$$

Where:

$$\rho = \text{correction factor} = 0.392 \left( \frac{P}{273 + T} \right)$$

P = atmospheric pressure (mmHg)

T = temperature (°C)

r = tip radius (cm)

m = shape factor ( $0 < m < 1$ ) For a perfectly rounded tip  $m = 1$ .

The finial tip is 2mm wide, using  $r = 0.1\text{cm}$  and applying the correction factor for the conditions in the laboratory on the day the corona inception voltages were measured, the critical field works out to  $592\text{kVm}^{-1}$  for a perfectly rounded tip. This value is much larger than the calculated value of around  $130\text{kVm}^{-1}$ . However finial tip is not perfectly rounded, it has a flat circular top with a well defined perimeter which will cause localised field enhancement. So the shape factor will be quite low, thus giving a value for corona inception voltage of around  $130\text{kVm}^{-1}$ .

Figure 4.4.2 and 4.4.3 show the equipotential field plots for the two situations. They show very clearly that grounding the sphere and applying a +ve voltage to the finial **is not** the same as grounding the finial and applying a -ve voltage to the sphere. This is due to the effect of the ground plane. However figure 4.4.7 shows that the field directly between the finial tip and the bottom of the sphere is approximately the same for the two different cases. The only difference being that the field strength is slightly greater closer to the “energised electrode” in each case.

This explains why the +ve corona inception voltage is lower when the voltage is applied to the finial as opposed to the sphere (14.8kV as opposed to 21.1kV).

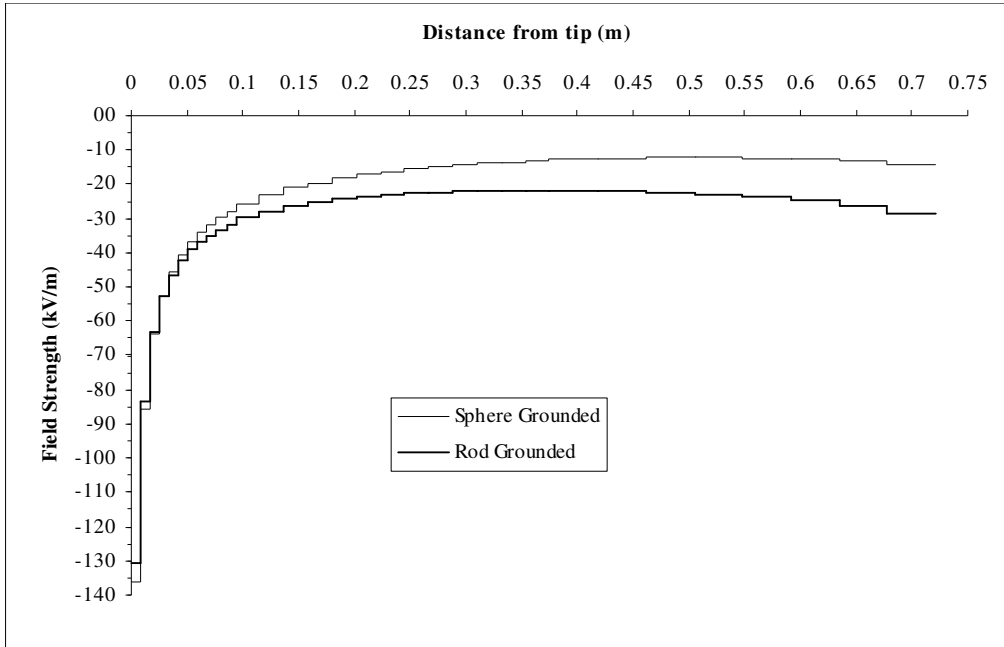


**Figure 4.4.7 :** Comparison of the two field strength distributions.

In the absence of being able to pre-stress the sphere as had been planned, applying +ve pre-stress to the finial has provided an insight into what would have happened if we had been able to pre-stress the sphere.

## 4.5 Tests on the artificial ESE device

The experiments conducted up until this point have concentrated on the passive finial and what effect that the permanent electric field (the pre-stressed case) has. Now the focus of the experiments switches to tests with the artificial ESE device, (documented in chapter 3).

### Corona Inception Times of the finial under its own excitation

Experiments were conducted to find how the artificial ESE device behaved on its own, i.e. with no simulated lightning strike.

#### **Method:**

The small impulse generator was set up to apply positive 1.2/50 $\mu$ s impulses to the lightning finial, with the sphere grounded. A photomultiplier was positioned to observe the corona discharge from the tip of the finial.

Impulses of different magnitude were applied to the rod, and the time to corona inception recorded. Times were measured from the moment the small impulse generator fired. Measurements were repeated 30 times at each voltage level.

#### **Results:**

The first observation to be made was that only **one** corona discharge occurred each time, this made recording the inception times much easier. A typical corona discharge observed with the photo multiplier is shown in figure 4.5.1.

For lower impulse voltages (below around +25kVp) corona became intermittent, i.e. not every impulse yielded a corona discharge. For impulse voltages below +17kVp no corona discharges were detectable from the tip of the finial.

The graph in figure 4.5.2 summarises the results obtained. At each test voltage the average corona inception voltage is shown. The maximum and minimum inception times obtained (within the sample size of 30 impulses) are also shown.

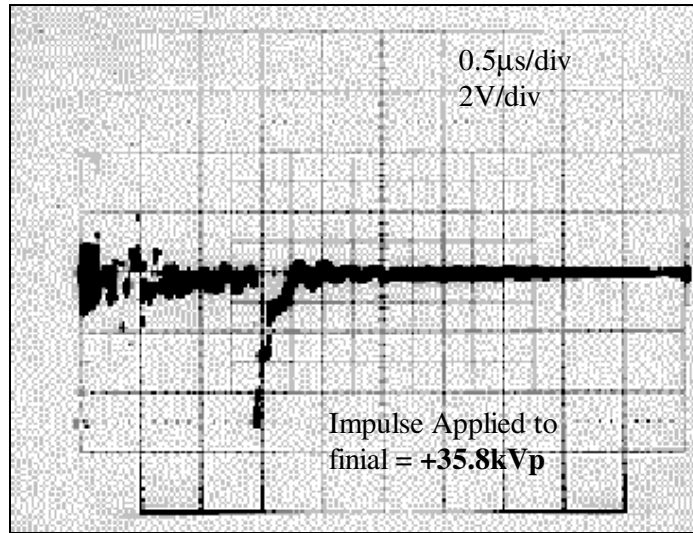


**Figure 4.5.1** : Typical observed corona discharge

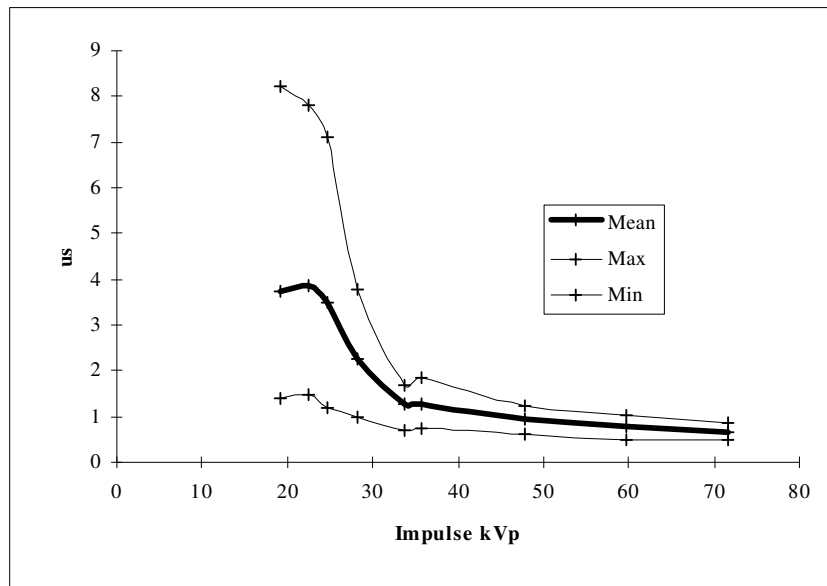


**Figure 4.5.2** : Corona inception times for 1.2/50 $\mu$ s wave applied to finial.

**Discussion:**

When analysing the data an important point to make is that the applied impulse is a 1.2/50 $\mu$ s wave, and this wave reaches its maximum value in about 2 $\mu$ s, then it starts to decay. This is a much faster fronted wave than the main impulse wave (500 $\mu$ s to peak) that explains why only one corona discharge had time to form each time.

For impulses above +40kVp the corona discharge always occurs on the front of the wave (i.e. in under 2 $\mu$ s). The range of corona inception times at higher impulse voltages is much smaller. As the impulse voltage increases the average time to corona slowly decreases. This is because as the impulse voltage rises the front dV/dt increases and thus the voltage at which corona takes place will be reached at an earlier time. However the average time to corona will not decrease forever because the corona themselves take a certain time to form after the application of the electric field.

For impulses below +30kVp the time to corona becomes much more varied, corona are observed after the voltage peak. This large variation in time to corona can be explained by the statistical nature of corona. There will always be a slight variation in time to corona because of the physical process involved, free electrons have to be in the right place at the right time etc. For large impulse voltages the corona inception voltage is passed very quickly, thus the time to corona is largely controlled by the time to reach corona inception voltage. When the peak impulse voltage is close to the corona inception voltage, the flat top of the impulse wave will emphasise the variation in time to corona.

**Time to Breakdown**

The last experiment to be conducted investigated the effect of varying the time delay before the application of the impulse to the finial, because the real ESE devices do not energise the finial until a certain point. This experiment studies the effect that varying the time to application of the finial voltage pulse has on the time to gap breakdown (and thus time to generation of a positive leader).

The magnitude of the impulse applied to the finial was chosen to be +40kVp, as can be seen from figure 4.5.2 this value is large enough to reliably put a corona discharge on the finial, and thus guarantee an injection of space charge around the tip of the rod.

The magnitude of the main impulse was chosen to be -725kVp for two reasons. Firstly because it is a value large enough to reliably cause breakdown on the front of the main wave (see figure 4.2.9). Secondly because an impulse of this magnitude generates a field between the sphere and the earth plane that is very close to that experienced in an actual lightning strike.

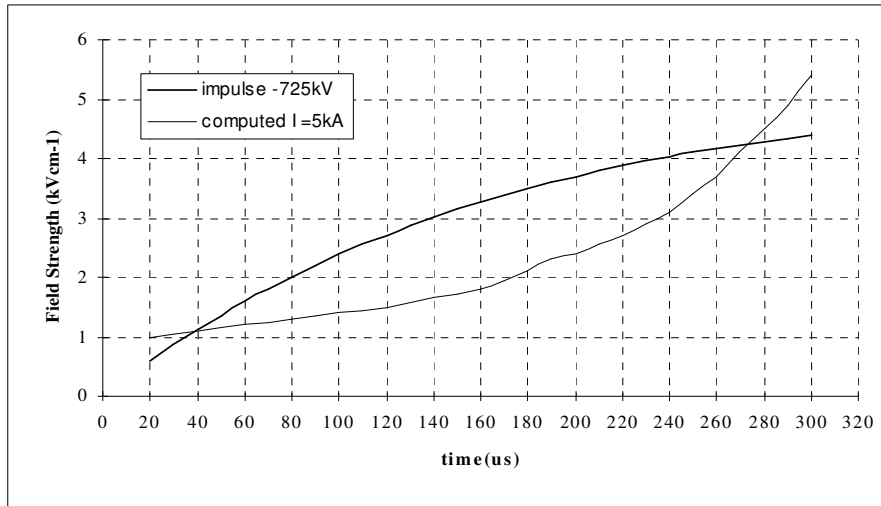


**Figure 4.5.3 :** Comparison between -725kV impulse and natural lightning.

Figure 4.5.3 shows the “average field strength” between the sphere and the ground plane for a -725kVp impulse applied to the sphere. The sphere is 1.5m above the ground plane, so “average field strength” is defined as  $V_{\text{sphere}}/150$ . Thus the impulse wave will rise to a peak “average field strength” of  $725/150 = 4.83\text{kVcm}^{-1}$ .

Also shown in figure 4.5.3 is the theoretical field strength at ground level for a lightning strike with a prospective current of 5kA [5] (medium sized lightning strike).

A -725kVp impulse wave will breakdown the finial-sphere gap in around 300 $\mu\text{s}$  the two curves shown in figure 4.5.3 compare very well for the range 0-300 $\mu\text{s}$ . Thus using a -725kVp impulse will provide a reasonably good simulation of a 5kA lightning strike.

**Method:**

A -725kVp impulse was applied to the sphere, and a +40kVp impulse was applied to the finial. The time delay to application of the +40kVp impulse was varied using the apparatus described in chapter 3, and the time to breakdown recorded 20 shots were taken at each voltage level. A photo-multiplier was also used to observe discharges from the tip of the finial, and the voltage on the finial was monitored.

**Results:**

Figure 4.5.4 shows the average time to breakdown for the different time delays, the thin lines show the 95% confidence limits for the data. Note that for delays between 230µs and 300µs no scatter was detectable in the time to breakdown.

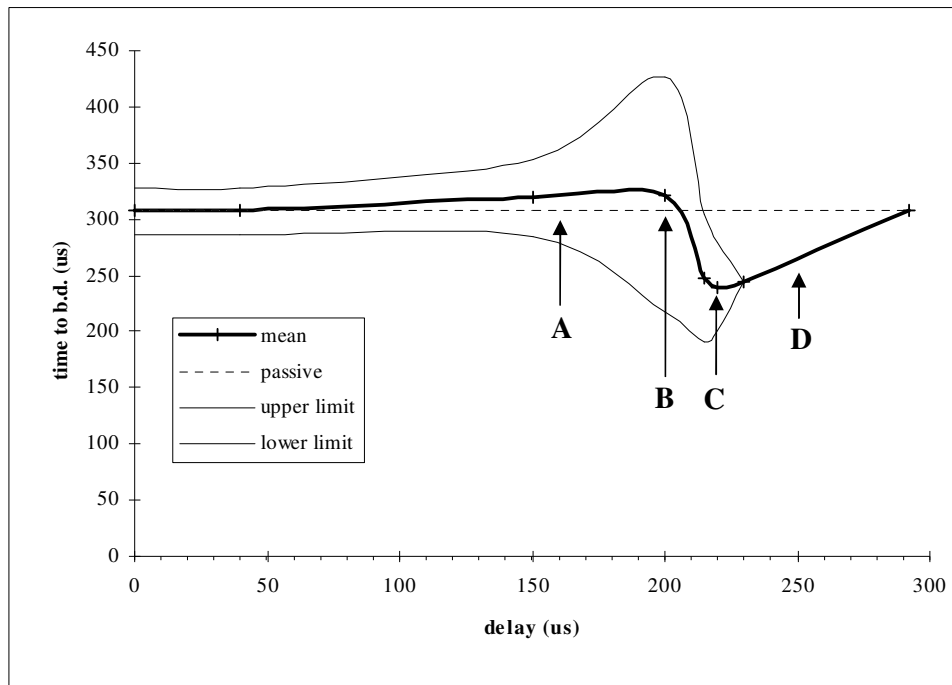


**Figure 4.5.4 :** Graph showing of how variation in time delay affects time to breakdown.

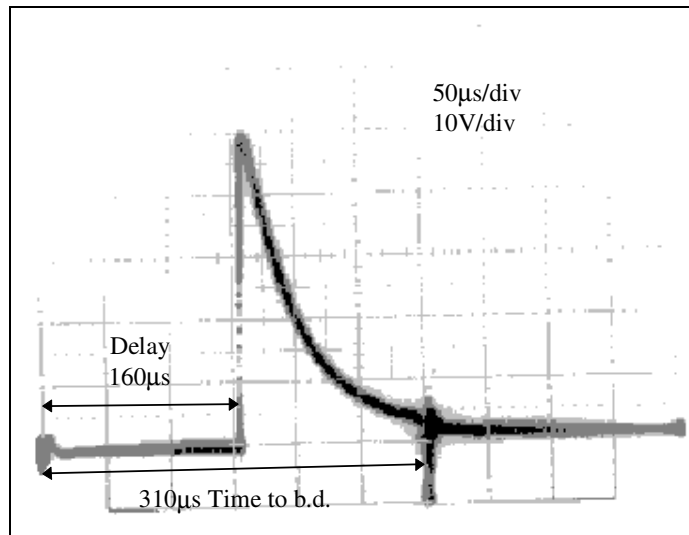


**Figure 4.5.5 :** Final voltage for 160µs delay (point A).

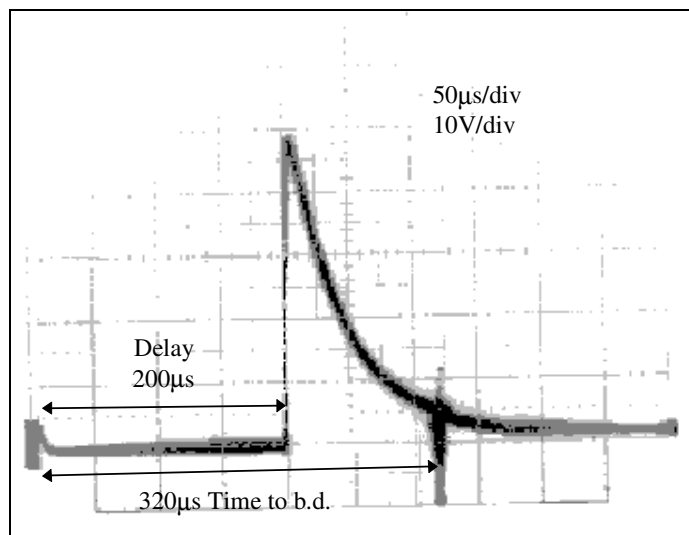


**Figure 4.5.6 :** Final voltage for 200µs delay (point B).

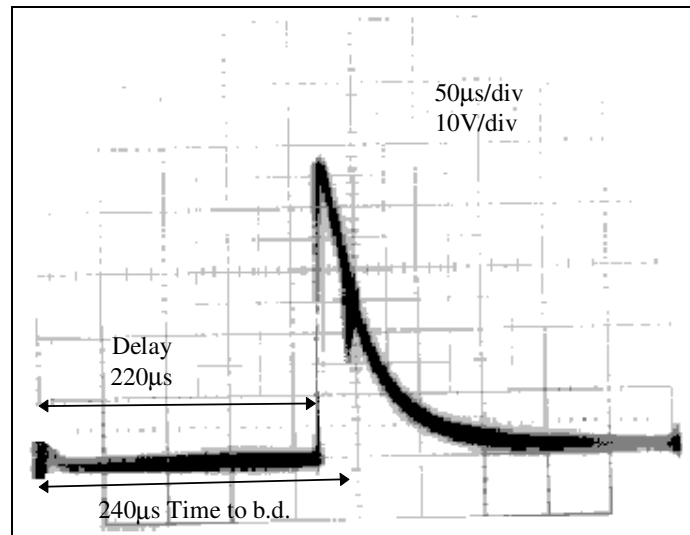


**Figure 4.5.7 :** Final voltage for 220 μs delay (point C).

Figures 4.5.5 to figures 4.5.8 show the voltage measured at the finial using a capacitive voltage divider. Breakdown appears as a sudden negative voltage pulse. This is because when the main gap breaks down the magnitude of the voltage at the finial rapidly rises until the protective spark gap on the small impulse generator breaks down. The three finial voltage measurements were taken at points marked **A**, **B** and **C** on figure 4.5.4.

Figures 4.5.8 and 4.5.9 on the next page show typical photo-multiplier measurements from the finial tip for delays in between points **A** and **B** on figure 4.5.4.

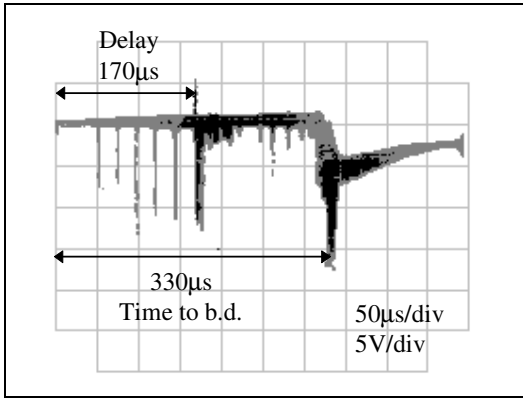


**Figure 4.5.8** : Photo multiplier measurement  
delay = 170 $\mu$ s.

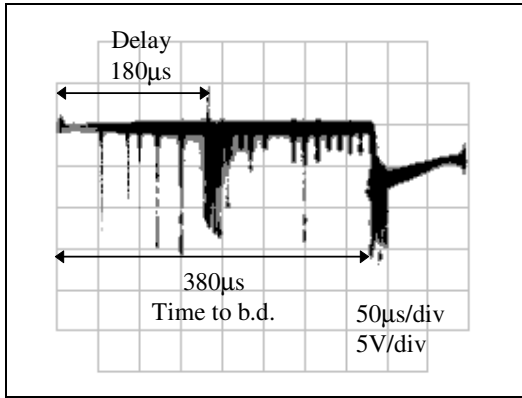


**Figure 4.5.9** : Photo multiplier measurement  
delay = 180 $\mu$ s.

Figures 4.5.10 and 4.5.11 show typical photo-multiplier measurements from the final tip for delays shown as points **C** and **D** on figure 4.5.4.

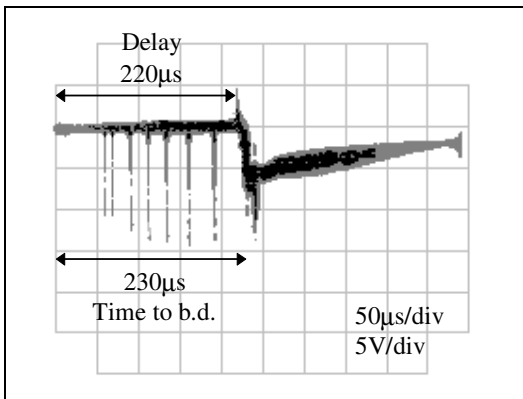


**Figure 4.5.10** : Photo-multiplier measurement  
delay = 220 $\mu$ s.

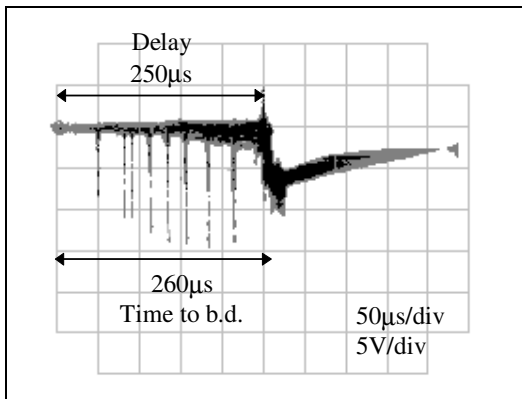


**Figure 4.5.11** : Photo-multiplier measurement  
delay = 250 $\mu$ s.

**Discussion:**

Up to a delay of 150 $\mu$ s (point A) the application of the impulse to the finial has little or no effect on the time to breakdown. The mean value of the breakdown time to breakdown is slightly later than in the passive case. From the photo-multiplier measurements it would appear that the application of the impulse deters further corona discharge that may go on to create a +ve leader, thus increasing the average time to breakdown.

As the delay is increased further the average time to breakdown becomes more scattered and the mean time to breakdown increases further. When a critical delay (220 $\mu$ s point C) is reached the applied impulse switches from inhibiting the the generation of a +ve leader to actually initiating a +ve leader. This is can be observed in figures 4.5.10 and 4.5.11 where the gap breaks down aproximatly 10 $\mu$ s after the impulse is applied.

For delays between 220 $\mu$ s and 300 $\mu$ s the time to breakdown can be accurately precisely controlled this is why this region of the graph has no scatter. The application of the finial impulse in this region always intiates a leader from the tip. The finial can be made to breakdown a maximum of 70 $\mu$ s earlier than the passive case by applying the impulse at point C (220 $\mu$ s delay). This time advantage can be converted into a distance advantage ( $\Delta L$  in figure 1.2.4) by assuming a constant positive leader velocity of 10<sup>4</sup>ms<sup>-1</sup> this works out to  $\Delta L = 70 \times 10^{-1} \times 10^4 = 7$ meters. However this value depends on the assumed leader velocity.

A 70 $\mu$ s time advantage is similar to that claimed by Berger [5] for tests on an actual ESE device, however he uses a greater value for leader velocity that gives a claimed 50m hieght advantage.

## **5. Conclusions**

The experiments have shown that a large amount of discharge activity occurs prior to the initiation of a leader from the tip of the finial. It is the long front time of the wave applied that allows multiple corona discharges to occur, however most of the corona observed occurred only on the front of the wave. This suggests that the early corona set up enough space charge at the tip of the finial to inhibit further corona.

The time to breakdown of the finial-sphere gap for a passive finial is dependant upon the peak impulse voltage. Since the front time of the impulse wave is constant then increasing the peak voltage will increase the wave front  $dV/dt$  thus causing the time to breakdown to decrease.

The permanent field that exists in nature prior to a lightning strike is equivalent to pre-stressing the finial-sphere gap. Pre-stressing the finial-sphere gap was investigated for a passive finial and it was found that pre-stress will slightly affect discharge from the tip depending on the level on pre-stress applied. In general the effect of pre-stress can be summarised as; decreasing the average time to first corona discharge, however pre-stress creates more space charge and this inhibits the generation of a positive leader thus increasing the mean time to breakdown.

For a wave simulating the field generated by a descending 5kA lightning strike it was shown that the artificial ESE device can produce an upward leader earlier than the passive finial. However the time delay to energisation of the finial is critical. If the finial is energised to early it will have little or no effect on the time to leader initiation. For a delay of 220 $\mu$ s a leader could be generated 70 $\mu$ s earlier than the passive case. This can be interpreted as an increase in striking distance ( $\Delta L$ ) depending on the choice of upward leader velocity.

The experiments have shown that a height advantage over the passive finial is possible in the controlled situations of the laboratory. However the time to finial energisation is *critical*. For practical ESE devices, such as one based on the circuit shown in figure 1.2.5 it would be impossible for the device to accurately energise the finial at the correct time. A mis-timed pulse on the finial would make the protective radius of an ESE device at best the same as a passive finial (and possibly even worse).

Another major point to make is the variability of lightning strikes, all lightning strikes are different. Presumably if different lightning strike magnitudes were simulated then slightly different time to breakdown vs. delay characteristics. The optimum delay time to produce the greatest  $\Delta L$  would probably also vary for different strikes.

To be effective the ESE device would have to get the correct delay for *every* lightning strike to be more effective overall than the passive finial. It is therefore my view that practical ESE devices are not more effective than the passive finial.

## **6. Appendix**

## 6.1 Main Impulse Generator Calibration Sheet

Test Object: **Passive finial Arrangement**

16/9/96

Temperature = **18.0°C**

Pressure = **765.5mm Hg**

Wave shape: **Negative 250/2500μs**

Correction factor =  $\frac{0.386 \times P}{(273 + t)} = \mathbf{1.015}$

Generator: **Main Impulse Generator**

No. of stages: **6**

Sphere diameter = **150cm**

Spark gap= **15cm**

Tabulated  $V_{50\%} = \mathbf{390kVp}$

Corrected flashover voltage:  $390 \times 1.015 = \mathbf{395.9kVp}$

Meter kV	
77	○
78	○ x ○ ○ ○ ○ ○ ○ ○ ○ ○ ○
79	x x ○ ○ ○ x x ○ x
80	x x x x

$$\text{Average} = (1 \times 77 + 6 \times 78 + 9 \times 79 + 4 \times 80) / 20 = \mathbf{78.8 \text{ kV}}$$

Spark gap= **18cm**

Tabulated  $V_{50\%} = \mathbf{462kVp}$

Corrected flashover voltage:  $462 \times 1.015 = \mathbf{468.9kVp}$

Meter kV	
93	○ ○ ○ ○ ○ ○ ○ ○ ○ ○
94	○ x x ○ ○ ○ x x ○ ○
95	x x x x x x

$$\text{Average} = (4 \times 93 + 10 \times 94 + 6 \times 95) / 20 = \mathbf{94.1 \text{ kV}}$$

## 6.2 Small Impulse Generator Calibration Sheets

Test Object: **Passive finial**

1/8/96

Temperature = **22.0°C**

Pressure = 759.2mm Hg

Wave shape: **Positive 1.2/50µs**

Correction factor =  $\frac{0.386 \times P}{(273 + t)}$  = **0.9934**

Generator: **Small Impulse Generator**

No. of stages: **8**

Sphere diameter = **10cm**

Spark gap= **1.2cm**

Tabulated  $V_{50\%}$  = **37.4kV**

Corrected flashover voltage:  $37.4 \times 0.9934$  = **37.2kV**

Meter kV	
<b>15.0</b>	○
<b>15.5</b>	x ○ ○ x ○ ○ ○ ○ ○ x ○
<b>16.0</b>	x x x x x x x x

$$\text{Average} = (3 \times 15.0 + 10 \times 15.5 + 7 \times 16.0) / 20 = \mathbf{15.6 \text{ kV}}$$

Spark gap= **1.8cm**

Tabulated  $V_{50\%}$  = **53.5kV**

Corrected flashover voltage:  $53.5 \times 0.9934$  = **53.1kV**

Meter kV	
<b>21.5</b>	○ ○ ○ ○ ○ ○ ○ ○
<b>22.0</b>	○ ○ ○ x x x ○ ○ ○ x ○
<b>22.5</b>	x x x x x x x x

$$\text{Average} = (4 \times 21.5 + 10 \times 22.0 + 6 \times 22.5) / 20 = \mathbf{22.05 \text{ kV}}$$

Spark gap= **2.4cm**

Tabulated  $V_{50\%}$  = **70.0kV**

Corrected flashover voltage:  $70.0 \times 0.9934$  = **69.5kV**

Meter kV	
<b>28.5</b>	○
<b>29.0</b>	○ ○ ○ x ○ ○ ○ ○ ○ ○ ○
<b>29.5</b>	x x x x x x x x x

$$\text{Average} = (1 \times 28.5 + 10 \times 29.0 + 9 \times 29.5) / 20 = \mathbf{29.2 \text{ kV}}$$

Test Object: **Passive finial**

7/8/96

Temperature = **21.2°C**

Pressure = 759.2mm Hg

Correction factor =  $\frac{0.386 \times P}{(273 + t)}$  = **0.9961**

Wave shape: **Positive 1.2/50µs**

Generator: **Small Impulse Generator**

No. of stages: **4**

Sphere diameter = **10cm**

Spark gap= **0.6cm**

Tabulated  $V_{50\%}$  = **19.9kV**

Corrected flashover voltage:  $19.9 \times 0.9961$  = **19.8kV**

Meter kV	
18.0	
18.5	○ ○ ○ ○ × × ○ ○ ○ ○ ○ ○
19.0	× × × × × × × × × × × ×

$$\text{Average} = (2 \times 18.0 + 10 \times 18.5 + 8 \times 19.0) / 20 = \mathbf{18.65 \text{ kV}}$$

Spark gap= **0.8cm**

Tabulated  $V_{50\%}$  = **26.0kV**

Corrected flashover voltage:  $26.0 \times 0.9961$  = **25.9kV**

Meter kV	
22.0	○
22.5	× ○ ○ ○ ○ ○ ○ ○ ○ ○ ○ ○ ○
23.0	× ○ ○ ○ ○ ○ ○ ○ ○ ○ ○ ○ ○
23.5	○ × × ○ × × × × × × × × ×
24.0	× ×

$$\text{Average} = (1 \times 22.0 + 3 \times 22.5 + 7 \times 23.0 + 7 \times 23.5 + 2 \times 24.0) / 20 = \mathbf{23.15 \text{ kV}}$$

Spark gap= **1.0cm**

Tabulated  $V_{50\%}$  = **31.7kV**

Corrected flashover voltage:  $31.7 \times 0.9961$  = **31.6kV**

Meter kV	
27.0	○ ○
27.5	× ○ ○ ○ × ○ ○ ○ × ×
28.0	○ ○ × ○ ○ ○ ○ ○ ○ ○ ○ ○ ○
28.5	× × × × × × × ×

$$\text{Average} = (2 \times 27.0 + 6 \times 27.5 + 8 \times 28.0 + 4 \times 28.5) / 20 = \mathbf{27.85 \text{ kV}}$$



## 6.4 Results for calculation of V50% for finial-sphere gap

Test Object: **Passive finial Arrangement**

16/9/96

Temperature = **18.0°C**

Pressure = **765.5 mm Hg**

Wave shape: **Negative 250/2500µs**

Generator: **Main Impulse Generator**

No. of stages: **6**

Meter kV	
<b>97</b>	○
<b>98</b>	○ X ○ ○ ○ X X X X X
<b>99</b>	X X ○ ○ X X X
<b>100</b>	X X X

$$\text{Average} = (5 \times 97 + 10 \times 98 + 7 \times 99 + 3 \times 100) / 25 = \mathbf{98.3 \text{ kV}}$$

## 6.5 References

1. Abdel-Salam, M. et al, Lightning Protection Using Energised Franklin Rods, Assiut University, IEEE 1995.
2. Allen, N.L. et al, A New Phenomenon Occurring in the Breakdown of Pre-Stressed Conductor-Rod Gaps Under Impulse Voltages, 9th International Symposium on High Voltage Engineering, 1995.
3. Allen, N.L. et al, Corona and Sparkover in the Pre-Stressed Conductor-Rod Gap, UMIST, CIGRE 1996.
4. Allen, N.L., On the Performance of Active and Passive Terminations in Lightning Protection, University of Leeds.
5. Berger, G., Determination of the Inception Electric Field of the Lightning Upward Leader, 8th International Symposium on High Voltage Engineering, 1993.
6. Cornick, K.J., MSc. Electrical Power Systems Engineering Lecture Notes, UMIST.
7. Darveniza, M. et al, Critical Review of Claimed Enhanced Lightning Protection Characteristics of Early Steamer Emission Air Terminals for Lightning Protection of Buildings, University of Queensland, CIGRE 1995.
8. Deller, L. et al, Lightning Stroke Simulation by means of the Leader Progression Model, IEEE 1990.
9. Gallagher, T.J. et al, High Voltage-Measurement, Testing and Design, Wiley 1984.
10. Grzybowski, S. et al, Effectiveness of Dissipators used for Lightning Protection of 13kV Distribution Lines-Model Tests, 9th International Symposium on High Voltage Engineering, 1995.
11. Nasser, E., Fundamentals of Gaseous Ionization and Plasma Electronics, Wiley 1971.
12. Petrov, N.I. et al, Determination of the Striking Distance of Lightning to Earthed Structures, University of Wales College of Cardiff, The Royal Society 1995.
13. Zhou, P.B. et al, Field Analysis and Optimum Design of Conducting Thunder Disperser, 9th International Symposium on High Voltage Engineering, 1995.